Perttu Hettula

Moment-rotation response of a flush end-plate splice

Thesis submitted for examination for the degree of
Master of Science in Technology

Espoo 29.05.2017
Thesis supervisor: Assistant prof. Arttu Polojärvi
Thesis advisor: M.Sc. Juha Kukkonen

Aalto-yliopisto
Insinööritieteiden
korkeakoulu

Aalto-yliopisto, PL 11000, 00076 AALTO
www.aalto.fi

Diplomityön tiivistelmä

Tekijä Perttu Hettula		
Työn nimi Päätylevyjatkosliitoksen momentti-kiertymäyhteys		
Koulutusohjelma Konetekniikka		
Pää-/sivuaine Teknillinen mekaniikka		**Koodi** K3006
Työn valvoja Apulaisprofessori Arttu Polojärvi		
Työn ohjaaja DI Juha Kukkonen		
Päivämäärä 29.05.2017	**Sivumäärä** 83 + 15	**Kieli** Englanti

Tiivistelmä

Päätylevyjatkosliitoksen taivutuskestävyys ja kiertymisjäykkyys voidaan määrittää momentti-kiertymäyhteyden avulla. Päätylevyjatkosliitoksen taivutuskestävyys ja kiertymisjäykkyys vaihtelevat paljon liitoksen geometriasta ja käytetystä materiaalista riippuen. Päätylevyjatkosliitoksen momentti-kiertymäyhteys voidaan määrittää Eurokoodi 3 perustuvalla analyyttisellä komponenttimenetelmällä tai elementtimenetelmään perustuvalla analyysillä.

Tässä työssä muodostetaan komponenttimenetelmään perustuva laskentaohjelma päätylevyjatkosliitoksen kiertymäyhteyden määrittämiseksi sekä tasossa tapahtuvassa taivutuksessa, että tasoa vastaan kohtisuorassa taivutuksessa. Eurokoodi 3:ssa on määritetty kattavat suunnitteluohjeet momentti-kiertymäyhteyden laskemiseksi tasossa tapahtuvassa taivutuksessa, mutta tasoa vastaan kohtisuoran taivutuksen tapausta ei ole tarkasti määritetty. Tässä työssä sovelletaan tasossa tapahtuvan taivutuksen suunnitteluohjeita ja muodostetaan laskentamalli myös tasoa vastaan kohtisuoralle taivutukselle.

Tässä työssä suoritetaan lisäksi parametrinen analyysi, jossa eri liitosgeometrioita tutkitaan sekä Eurokoodin perustuvalla analyyttisellä mallilla, että Ansys elementtimenetelmäohjelmistolla muodostetulla numeerisella mallilla. Parametrisessa tutkimuksessa käsitellään yhteensä kahdeksan eri liitosgeometriaa, joissa vaihdellaan liitoksen päätylevyjen paksuutta ja pulttien halkaisijaa. Lisäksi tutkimuksessa tarkastellaan yhdistetyn taivutuksen ja aksiaalisen kuorman, sekä pulttien esijännityksen vaikutusta liitoksen taivutuskestävyyteen ja kiertymisjäykkyyteen.

Työn tuloksena voidaan muodostaa kattava käsitys päätylevyjatkosliitoksen momentti-kiertymäyhteydestä puhtaassa taivutuksessa sekä yhdistetyssä taivutuksen ja aksiaalisen kuorman tapauksessa niin tason taivutuksessa, kuin tasoa vastaan kohtisuorassa suunnassa tapahtuvassa taivutuksessa. Lisäksi kattavan elementtimenetelmään perustuvan analyysin avulla voidaan tunnistaa päätylevyjatkosliitoksen suunnitteluohjeiden puutteet ja heikkoudet.

Avainsanat Päätylevyjatkosliitos, tasossa tapahtuva taivutus, tasoa vastaan kohtisuora taivutus, momentti-kiertymäyhteys, momenttiliitokset, Eurokoodi 3, FEM

Aalto University
School of Engineering

Aalto University, PL 11000, 00076 AALTO
www.aalto.fi

Abstract of master's thesis

Author Perttu Hettula		
Title of thesis Moment-rotation response of a flush end-plate splice		
Degree programme Mechanical Engineering		
Major Technical Mechanics		**Code** K3006
Thesis supervisor Assistant professor Arttu Polojärvi		
Thesis advisor M.Sc. Juha Kukkonen (tech.)		
Date 29.05.2017	**Number of pages** 83 + 15	**Language** English

Abstract

Resistance and stiffness of a flush end-plate splice can be determined through moment-rotation analysis. Moment-rotation characteristics vary significantly, depending on the geometrical and material properties of the joint. A prediction of a moment-rotation response of a flush end-plate splice can be determined analytically according to Eurocode 3 based component method or through a more advanced finite element analysis.

In this thesis, an analytical calculation spreadsheet is conducted for flush end-plate splices both in in-plane and in out-of-plane bending. Although Eurocode 3 only provides design rules for in-plane bending, a proposal for out-of-plane bending is presented in this thesis. In addition, a suitable finite element modelling technique is formed for bolted steel connection and the chosen methods are validated with experimental results found in the literature.

This thesis also includes a parametric study, in which different joint geometries are analysed both analytically and numerically by using the calculation spreadsheet and Ansys finite element software. In the parametric study, a total of eight different joint geometries are studied by varying the end-plate thickness and the bolt diameter. Also the effect of combined bending and axial loading as well as the effect of preloading the bolts are studied for each joint configuration.

As a result of this thesis, a more thorough understanding of the moment-rotation response of a flush end-plate splice is formed both for pure bending and for combined bending and axial loading in in-plane and in out-of-plane bending. In addition, through an extensive finite element analysis, the weaknesses related to the standardised design rules for flush end-plate splices are identified.

Keywords End-plate splice, in-plane bending, out-of-plane bending, moment-rotation, moment resisting joint, Eurocode 3, FEM

Preface

This master's thesis was done in Sweco Rakennetekniikka Oy in order to enhance the understanding of the moment-rotation response of a flush end-plate splice. The financial support for the thesis is gratefully acknowledged.

I would like to present my gratitude for Juha Kukkonen (M.Sc.) for the thesis subject and for the advice throughout the thesis. The valuable comments regarding the design of steel joints and steel structures have been extremely helpful. I would also like to thank my coworkers for the support and help with everyday issues faced with this thesis. A special thanks goes to the thesis supervisor Assistant Professor Arttu Polojärvi for providing the ideas for improving the thesis.

Finally, I would like to thank my family and friends for the extensive support they have provided not only during this thesis, but also throughout my studies in Aalto University. Without the help and support, the academic journey would have been completely different.

Espoo 29.05.2017

Perttu Hettula

Table of contents

List of Appendices

1 Introduction

1.1 Background

Splicing of structural members is required to keep member lengths within manageable limits for manufacturing, for transportation and for assembling ease. In some structures with steel columns, splicing is also necessary for the required changes in the cross-section of the columns. There are multiple ways for splicing structural members, but the main principle is that with the chosen splice, an appropriate level of continuity needs to be achieved. The standardized design rules for moment resisting joints are provided in Eurocode 3, mostly in EN 1993-1-8 [1] and additionally in standards EN 1993-1-1, EN 1993-1-2, EN 1993-1-3 and EN 1993-1-5 [2-5].

The benefits of steel construction are especially the capability of constructing challenging geometries quickly and cost efficiently. The efficiency of steel construction is based on the prefabrication of the structural members and the quick assembly at the construction site. Due to the high degree of prefabrication and quick assembly, the joints used in the structure have a significant effect on the ease of assembly and the total costs of construction. In this thesis, the study is concentrated on a flush end-plate splice. Although flush end-plate splices are not the stiffest moment resisting joints available, they still offer sufficient rigidity and continuity for spliced members [6]. For example, a flush end-plate joint offers cost efficient manufacturing and quicker assembling compared to a stiffer cover plate joint. End-plate joints and splices are generally used especially in industrial buildings. An example structure, in which such splicing is used is presented in Fig. 1.1. In this example, the roof structure was divided into smaller assemblies to enable the transportation from the workshop to the construction site. In this structure, the end-plate splices have been used for splicing the horizontal beams.

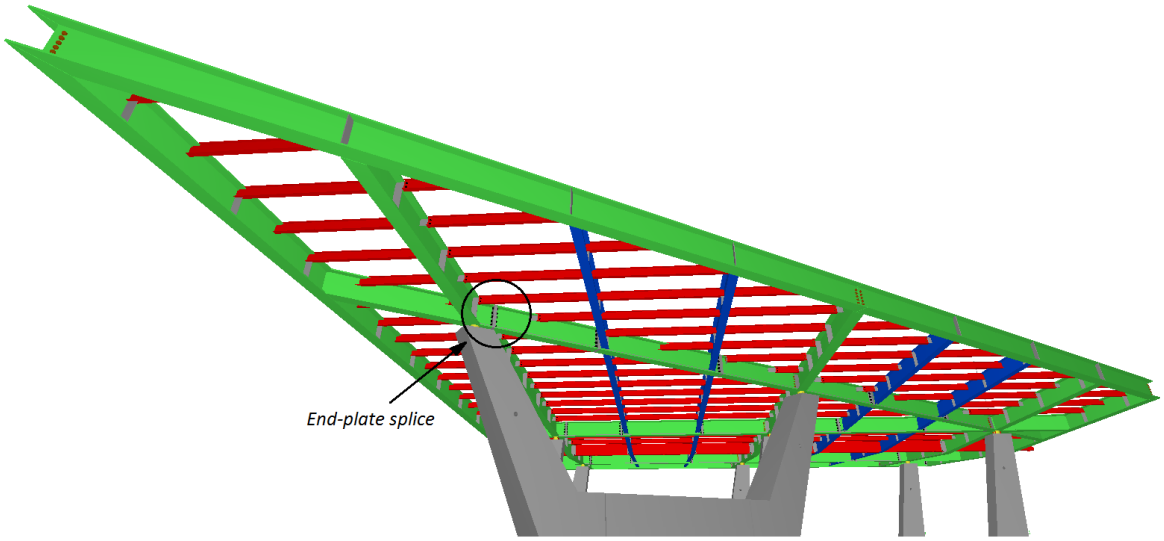

Fig. 1.1 An example of a roofing structure, in which the structural members have been spliced by using end-plate splices. In this example, the horizontal beams have been spliced to enable transportation from the workshop to the construction site. (Roofing structure in Länsiterminaali, Helsinki 2017)

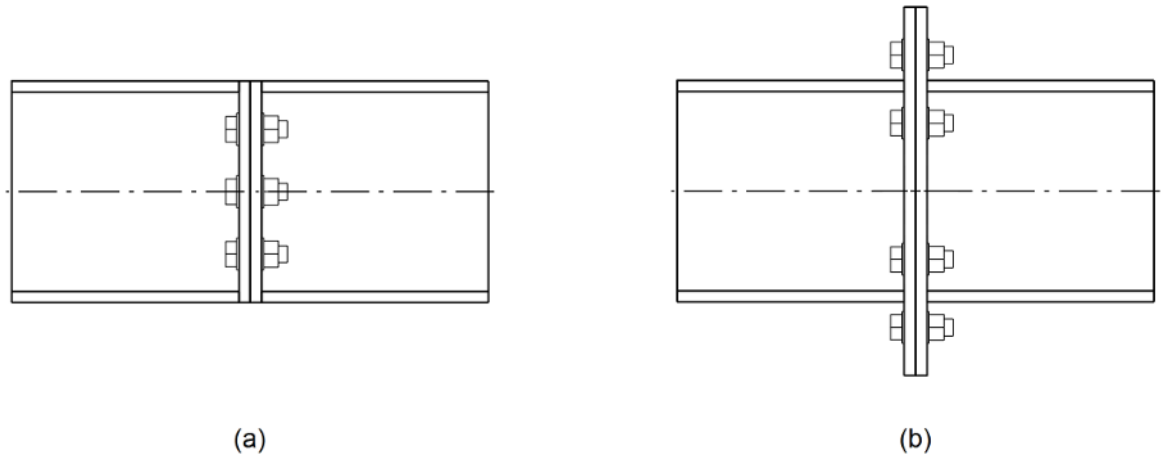

Fig. 1.2 Flush end-plate splice in (a) and extended end-plate splice in (b) for beams and columns.

Different end-plate splices are presented in Fig. 1.2. A flush end-plate joint consist of end-plates, which are not extended outside of the beam flanges. Due to smaller end-plates, all bolt rows are located between the beam flanges. An extended end-plate joint is otherwise similar, except that the end-plates are extended to reach outside the beam flanges. With extended end-plates, the stiffness of the joint can be improved due to longer lever arms for the bolts and also due to the possibility to use more bolts, since some bolt rows can be located outside of the beam flanges. Due to enhanced moment-rotation characteristics of an extended end-plate joint, it should always be preferred over a flush end-plate joint. However, architectural or structural restrictions may lead to situations, in which a flush end-plate splice is the only possibility for splicing the structural members.

End-plate joints can be used to splice structural members, but also to connect beams to columns. Although beam-to-column end-plate joints are widely researched in in-plane bending, only little research has been conducted in out-of-plane bending [7,8]. The existing research on beam-to-column end-plate joints is beneficial for this thesis, since the actual flush end-plate splice for beam-to-beam connections is very little researched. Some research has been conducted by Urbonas and Daniunas in [9,10] and by Mohamadi-shooreh and Mofid in [11]. A connecting factor within these studies on flush end-plate splices is that they are limited to only a few geometrical configurations, so no general conclusion can be made on the moment-rotation response of this specific end-plate splice. Also the behavior of end-plate splices under combined bending and axial loading is very little researched.

1.2 Objectives and scope

This thesis concentrates in the calculations of the moment-rotation response of a flush end-plate splice both in in-plane and in out-of-plane bending. Although the Eurocode 3 [1] only provides thorough design rules for in-plane bending, both in-plane and out-of-plane bending of a flush end-plate splice are considered in this thesis. The two bending cases are shown in Fig. 1.3. With I-profiles, in-plane and out-of-plane bending are sometimes referred to as strong axis and weak axis bending. The consideration of both directions is important, since especially in industrial steel frames, bending can occur in both directions.

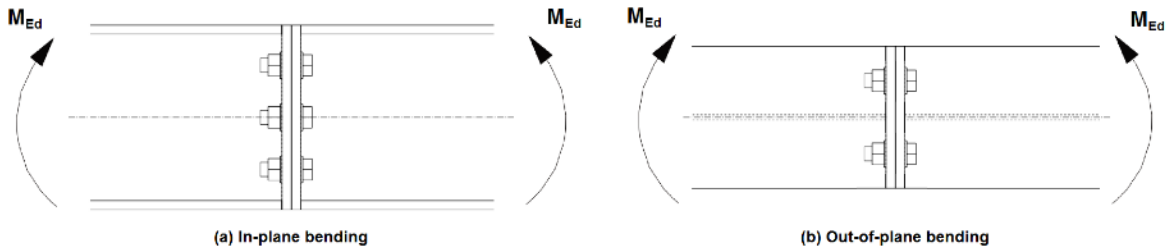

Fig. 1.3 (a) shows the in-plane bending and (b) the out-of-plane bending of an end-plate splice with six bolts. M_{Ed} is the design bending moment.

Objective in this thesis is to form better understanding of the behavior of a flush end-plate splice in both directions in pure bending cases and also under combined bending and axial loading. Especially the out-of-plane bending and the combined loading cases are considered of high importance, since these cases are little researched and the common design standards do not provide thorough design rules for calculating neither the initial stiffness nor the ultimate moment resistance of an end-plate splice in out-of-plane bending and under combined loading. The moment-rotation response of a flush end-plate splice in biaxial bending and under torsion is not studied in this thesis.

Another objective is also to study the different failure mechanisms developed with end-plate splices and to see if it is possible to achieve relatively stiff joints while still presuming appropriate levels of ductility. Some examples on how moment resisting joints can affect the global analysis of the whole structure are presented, but more accurate frame analysis and the impact on the surrounding structure are not handled in this thesis.

This thesis consists of two major parts: determining the moment-rotation response of a flush end-plate splice according to Eurocode 3 and on the comparative calculations conducted with finite element analysis. The comparative analysis consists of a parametric study, in which two geometrical parameters of an end-plate splice are varied. The parametric study includes also analysis with non-preloaded and preloaded bolts as well as with combined bending and tension and combined bending and compression. The numerical analysis are performed with Ansys finite element software. In the results section, the analytical and numerical results are compared and the development of different failure mechanism is explained in detail.

1.3 Thesis structure

This thesis is divided into four separate sections. In the first section, different connection types and the Eurocode based classification system is presented alongside with an example analysis of a simple steel frame. The simple steel frame analysis is presented to visualize the importance of accurate assumptions made in the global analysis of structures. In the second section, the Eurocode 3 based design of flush end-plate joints is presented and a calculation sheet is formed. The third section concentrates on the validation of chosen finite element methods and techniques and on the formulation of a full size end-plate splice model. The parametrized study and the tools for comparing the different parametrizations are also presented in the third section. In the results section, the results of the parametric study are presented and the numerical results are compared to the results obtained with the Eurocode based calculation sheet.

2 Connection types

This thesis concentrates on the moment resisting joints used in steel construction. There are multiple types of steel joints and they are categorized according to their characteristics. In general, moment resisting joints are more expensive to fabricate than simple shear only connections [12]. Although the use of material is not significantly increased with moment resisting joints, they usually require more welding than other connection types, especially if additional stiffeners are used. The effort made for the design of moment resisting joints would be significantly reduced, if the structural members were welded to each other on-site. However, this is not preferred, since on-site welding usually occurs in difficult conditions and it is slow and expensive. The classification of joints and the aspects that should be accounted for in the design of moment resisting joints are presented in the following subsections.

2.1 Classification of joints

In the design of steel frames, the joints should be designed so that they meet the assumptions made in the applied design method without adversely affecting any other part of the structure. According to Eurocode 3 [1], joints can be classified by their stiffness and by their strength. The Eurocode based classification of end-plate splices is presented in the following subsections.

2.1.1 Classification by stiffness

An end-plate splice can be classified by stiffness as *rigid*, *semi-rigid* or *nominally pinned*. The initial rotational stiffness of the joint is the determining factor while defining the joint classification. The Eurocode based joint classification is presented in Fig. 2.1. The joints classified as *rigid* may be assumed to have sufficient rotational stiffness to justify analysis based on full continuity. The stiffness criteria for rigid joint is as follows

$$S_{j,ini} \geq k_b \frac{E I_b}{L_b} \tag{2.1}$$

in which $S_{j,ini}$ is the initial stiffness of the joint, E is the Young's modulus of the material, I_b is the second moment of area of the connected member, L_b is the span of the beam and the coefficient $k_b = 8$ for braced frames. For other frames, which do not meet the Eurocode based criteria for braced frames $k_b = 25$. All stiffness classifications in this thesis are performed under the assumption of braced frames.

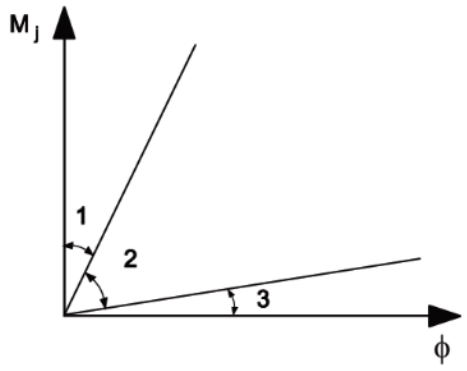

Fig. 2.1 Classification of joints by stiffness according to Eurocode 3 [1]. M_j is the bending moment and ϕ is the corresponding rotation angle.

The stiffness criteria for *nominally pinned* joints is the following

$$S_{j,ini} \leq 0.5 \frac{EI_b}{L_b}. \tag{2.2}$$

A nominally pinned joint should be capable of transmitting the internal forces without developing significant moments to the surrounding structure. A nominally pinned joint should also be capable of accepting the resulting rotations under the design loads. All joints, which do not meet the criteria for rigid joint of a nominally pinned joint, should be classified as *semi-rigid*. Semi-rigid joints should be capable of transmitting the internal forces and moment and they provide a predictable degree of interaction between the connected members. With semi-rigid joints, the interaction is never full continuity, so to determine the impact to the surrounding structure, the moment-rotation characteristics should always be defined [12].

As can be seen from expressions (2.1) and (2.2), the classification by stiffness is always relative to the connected members. For example, the stiffer the connected members, the higher the criteria for rigid joints. The same goes for the length of the span, as the shorter the beam span, the higher the rigidity criteria. Practically this means that with short and relatively stiff members, a rigid joint is more difficult to achieve and more expensive to manufacture. Sometimes the stiffness classification of joints is also done based on the continuity it provides to the connected members. Joints that are classified as pinned can be referred to as simple connections, which do not distribute significant internal moments. Rigid joints can provide full continuity and semi-rigid joint are capable of providing continuity to some extent.

2.1.2 Classification by strength

An end-plate splice can be classified by strength as *full-strength, partial strength* or *nominally pinned*. The classification is done by comparing the design moment resistance $M_{j,Rd}$ of the joint with the design moment resistance of the members it connects. Here, the design moment resistance is the limit for the bending moment leading to failure of a structural member. The classification by strength is relevant when plastic analysis are used for frame analysis [12].

For *full-strength* joints, the design moment resistance should not be less than that of the connected members

$$M_{j,Rd} \geq M_{b,pl,Rd}. \tag{2.3}$$

in which $M_{j,Rd}$ is the design moment resistance of the joint and $M_{b,pl,Rd}$ is the design moment resistance of the adjacent member. An end-plate splice can be classified by strength as *nominally pinned* if $M_{j,Rd}$ is less than $0{,}25 \cdot M_{b,pl,Rd}$. A nominally pinned joint should be capable of transmitting the internal forces without developing significant moment to the surrounding structure and it should be capable of accepting the resulting rotations under the design loads. An end-plate splice is classified as *partial strength* if it does not meet the criteria for a nominally pinned joint or a full-strength joint. Similarly, as with the classification by stiffness, also with the strengths classification, the classification is relative to the connected members

meaning that members with high moment resistance lead to higher criteria for full-strength joints.

2.2 Influence of assumptions on the surrounding structure

The intent in the design of frames including moment-resisting joints would be that such joints are classified as rigid. However, quite often the full rigidity is not achieved and the moment-resisting joints are classified as semi-rigid. [12] The lack of sufficient rigidity might be due to limited space around the connection area or due to some other restrictions concerning the geometrical properties of the joint. On the contrary to rigid joints, sometimes pinned joints are required to obtain favorable behavior of the structure and if the moment-rotation response of the designed joint is stiffer, the assumption made in the global analysis is wrong. Semi-rigidity of the joint has a significant influence on the frame behavior and stability as can be seen in the following simple frame analysis.

In Eurocode 3 [2] it is determined that the joint behavior can be neglected in the global analysis of the structure if joints have only minor changes to the deformations and the global distribution of internal forces and moments. The joint behavior cannot be neglected with joints that provide semi-continuity, whereas with simple and with full continuity joints, pinned and rigid assumption can be made in the global analysis of the structure. Especially for multistorey unbraced frames, the rotational stiffness of the joint is fundamental to the determination of the frame stability [12].

In the design procedure of steel frames that include moment-resisting semi-rigid joints, all of the assumptions concerning the connectivity between the members should be done as accurately as possible. A common method of including the joint characteristics to the global frame model is to connect the structural members with rotational springs. Rotational springs have a significant impact on the global frame behavior, as with small values of rotational stiffness, the sway of the frame increases significantly. In Eurocode 3 [2], steel frames are categorized into sway and non-sway frames according to the coefficient

$$\alpha_{cr} = \frac{F_{cr}}{F_{Ed}} \tag{2.4}$$

in which F_{Ed} is the design loading on the structure and F_{cr} is the elastic critical buckling load for global instability mode based on initial elastic stiffness. With non-sway frames, second order effects determined in Eurocode 3 [2], do not have to be taken into account. The limit for non-sway frame with elastic analysis is $\alpha_{cr} \geq 10$.

To visualize the impact of different joint characteristics, a simple frame analysis was performed with Dlubal RFEM software. The sway of the one-bay, two-storey frame under given loading conditions is presented in Fig. 2.2. The analysis was performed with two different rotational springs: in Fig. 2.2 (b) $C_1 = 200$ kNm/° and in Fig. 2.2 (c) $C_2 = 1200$ kNm/°. Although the stiffness coefficients differ quite significantly, according to Eurocode 3, both of these rotational springs would be classified by stiffness as semi-rigid.

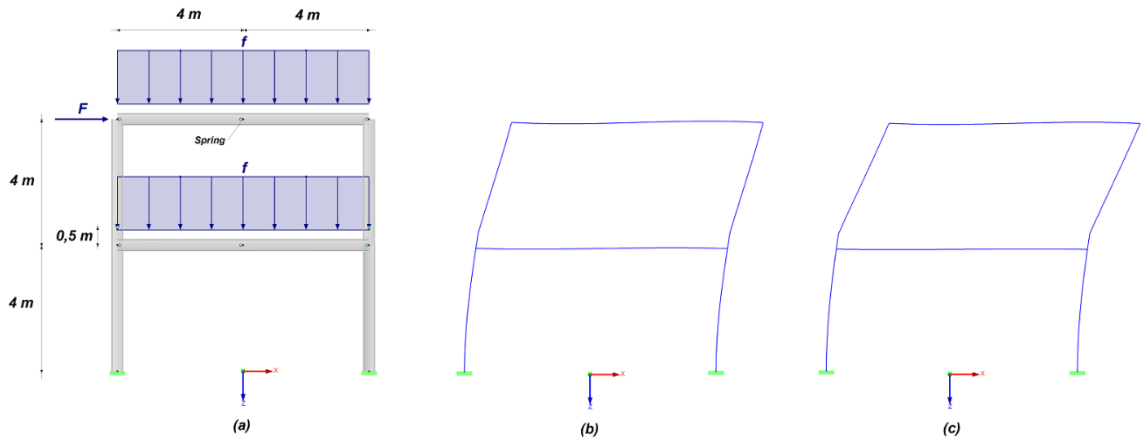

Fig. 2.2 Frame analysis performed with Dlubal RFEM software. Steel members of the frame are HEB400 steel profiles and they are connected with linear rotational springs. The external load $F = 400$ kN and the uniformly distributed load $f = 150$ kN/m. (a) is presenting the loading and the geometrical properties of the frame. The points are indicating the locations of the rotational springs, which represent the end-plate joints. (b) is showing the first global buckling mode of the structure with rotational springs with stiffness coefficients of $C_1 = 400$ kNm/° and (c) is showing the first global buckling mode of the frame with rotational spring with stiffness coefficient of $C_2 = 200$ kNm/°.

Although both joints used in the frame analysis are classified as semi-rigid, it was found that with the lower rotational stiffness joint, $\alpha_{cr} = 6{,}77$ and with the stiffer joint $\alpha_{cr} = 11{,}02$. This means that the lower stiffness leads to a sway frame and second order effects should be considered. The simple analysis performed here shows that if the initial stiffness of the semi-rigid joints is not accurately determined, it can lead to fatal errors in the global analysis of structures. Errors in the stiffness calculations can also cause major problems in earthquake sensitive areas, since for example, if the initial stiffness of an end-plate joint is over-estimated, it leads to under-estimated storeydrifts and to lower natural frequencies than predicted [6].

As well as with whole structural frames, the joint stiffness plays a significant role also in the stability and load carrying capacity of an individual column. Another significant factor is the location of the column splice. [13,14] In steel construction, columns should be spliced at floor level, but due to practical restrictions this usually occurs at a convenient distance above the floor beam level. [15,16] In Eurocode 3 [4], it is determined that splices and end-plate joints connecting members subject to compression, should either have at least the same resistance as the cross-section of the connected members or to be designed to resist an additional bending moment due to second-order effects in the connected members. The second-order effects should be taken in addition to the internal compressive force and the internal bending moments about both axis, obtained from the global analysis of the structure.

Usually the determining factor in the design of columns in practical cases is the buckling of the columns. Snijder and Hoenderkamp [16] proposed an analytical model for determining the criteria for the required stiffness of column splices. The proposed analytical model is based on the assembly of two separate subsystems as presented in Fig. 2.3. The Euler buckling load of a spliced column $N_{cr,spl}$ can be estimated by combining the Euler buckling loads for the two subsystems. In subsystem 1, the rotational stiffness C of the splice is assumed infinite while the bending stiffness EI of the column is finite. In subsystem 2 on the right, the rotational stiffness C is finite and the connected column members are assumed rigid.

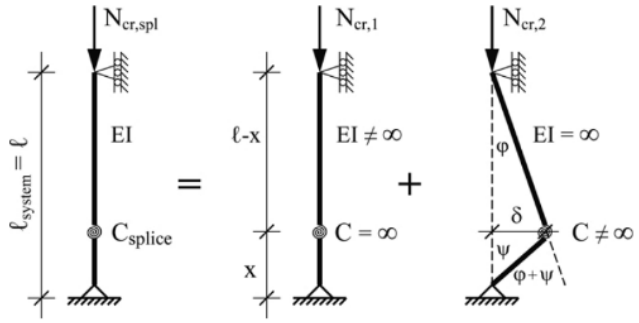

Fig. 2.3 Column model for stiffness requirements of a column splice. [16]

The Euler buckling load for column 1 in Fig. 2.3 is the following

$$N_{cr,1} = \frac{\pi^2 EI}{l^2} \tag{2.5}$$

in which E is the Young's modulus, I is the second moment of area and l is the system length. The Euler buckling load for subsystem 2 can be derived by the equilibrium equation in the deformed state. In the final equilibrium state, the moment caused by the external load should be equal to the internal moment at the splice as follows

$$N_{cr,2} = C(\psi + \varphi) \tag{2.6}$$

in which C is the rotational stiffness of the splice and $\psi + \varphi$ is the total rotation angle of the splice. The moment arm for the external load can be derived by using the geometrical conditions

$$\delta = \varphi(l - x) \tag{2.7}$$

in which x is the location of the splice. Angle ψ can also be derived from the geometry by assuming small angle rotations

$$\psi = \varphi \frac{l - x}{x}. \tag{2.8}$$

Substituting equations (2.7) and (2.8) into (2.6) and simplifying leads to

$$N_{cr,2} = \frac{Cl}{x(l - x)}. \tag{2.9}$$

Now the Euler buckling load of the spliced column can be calculated by using the Dunkerley formula from [17] as follows

$$\frac{1}{N_{cr,spl}} = \frac{1}{N_{cr,1}} + \frac{1}{N_{cr,2}} \tag{2.10}$$

in which $N_{cr,spl}$ is the Euler buckling load of a spliced column. By substituting equations (2.5) and (2.9) into (2.10) yields the following equation for the Euler buckling load of the spliced column

$$N_{cr,spl} = \frac{1}{\frac{l^2}{\pi^2 EI} + \frac{x(l-x)}{Cl}} \tag{2.11}$$

Snijder and Hoenderkamp proposed an acceptance of 5 % reduction in Euler buckling load due to the splice stiffness. By applying this, the following criteria can be derived for the Euler buckling load of spliced columns

$$N_{cr,spl} \geq 0.95 \frac{\pi^2 EI}{l^2}. \tag{2.12}$$

Now, substituting equation (2.11) into (2.12) gives the following expression

$$\frac{Cl}{\frac{Cl^3}{\pi^2 EI} + x(l-x)} \geq 0.95 \frac{\pi^2 EI}{l^2}. \tag{2.13}$$

Equation (2.13) can be further simplified to obtain a criteria for a splice stiffness as follows

$$C \geq 19 \frac{\pi^2 EI}{l^2} \frac{x(l-x)}{l}. \tag{2.14}$$

By assuming the location of the splice at $x = l/4$, the criteria can be written into the following simplified form

$$C \geq \frac{57\pi^2 EI}{16l}. \tag{2.15}$$

The criteria proposed in [16] is of the same form as the Eurocode based criteria for a rigid joint. However, by comparing the expressions (2.1) and (2.15) it can be clearly seen that the Eurocode based criteria for rigid joints is significantly lower than the criteria based on Euler buckling. Reason for this might be that the stiffness calculation rules provided in Eurocode 3 [1] are only applicable to joints connecting members in which the axial force does not exceed 5 % of the plastic design resistance $N_{pl,Rd}$ of the cross-sections of the connected members. Another reason could be that the same rigidity rule is not only applied for splices, but also for other moment resisting joints. The criteria for the level of axial loading is hardly ever fulfilled with column splices, since columns are always designed to carry high compressive forces. The criteria based on Euler buckling suggests that with column splices, the stiffness of the splice should be accounted for in the global analysis of the structure even if the Eurocode based classification for the joint is rigid.

These few examples are indicating the significance of the moment-rotation response of the joint on the behavior of the whole structure. The exact value of the rotational stiffness of the joint was presented to have a notable impact on the behavior of the structure and that erro-

neous stiffness can lead to fatal mistakes in the global analysis of the structure. All this highlights the importance of suitable design methods for different joint types in varying loading conditions.

3 Ultimate limit state calculations

Ultimate limit state calculations consist of the theoretical models used for standardized design of moment resisting steel connections. The theoretical model is called the component method, which is based on Eurocode 3, standard EN 1993-1-8 [1]. The component method can be applied to all planar joints provided that the axial force in the connected members does not exceed 5 % of the design resistance $N_{pl,Rd}$ of their cross-section. In steel design, the component method refers to a spring model, which represents the steel connection as a set of linear springs. A considerable effort for developing the component method has been performed already in 1974 by Zoetemeijer [18] and the development has then been continued by Jaspart in [19,20]. The formulation of the components, as well as other standardized design procedures, are based on a large number of experimental research programs carried out by multiple research institutes.

The component method presented in this section is used for the calculation spreadsheet formulated as part of this thesis. An output print of an example design of an individual T-stub is presented in Appendix 2 and of a flush end-plate splice is presented in appendix 3 and 4. The calculation spreadsheet is used later in this thesis to derive the Eurocode based analysis of the parametric study. The Eurocode based results and the numerical results are compared in section 5.

3.1 Terms and definitions of component method

The idea of the component method is to form a mathematical model, in which the individual components make an identified contribution to one or more of the structural properties of the connection. The design moment-rotation characteristic of a joint depends on the properties of its basic components. The linear spring-system is shown in Fig. 3.1.

In Fig. 3.1, as a result of the combination of the linear spring system, the joint configuration is represented as a rotational stiffness spring, in which the rotation center is at the center of the intersection of the connected members. The Eurocode based component method can be applied to multiple planar moment resisting joint types, but only the end-plate connections are considered in this section. In Eurocode 3 [1], the method for the end-plate connections is presented only for beam-to-column connection, but the standard gives additional rules for extending the design procedure to end-plate splices.

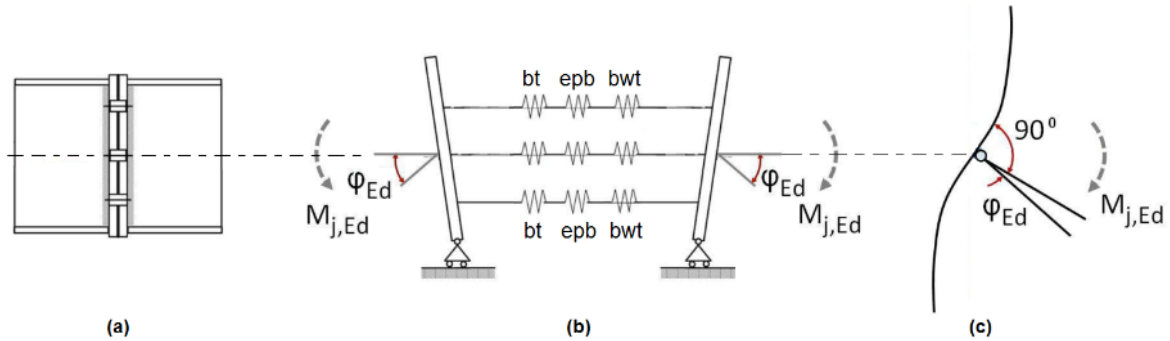

Fig. 3.1 The combination of the linear spring system can be represented as a rotational spring. (a) is showing the beam splice geometry, (b) the linear spring system in which *bt* indicates bolts in tension, *epb* end-plate in bending and *bwt* beam web in tension, (c) represents the equivalent rotational spring. $M_{j,Ed}$ is the bending moment and φ_{Ed} the corresponding rotation angle.

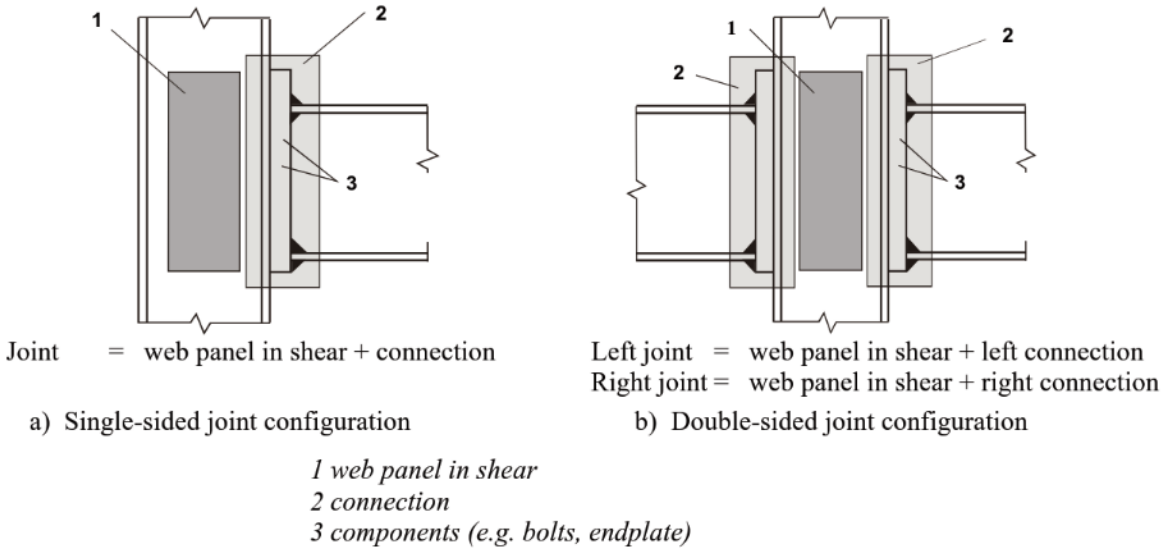

Fig. 3.2 Parts of a beam-to-column joint configuration. [1]

The distinction between the terms: basic component, connection and joint is presented in Fig. 3.2. A connection refers to a location where two or more structural elements meet. For design purposes, a connection is the assembly of the basic components. A joint is a zone, where two or more structural members meet. Members are, for example, the jointed beams and columns.

The typical components of an end-plate splice are basically the same as those of a beam-to-column end-plate connection except that all the items related to the column are omitted. In a beam-to-column end-plate connection, there are the following components: (i) column web panel in shear, (ii) end-plate in bending, (iii) column flange in bending, (iv) beam web in tension, (v) column web in compression (vi) beam web in tension, (vii) beam flange and web in compression, (viii) bolts in tension and (ix) welds. The typical components are shown in appendix 1. [1]

In this study, the component method is not handled generally, but by applying the component method to a flush end-plate splice. Firstly, this is done by studying the behavior of the individual T-stubs under tension and then by identifying and designing all the necessary components of a flush end-plate splice.

3.2 Equivalent T-stub under tension

For comprehensive analysis of the moment resisting connections, it is important to understand the behavior of the bolted T-stub. This is due to the fact that typical end-plate connections and splices are usually build-ups of individual bolted T-stubs under tension. An end-plate splice consisting of individual T-stubs is shown in Fig. 3.3. The equivalent T-stub approach is used for defining the limiting yield mechanism of the end-plate splice. The equivalent T-stub presented in this sections and the analytical calculations of the T-stub will also be used in section 4 for comparative analysis of the finite element validation model.

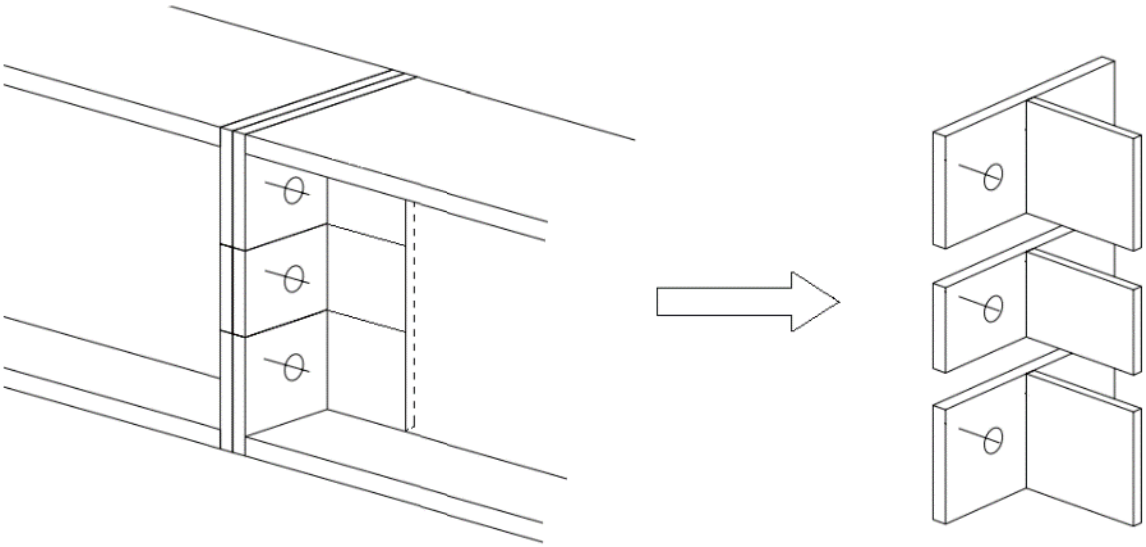

Fig. 3.3 End-plate splice consisting of individual T-stubs under tension.

3.2.1 Failure mechanisms of the T-stub

In the case of Fig. 3.4, it might be mistakenly considered that the bolt forces are the total tension force T devided by the number of the bolts. This is not always true, since because of the deflection of the flanges, some internal prying forces can occur. [18] Due to the internal prying forces, the failure mechanism and also the design resistance of the T-stub needs to be thoroughly analyzed. The development of the failure mechanisms is studied in this section.

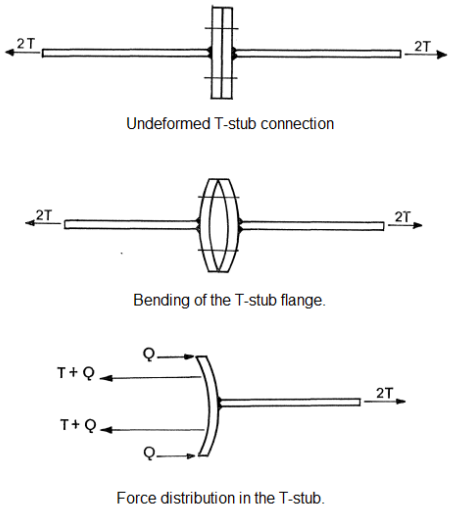

Fig. 3.4 Basic T-stub under external tension load.

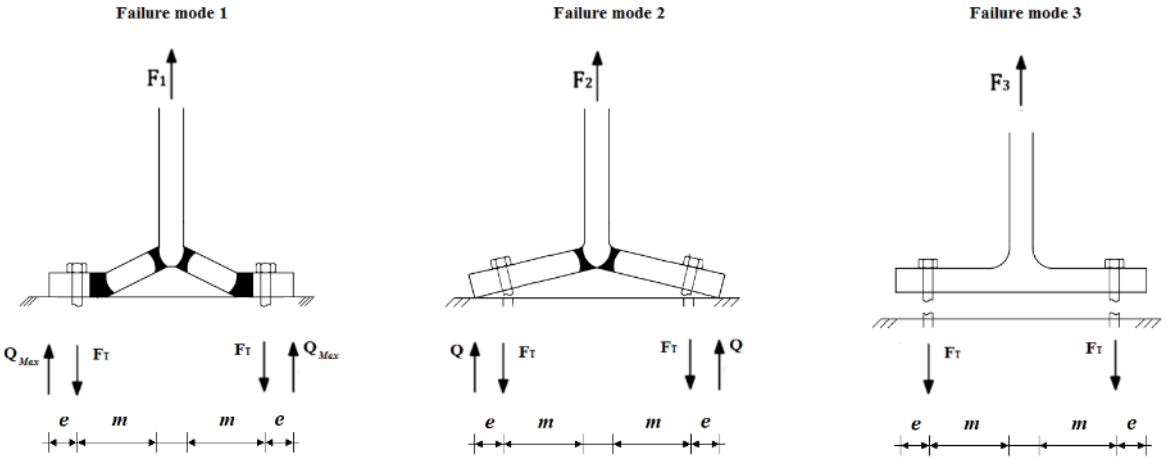

Fig. 3.5 Failure mechanisms according to Eurocode 3. F_T is the tension force in the bolt, Q is the internal prying force, e is the distance from the edge of the T-stub to the center of the bolt and m is the lever arm for the internal moment, which develops the plastic hinge $M_{pl,Rd}$. F_1, F_2 and F_3 correspond to the design tension resistance of different failure modes.

In Eurocode 3 [1], the resistance of the bolted T-stubs is based on the identification of the three possible failure mechanisms. These failure mechanisms are usually referred to, as type-1: *complete flange yielding*, as type-2: *simultaneous flange yielding and bolt fracture* and as type-3: *bolt fracture*. Such failure mechanisms are presented in Fig. 3.5. Lever arm m in Fig. 3.5 is calculated as follows

$$m = \frac{p - t_w}{2} - 0.8r \tag{3.1}$$

in which p is the horizontal distance between the bolts, t_w is the web thickness, r is the fillet radius and e is the distance from the edge of the T-stub to the center of the bolt. 0.8 is a factor provided in the standard, which determines that the plastic hinge is not formed right in the beginning of the fillet rounding, but instead it surges 20 % into the fillet. The dimension m has a significant contribution to the amplitude of the tension force in the bolts as can be seen in equations (3.2) and (3.3). As seen in Fig. 3.5, in mechanism type-1 the prying force Q at the ends of the span n reaches its maximum value and causes the plastic hinges to form at the bolt lines. [18]

According to Eurocode 3 [1], the tension resistance of the T-stub flange should be taken as the minimum of the following values

Type-1:

$$F_{T,1,Rd} = \frac{4M_{pl,1,Rd}}{m} \tag{3.2}$$

Type-2:

$$F_{T,2,Rd} = \frac{2M_{pl,1,Rd} + e\sum F_{t,Rd}}{m} \tag{3.3}$$

Type-3:

$$F_{T,3,Rd} = \sum F_{t,Rd} \tag{3.4}$$

in which $F_{t,Rd}$ is the design tension resistance of an individual bolt according to [1] and symbols m and e are as presented in Fig. 3.5. The bending resistance of the flanges is as follows

$$M_{pl,1,Rd} = \frac{0{,}25 b_{eff} t_f^2 f_y}{\gamma_{M0}}. \tag{3.5}$$

In the expression of the bending resistance of the flange, b_{eff} is the length of the corresponding yield line pattern, t_f is the flange thickness, f_y is the ultimate yield strength and γ_{M0} is the partial safety factor for the resistance of cross-section in tension to fracture according to Eurocode 3 [2].

In Eurocode 3 [1], there is also an alternative way of calculating the design resistance of the type-1 failure mode. This alternative method takes into account the effect of the bolt head, nut and washer with the following expression

$$F_{T,1,Rd} = \frac{(8n - 2e_w) M_{pl,1,Rd}}{2me - e_w(m + e)} \tag{3.6}$$

in which the defined factor $e_w = \frac{d_w}{4}$ and d_w is the washer diameter.

The design practice presented in Eurocode 3 is based on elastic and pure plastic theories presented in [19,21,22] and [18,23] respectively. In Fig. 3.6, the locations of the plastic hinges and internal moment diagrams can be seen in different failure mechanisms. Taking into account the internal moments and cross-sectional properties, it can be easily determined that the plastic hinges will form in the locations, where the internal moments are highest and the cross-sections weakest. From Fig. 3.6, it can also be seen, that in all failure mechanisms, the highest internal moment occurs right below the web. However, the cross-section of the flange is stronger under the web because of the support of the web and the fillets, so the plastic hinge will form right next to the fillet. The other location for the plastic hinge goes through the bolt line, which is weakened by the bolt holes.

From the practical point of view, it can be intuitively concluded that the type-1 failure mechanism usually occurs when the flange is relatively thin, whereas the type-3 occurs when thick flanges are bolted with relatively small bolts. The type-2 failure mechanism usually occurs when neither the strength of the flange nor the strength of the bolts is overcoming the other. For predicting the failure mechanism of the T-stub, a mathematical model has been proposed in [24]. The mathematical model is based on factor β_{Rd}, the ratio between the flexural strength of the flange and the axial strength of the bolts

$$\beta_{Rd} = \frac{4M_{pl,Rd}}{2F_{t,Rd} \cdot m} \tag{3.7}$$

and on the non-dimensional parameter λ

$$\lambda = \frac{e}{m} \tag{3.8}$$

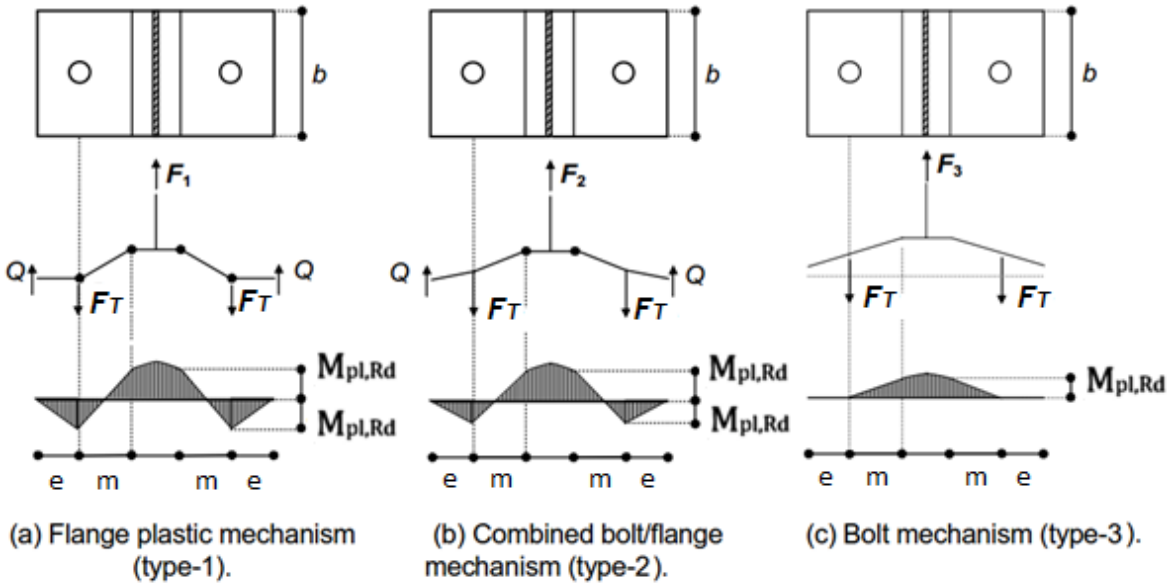

Fig. 3.6 Locations of the plastic hinges. Symbols are the same as in Fig. 3.5. [25]

in which n and m are as presented in Fig. 3.6. Using these ratios and the following conditions

Type-1: $$\beta_{Rd} \leq \frac{2\lambda}{1+2\lambda} \tag{3.9}$$

Type-2: $$\frac{2\lambda}{1+2\lambda} \leq \beta_{Rd} \leq 2 \tag{3.10}$$

Type-3: $$\beta_{Rd} > 2 \tag{3.11}$$

the failure mode of the equivalent T-stub can be predicted.

3.3 Analytical model of the T-stub

Analytical model of the T-stub can be used for predicting the initial stiffness and the ultimate strength of the T-stub in tension. The analytical model presented here has already been studied in [24,26,27] These analytical models are based on Eurocode 3 [1] and they utilize the spring component system. Building the analytical model is quite straight forward, but defining all spring components of the connection can be tedious. Due to the laborious design calculations, a parametric calculation sheet was formulated as part of this thesis. The basic theory of the analytical model is studied in this section, but the actual calculations and results are studied in section 4 as a comparative calculation method to numerical results. The idea is to study how accurate results an analytical model can reproduce compared to a finite element model.

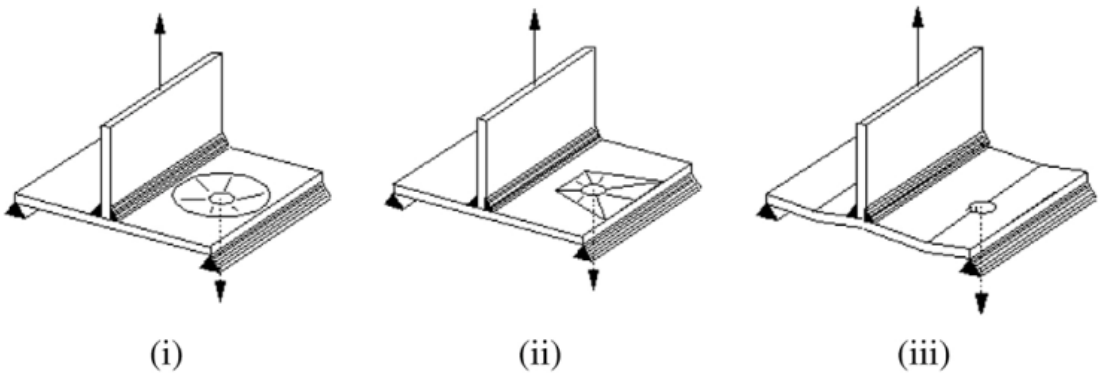

Fig. 3.7 Yield line patterns of a T-stub with two bolts per row: (i) circular pattern, (ii) non-circular pattern and (iii) beam pattern. [28]

3.3.1 Ultimate design resistance of the T-stub according to Eurocode 3

The design resistance of the T-stub can be calculated as presented in section 3.2.1 but in addition, one must also define the effective lengths of the yield lines. According to Eurocode 3 [1] three yield line patterns can arise: *circular pattern, non-circular pattern or beam pattern*. These yield lines of single bolt rows can be seen in Fig. 3.7.

Circular pattern forms due to the local deformations under bolt head and nut. Beam pattern usually occurs when the width of the T-stub is small and the T-stub is only a little affected by the three dimensional behavior. Non-circular pattern is conventional with wide T-stub flanges and with strong three dimensional behavior. [28] Strong 3D behavior usually occurs, for example, in the T-stubs which are close to beam flanges.

The expressions for the effective lengths of the yield lines according to Eurocode 3 [1] are the following

$$l_{eff,cp} = 2\pi m \tag{3.12}$$

$$l_{eff,nc} = 4m + 1.25e \tag{3.13}$$

$$l_{eff,bp} = b \tag{3.14}$$

The parameters m and e are defined as in Fig. 3.5 and b is the width of the T-stub flange. Indexes *cp*, *nc* and *bp* refer to circular pattern, non-circular pattern and beam pattern respectively.

Concerning the non-circular pattern, the model proposed in Eurocode 3 is a simplification of a more complex mechanism developed by Zoetemeijer [18]. Model by Zoetemeijer for type-1 failure mechanism, in which four plastic hinges develop is

$$l_{eff,1,nc} = 4m + 1.25e \tag{3.15}$$

and for type-2 failure mechanism, in which only two plastic hinges develop is

$$l_{eff,1,nc} = 5.5m + 4e \tag{3.16}$$

The advantage of the Eurocode simplification is that it always gives conservative results, so the design values are always on the safe side of the true design capacity.

According to Zoetemeijer [18], the study of the yield line models can be carried out by applying the principle of virtual work, in which the work done by the external load equals the work developed by the yield lines. Within this approach, the elastic deformations are neglected and rigid-plastic behavior is assumed [28].

In this case, employing the principle of virtual work basically means that the minimum energy required to develop a failure mechanism needs to be found. The minimum energy required for forming the failure mechanism can be calculated by determining the minimum moment resistance for the plastic hinge. According to the formula (3.5), $M_{pl,1,Rd}$ is proportional to the effective length. This means that the minimum collapse energy occurs with the shortest effective length of the yield line pattern.

3.3.2 Initial stiffness of the T-stub according to Eurocode 3

According to the component method in Eurocode 3 [1], the initial stiffness of the T-stub can be described as a linear spring system. The simple spring system of the T-element is composed of the axial stiffness due to the T-stub flange

$$K_f = E\frac{0{,}9 \cdot b_{eff} \cdot t_f^3}{m^3} \tag{3.17}$$

and due to the stiffness of two bolts per bolt row

$$K_b = E\frac{1{,}6 \cdot A_b}{L_b} \tag{3.18}$$

in which b_{eff}, t_f and m as already presented with equation (3.5) and A_b is the tension area of the bolt and the elongation length of the bolt is as follows

$$L_b = 2t_f + 2t_w + \left(\frac{t_{bh}+t_n}{2}\right). \tag{3.19}$$

The elongation length consists of the flange thickness t_f, the washer thickness t_w and the average value of the height of the bolt head t_{bh} and the height of the nut t_n.

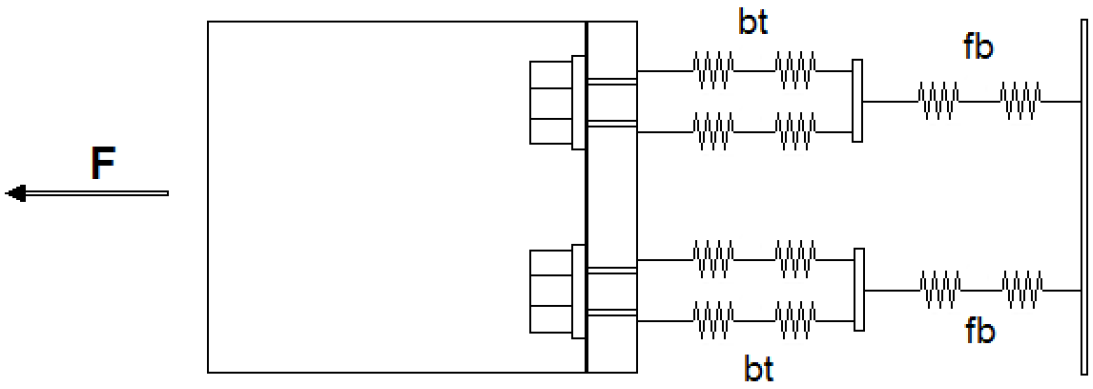

Fig. 3.8 The linear spring system of the equivalent T-stub with two bolt rows and two bolts per bolt row. *bt* indicates bolts in tension and *fb* the flange in bending. *F* is the external tension force.

The linear spring system is then formed as presented in Fig. 3.8. From the assembly in Fig. 3.8 it can be seen, that the bolts are assembled parallel with each other and then the equivalent stiffness of the T-stub flange for two bolt rows is attached in series. With this assembly, the initial stiffness of the T-stub with two bolt rows can be calculated as follows

$$K = \left(\frac{4}{K_f} + \frac{2}{K_b} \right)^{-1}. \tag{3.20}$$

Now since there are two bolt rows in parallel with two bolts in each row, the inverse of K_f is multiplied by four and the inverse of K_b is multiplied by two in the previous equation.

The analytical stiffness model proposed in Eurocode 3 [1], can be approximated by a force-displacement curve as shown in Fig. 3.9. In the approximation, the elastic range is limited to two thirds of the design plastic resistance of the T-stub. After the yielding point, since the Eurocode based model only governs the linear material models, the nonlinear behavior of the stiffness is accounted for with the factor

$$\mu = \left(\frac{F_{Ed}}{F_{Rd}} \right)^{\psi} \tag{3.21}$$

in which F_{Ed} is the acting tension force, F_{Rd} the design tension resistance and the factor $\psi = 2{,}7$ for bolted end-plates. For the nonlinear part of the force-displacement curve, the secant stiffness is calculated by dividing the initial stiffness by a factor μ as follows

$$K_j = \frac{K}{\mu}. \tag{3.22}$$

After the design tension resistance, the axial stiffness of the T-stub is assumed to be zero.

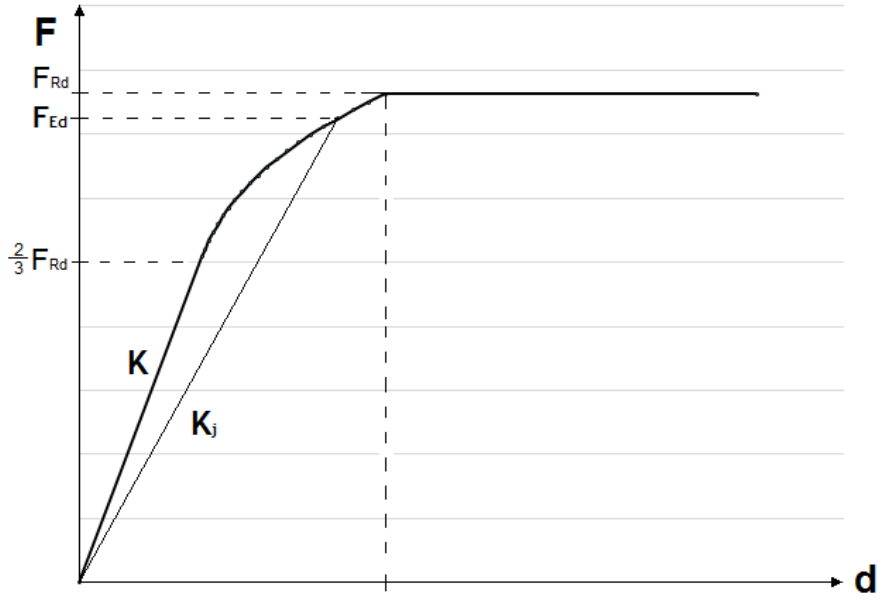

Fig. 3.9 Approximation of the force-displacement curve according to Eurocode 3 [1]. *F* represents the external tension force and *d* the corresponding displacement. F_{Rd} is the design tension resistance of the T-stub, F_{Ed} the acting tension force, *K* the initial stiffness as in (3.20) and K_j the secant stiffness as defined in equation (3.22).

A more accurate post-limit stiffness of the connection could be obtained as presented by da Silva et al. in [29]. This model is built by defining the post-limit stiffness for each basic component and then superposing them to form the post-limit stiffness of the whole joint. Although this method is more accurate, the complexity of the model makes it impossible to use in everyday design practices so the simplified Eurocode based model is generally preferred.

3.4 Basic components of an end-plate splice

In component method, it is essential to identify the individual components of the connection and to understand their behavior under proposed loading. When an end-plate connection is under combined bending and axial loading, the identification of the compression and tension components cannot be known in advance [30]. However, for pure bending, the identification of the tension and compression components is rather straightforward. The following subsections are presenting the active components used is the Eurocode based calculation sheet.

3.4.1 Tension components

The tension components of an end-plate splice consist of bolts in tension, end-plate bending and beam web in tension. The resistances for each basic tension component are given in Eurocode 3 [1] and the following procedure follows these design rules. The tension components of an end-plate splice are presented in Fig. 3.10.

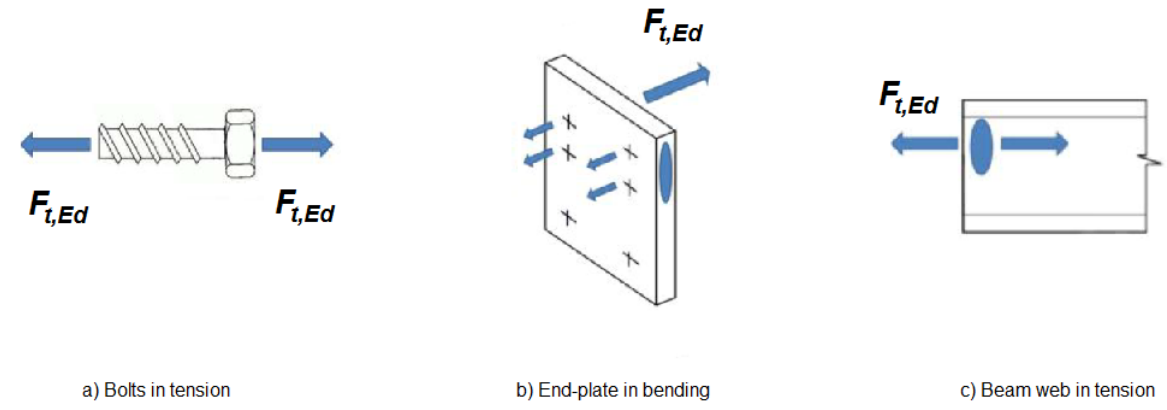

Fig. 3.10 Tension components of an end-plate splice according to [1].

Bolts in tension

The design resistance for the individual bolts subjected to tension should be taken according to [1] as follows

$$F_{t,Rd} = \frac{k_2 f_{ub} A_s}{\gamma_{M2}} \tag{3.23}$$

in which k_2 is the factor which takes into account the type of the bolt, f_{ub} is the ultimate tensile strength of the bolt, A_s is the tensile stress area of the bolt and γ_{M2} is the partial safety factor for the resistance of cross-section in tension to fracture [2]. In Eurocode based approach, bolts are always modeled as tension only springs, so if some bolts are located in the compression area of the joint, they are left idle in the calculation model.

End-plate in bending

The design resistance of an end-plate should be taken as similar to that of an equivalent T-stub flange. Due to the geometry of the connection, some three dimensional behavior occurs when the end-plates are subject to bending. To take into account the 3D behavior, the Eurocode based approach defines a method how to consider all of the equivalent T-stubs of the connections individually or as part of a group. This can be done by finding the minimum effective length of the yield lines for an individual bolt row under tension or for an individual group of bolt rows under tension. [1] This is exactly the same procedure as defined in [18], so the idea is to determine whether the collapse energy is obtained locally for an individual bolt row or globally for a group of bolt rows. The dimensions required for the equivalent T-stub calculations in case of a welded end-plate are presented in Fig. 3.11.

With welded end-plates, instead of considering the rounding radius of the fillet, the width a is the a-dimension of the fillet weld. Although the vertical spacing of the bolts can vary as presented in Fig. 3.11, in all of the example cases considered in this thesis, the bolts are equally distributed in horizontal and vertical direction.

Table 3.1 shows how the effective lengths are calculated for both circular and non-circular yield mechanisms, when an individual bolt row is considered. In Table 3.2, the same yield

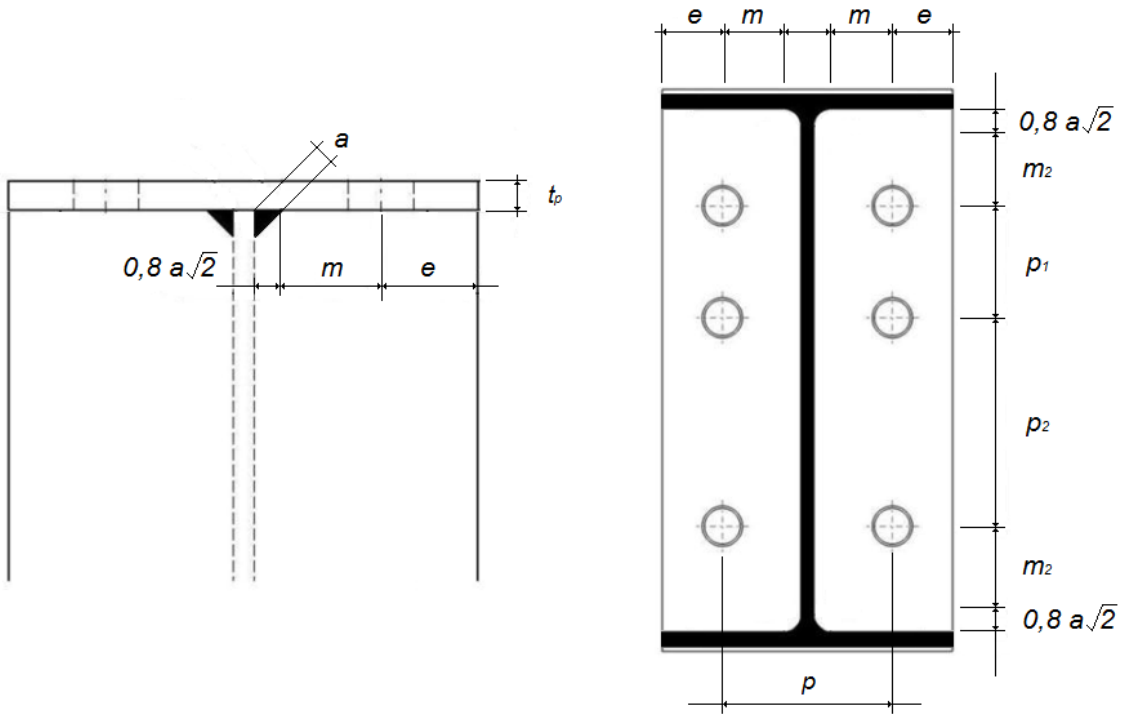

Fig. 3.11 Dimensions of an equivalent T-stub in case of an end-plate under bending. *m* and *e* are measured as in Fig. 3.5, *a* is the width of the fillet weld, m_2 is similar compared to *m*, but m_2 is in vertical direction, p_1 is the distance between bolt rows 1 and 2 and p_2 is the distance between bolt rows 2 and 3.

mechanisms can be seen for an individual group of bolts rows. In Table 3.1 and Table 3.2, the yield line factors α_1 and α_2 appear for the bolt row adjacent to the beam flanges. To obtain these factors one needs to assess the following factors:

$$\lambda_1 = \frac{m}{m+e} \tag{3.24}$$

$$\lambda_2 = \frac{m_2}{m+e} \tag{3.25}$$

in which the dimensions *m*, *e* and m_2 are as presented Fig. 3.11. After finding the values for λ_1 and λ_2, they can be used to graphically obtain the values for α_1 and α_2 from Eurocode 3 [1].

Using Table 3.1 and Table 3.2, the minimum effective lengths of each bolt row can be found. The comparison must be done first for the circular patterns of individual bolt rows and the same patterns of the group of bolt rows and secondly for the non-circular patterns of individual bolt rows and the same patterns of the group of bolt rows.

Table 3.1 Circular and non-circular yield line patterns when each bolt row is considered individually. Symbols e, m and m_2 are taken as presented in Fig. 3.5.

Circular patterns		
Bolt row 1	**Bolt row 2**	**Bolt Row 3**
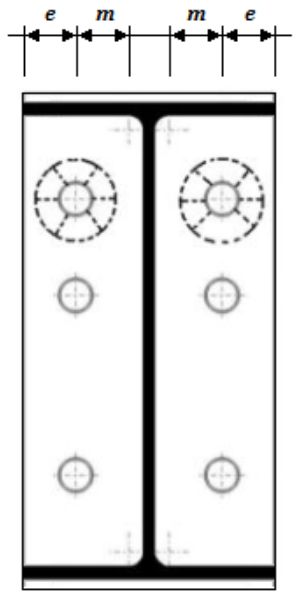	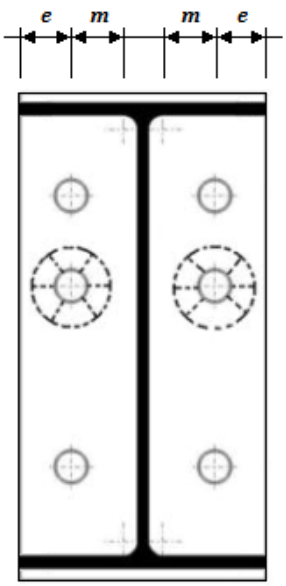	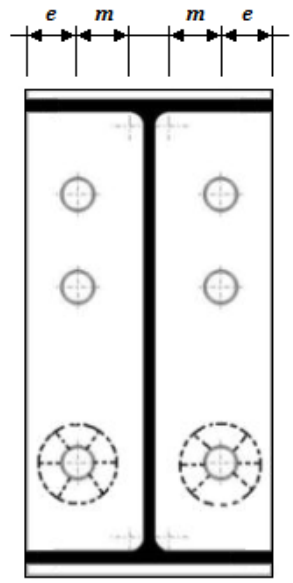
$l_{eff,cp} = 2\pi m$	$l_{eff,cp} = 2\pi m$	$l_{eff,cp} = 2\pi m$
Non-circular patterns		
Bolt row 1	**Bolt row 2**	**Bolt Row 3**
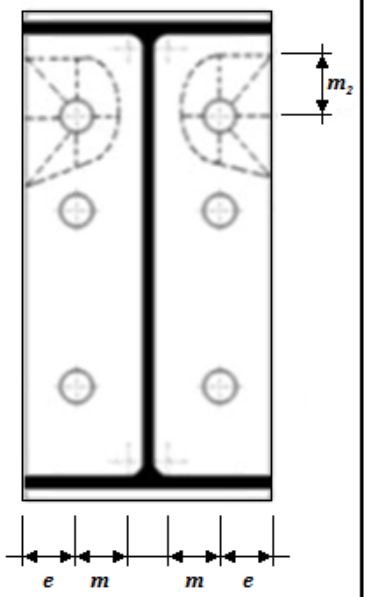	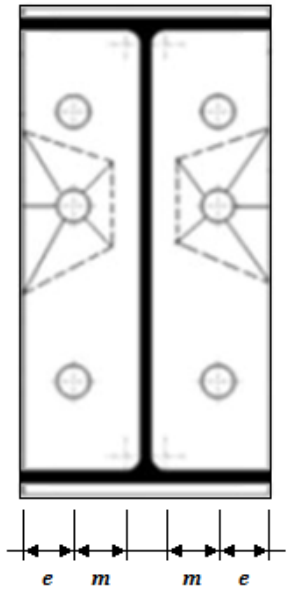	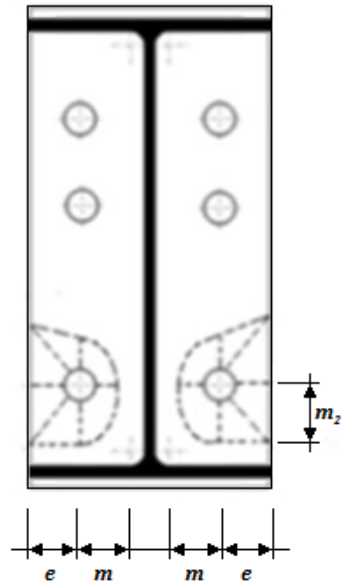
$l_{eff,nc} = \alpha_1 m$	$l_{eff,nc} = 4m + 1.25e$	$l_{eff,nc} = 4m + 1.25e$

Table 3.2 Circular and non-circular yield line patterns when an individual group of bolt rows is considered. Symbols *e*, *m* and m_2 are taken as presented in Fig. 3.5.

<table>
<tr><th colspan="3">Circular patterns</th></tr>
<tr><th>Group 1+2</th><th>Group 2+3</th><th>Group 1+2+3</th></tr>
<tr>
<td> 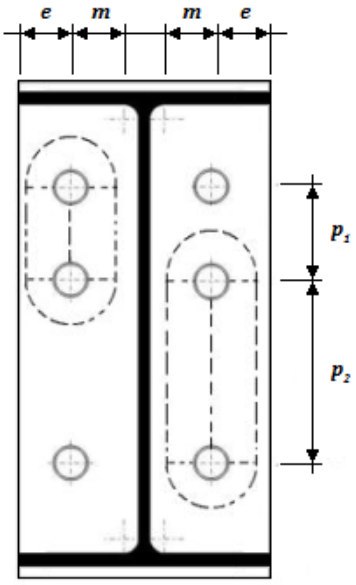

$l_{eff,cp} = \pi m + p_1 + 2p_1$</td>
<td>

$l_{eff,cp} = 2p_2 + \pi m + p_2$</td>
<td> 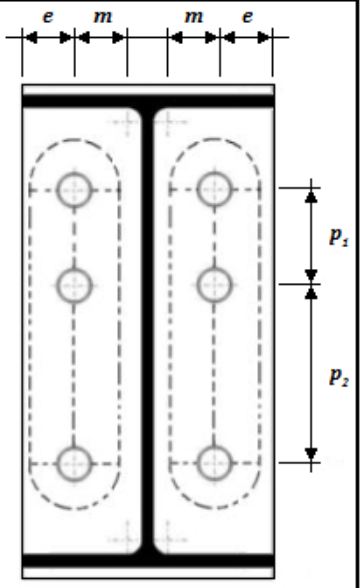

$l_{eff,cp} = (\pi m + p_1) + (p_1 + p_2) + (\pi m + p_2)$</td>
</tr>
<tr><th colspan="3">Non-circular patterns</th></tr>
<tr><th>Group 1+2</th><th>Group 2+3</th><th>Group 1+2+3</th></tr>
<tr>
<td> 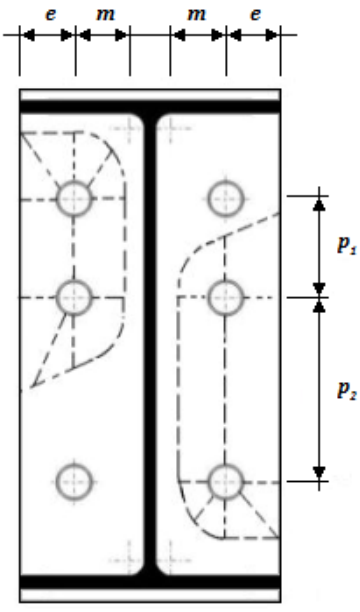

$l_{eff,nc} = 0.5p_1 + \alpha_1 m - (2m + 0.625e) + p_1$</td>
<td>

$l_{eff,nc} = p_2 + 2m + 0.625e + 0.5p_2$</td>
<td> 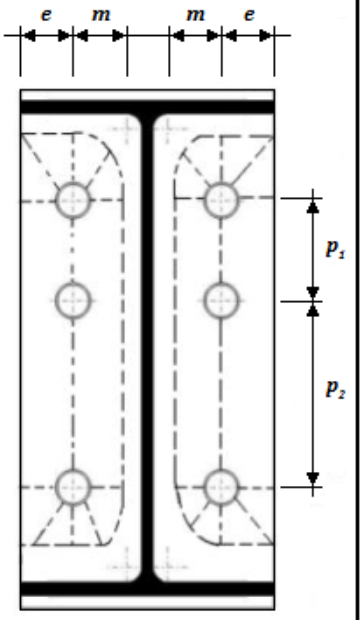

$l_{eff,nc} = 0.5p_1 + \alpha_1 m - (2m + 0.625e) + p_2 + 2m + 0.625e + 0.5p_1$</td>
</tr>
</table>

After finding the minimum values, the effective lengths for the equivalent T-stub of the end-plate for different failure mechanisms for individual bolt rows are the following:

Failure mechanism type-1 for individual bolt row

$$l_{eff,1} = l_{eff,nc} \quad \text{but} \quad l_{eff,1} \leq l_{eff,cp} \tag{3.26}$$

Failure mechanism type-2 for individual bolt row

$$l_{eff,2} = l_{eff,nc} \tag{3.27}$$

For individual groups of bolts rows, the effective lengths for different failure mechanisms can be obtained similarly, except that now they are considered as the sum of individual lengths:

Failure mechanism type-1 for individual group of bolt rows

$$\sum l_{eff,1} = \sum l_{eff,nc} \quad \text{but} \quad \sum l_{eff,1} \leq \sum l_{eff,cp} \tag{3.28}$$

Failure mechanism type-2 for individual group of bolt rows

$$\sum l_{eff,2} = \sum l_{eff,nc}\,. \tag{3.29}$$

The plastic moment resistance for particular failure mechanism is obtained as in equation (3.5) but now the T-stub parameters are replaced by the end-plate values as follows

$$M_{pl,i,Rd} = \frac{0{,}25 l_{eff,i} t_p^2 f_y}{\gamma_{M0}} \tag{3.30}$$

in which $l_{eff,i}$ is the effective length for the failure mode i, t_p is the thickness of the end-plate, f_y is the yield strength of the end-plate and γ_{M0} is partial safety factor for resistance of cross-section according to [2]. The design tension resistance $F_{T,Rd}$ is then determined for each failure mode by following expressions (3.2) - (3.4).

With joints consisting of relatively thick end-plates, an additional reduction factor may have to be taken into account when determining the design tension resistance of an individual bolt row. The additional reduction factor needs to be taken into account when the effective design tension resistance $F_{tx,Rd}$ of one of the previous bolt rows x is greater than $1{,}9F_{t,Rd}$. When the additional reduction factor is considered, the effective design tension resistance $F_{tr,Rd}$ for bolt row r should be reduced in order to ensure that

$$F_{tr,Rd} \leq F_{tx,Rd} \frac{h_r}{h_x} \tag{3.31}$$

in which h_r is the distance from bolt row r to the center of compression and h_x is the distance from bolt row x to the center of compression.

Beam web in tension
The design tension resistance of the beam web should be obtained as presented in the following equation

$$F_{T,wb,Rd} = \frac{b_{eff,t,wb} t_{wb} f_{y,wb}}{\gamma_{M0}} \tag{3.32}$$

where $b_{eff,t,wb}$ should be taken as equal to the effective length of equivalent T-stub representing the end-plate under bending, t_{wb} as the beam web thickness, $f_{y,wb}$ as the beam web yield strength and γ_{M0} as the partial safety factor for resistance of the cross-section.

3.4.2 Compression components

An end-plate splice has only one compression component: beam flange and web in compression. The resultant of the design compression resistance of a beam flange and the adjacent compression zone of the beam web may be assumed to act at the center of the compression flange. This is a simplification proposed in [1]. An end-plate splice under bending and the location of the compression center is shown in Fig. 3.12.

The design compression resistance of the combined beam flange and web is given by the following expression

$$F_{c,fb,Rd} = \frac{M_{c,Rd}}{h - t_{fb}} \tag{3.33}$$

in which h is the height of the beam, t_{fb} is the flange thickness of the connected beam and $M_{c,Rd}$ is the design moment resistance of the beam cross-section according to [2]. The design moment resistance can be calculated as follows:

$$M_{c,Rd} = M_{pl,Rd} = \frac{W_{pl} f_{yb}}{\gamma_{M0}} \tag{3.34}$$

in which W_{pl} is the plastic section modulus of the cross-section, f_{yb} is the yield strength of the beam and γ_{M0} is the partial safety factor for resistance of cross-section.

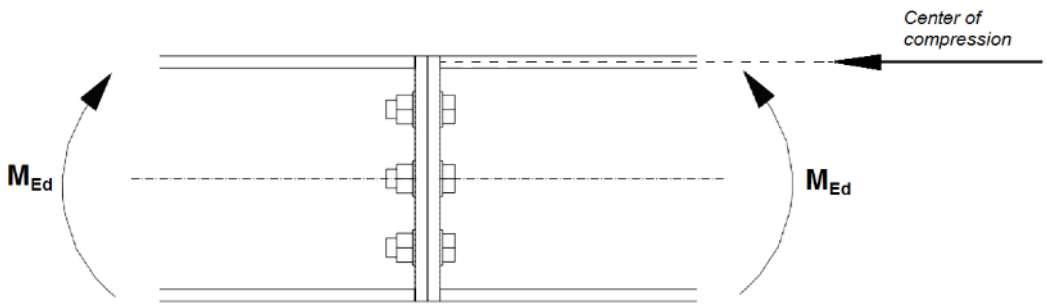

Fig. 3.12 Compression center of an end-plate splice under bending. $M_{j,Ed}$ is the design bending moment.

3.5 Assembly of the basic components and the design moment resistance

The failure mechanism of the joint will be controlled by the weakest component of the system. On each bolt row, the failure can be reached with a different magnitude of resistance and with a different failure mechanism. In the parametric study, which will be presented in section 5, the limiting components are always the tension components of the joints. In this section, the assembly of the components is presented for in-plane and out-of-plane bending and the presented assembly is then used in the formulation of the Eurocode based calculation sheet conducted as part of this thesis.

3.5.1 Design moment resistance for in-plane bending

The design moment resistance of an end-plate splice for in-plane bending can be calculated using the expression from Eurocode 3 [1]

$$M_{j,Rd} = \sum_{r} h_r F_{tr,Rd} \tag{3.35}$$

where $F_{tr,Rd}$ is the effective design tension resistance of bolt row r taking into account the equivalent T-stub, h_r is the distance from bolt row r to the center of compression and r is the bolt row number starting from the bolt row farthest from the compression center.

The effective design tension resistance $F_{tr,Rd}$ for each bolt row needs to be determined in sequence, starting from bolt row 1 and then progressing towards the center of compression. When determining the design tension resistance $F_{tr,Rd}$ for bolt row r, the effective design tension resistance of all other bolt rows closer to the center of compression should be ignored. The detailed procedure for determining the effective design tension resistance for each bolt row and the details on how to do the possible reductions depending on the failure mechanism are presented in [1].

3.5.2 Design moment resistance for out-of-plane bending

The Eurocode 3 [1] only proposes guidance for planar joints, so the design moment resistance for out-of-plane bending is excluded from the standard. However, some research about the out-of-plane bending of a beam-to-column end-plate connection has been concluded in [7,8] and it was found in the parametric finite element study that for out-of-plane bending, similar tension and compression components exist. The only difference is that the formulation of some yield line patterns need to be modified.

Some research has also been done on the extension of the component method into three dimensional behavior. A proposal for the extension has been concluded by Heinisuo et al. in [31]. In their study it was proposed that although component method is rather generic, it can be applied to the three dimensional cases by logically using the basic components that are active in out-of-plane bending. Heinisuo et al. present a method for applying the component method to a base plate joint. A similar method is used here, first by defining the active tension and compression components and then by applying the Eurocode based principles on the component method. In Fig. 3.13, these basic components are presented in different load cases.

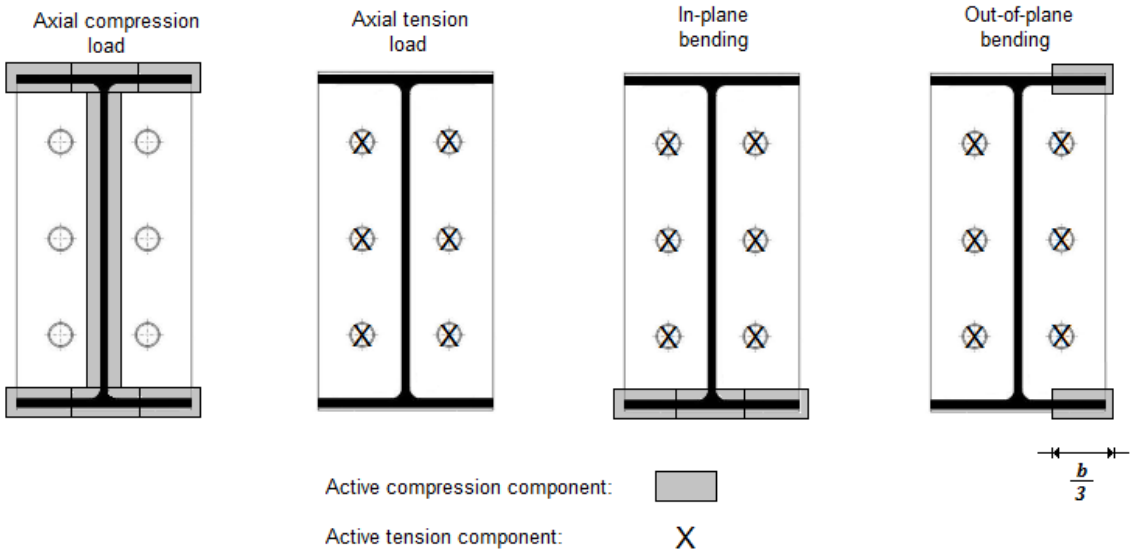

Fig. 3.13 The basic components that are active in different loading cases. *b* is the width of the beam flange.

As it can be seen in Fig. 3.13, in pure out-of-plane bending it is certain that at least the bolts on the left hand side are in tension, but depending on the horizontal location of the bolts and on the stiffness of the connected member, it may become challenging to determine whether the right hand side bolts are in tension. Here an analytical method is proposed for a case in which all bolts are in tension and one third of the flanges is considered to be in compression.

End-plate in bending

Here for the end-plate bending, it is assumed that the yield lines given in [1] do apply and in this case the possible yield line patterns are: (i) circular pattern for an individual bolt row, (ii) non-circular pattern for an individual bolt row, (iii) circular pattern for a group of bolt rows and (iv) non-circular pattern for a group of bolt rows. Although the yield mechanisms are similar in out-of-plane bending and in in-plane bending, it has to be taken into account that the Eurocode based formulas are assuming two bolts per bolt row. In out-of-plane bending, there is only one bolt active on each bolt row in each case considered. This means that the design tension resistance for an equivalent T-stub has to be divided by two to take into account only one vertical bolt row at a time.

In Table 3.3, the yield line patterns are shown for individual bolt rows and in Table 3.4 the yield line patterns are shown for groups of bolt rows. Now a similar procedure as with in-plane bending needs to be followed, so the critical yield lines are searched by going through all bolt rows in sequence. The case studies in section 4 and 5 show that the probable yield line patterns are: (i) each bolt row individually or because of the equally distributed vertical spacing of the bolts, (ii) as a group of three bolt rows as shown in Table 3.4. If necessary, as well as in in-plane bending, also with out-of-plane bending, the additional reduction factor is similarly accounted for as presented in subsection 3.4.1.

Table 3.3 Circular and non-circular yield line patterns for individual bolt rows in out-of-plane bending. Symbols e, m and m_2 are taken as presented in Fig. 3.5.

Circular patterns		
Bolt row 1	**Bolt row 2**	**Bolt Row 3**
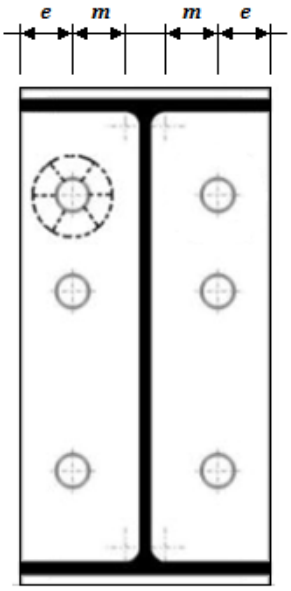 $l_{eff,cp} = 2\pi m$	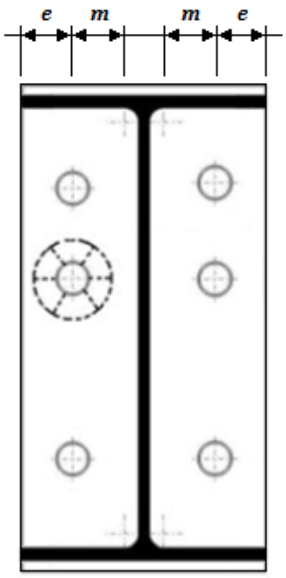 $l_{eff,cp} = 2\pi m$	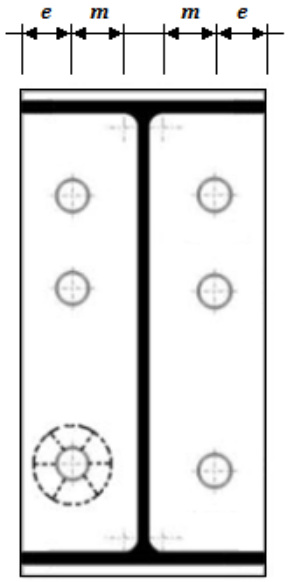 $l_{eff,cp} = 2\pi m$
Non-circular patterns		
Bolt row 1	**Bolt row 2**	**Bolt Row 3**
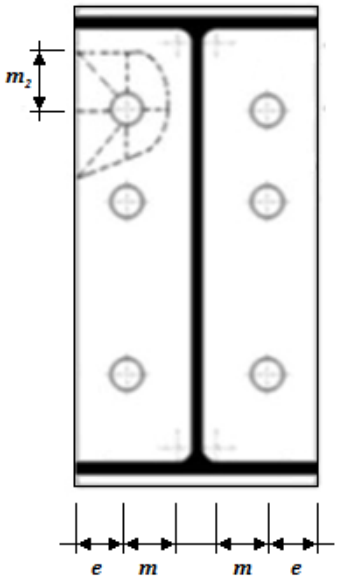 $l_{eff,nc} = 4m + 1.25e$	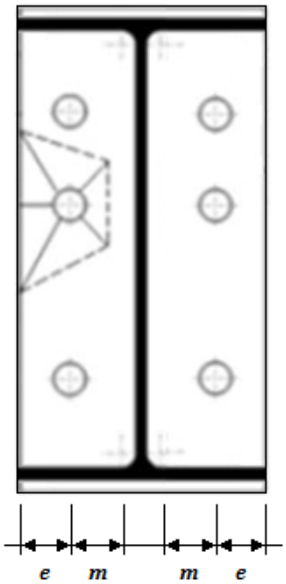 $l_{eff,nc} = 4m + 1.25e$	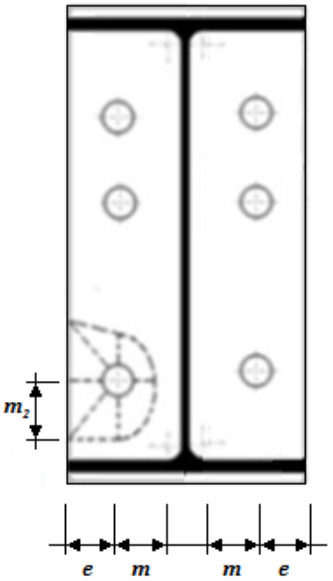 $l_{eff,nc} = 4m + 1.25e$

Table 3.4 Circular and non-circular yield line patterns for groups of bolt rows in out-of-plane bending. Symbols e, m and m_2 are taken as presented in Fig. 3.5.

Circular patterns		
Group 1+2	**Group 2+3**	**Group 1+2+3**
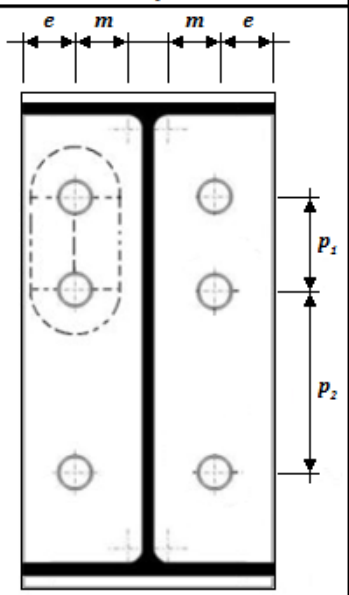	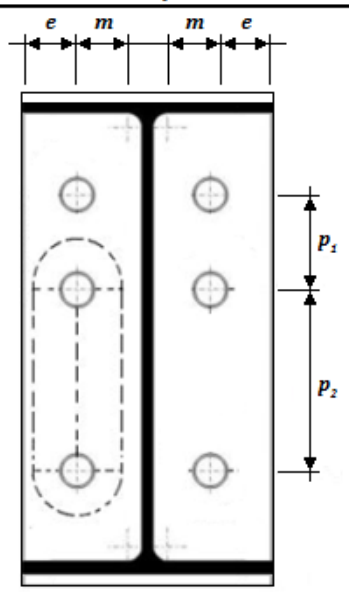	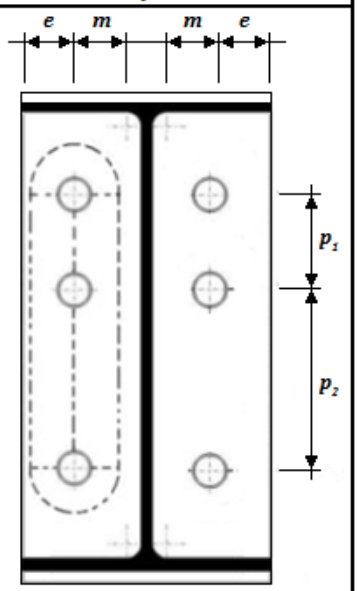
$l_{eff,cp} = \pi m + p_1 + 2p_1$	$l_{eff,cp} = 2p_2 + \pi m + p_2$	$l_{eff,cp} = \pi m + p_1 + 2p_2 + \pi m + p_2$
Non-circular patterns		
Group 1+2	**Group 2+3**	**Group 1+2+3**
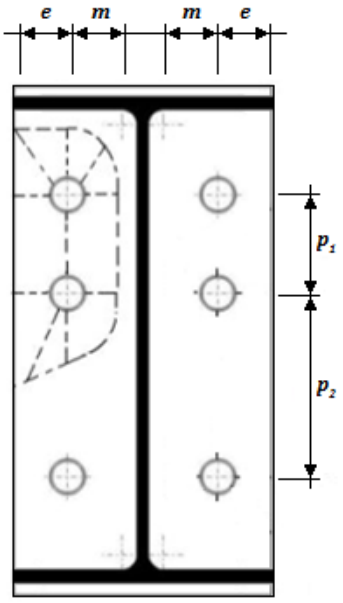	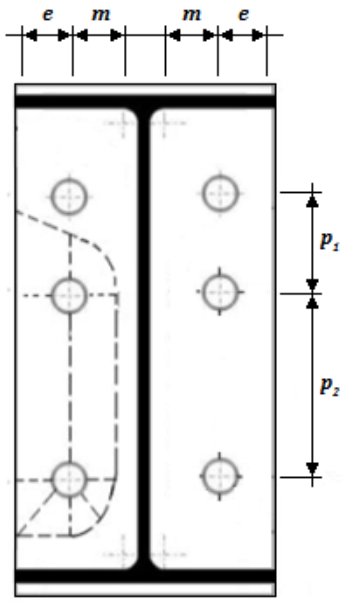	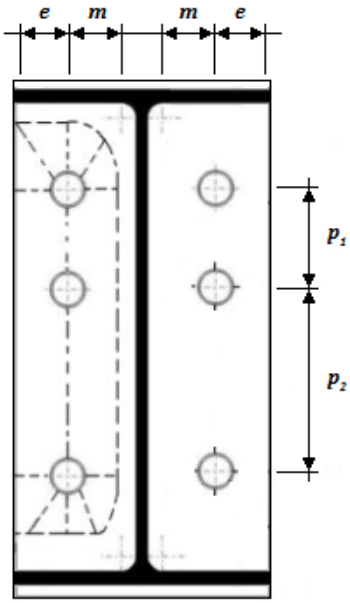
$l_{eff,nc} = 2m + 0.625e + 0.5p_1 + p_1$	$l_{eff,nc} = p_2 + 2m + 0.625e + 0.5p_2$	$l_{eff,nc} = 2m + 0.625e + 0.5p_1 + p_1$ $2m + 0.625e + 0.5p_2$

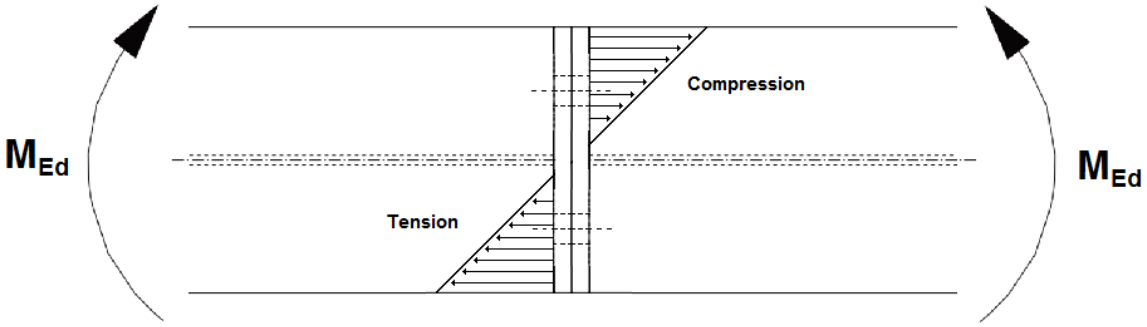

Fig. 3.14 Stress distribution in out-of-plane bending. M_{Ed} is the design bending moment.

Compression components
The compression component is assumed to be one third of the beam flange width as shown in Fig. 3.13. The force resultant of the compression is located in the middle of this compression area [31]. This is obviously a simplification, since as shown in Fig. 3.14, the stress distribution in the beam cross section is linear and the maximum compression stress is at the end of the beam flanges.

Even though the compression force resultant and its location is only an approximation, it can be taken as accurate enough in these cases, since the compression component is hardly ever the limiting component in end-plate splices. The compression force resultant can be expressed as follows

$$F_{c,Rd} = f_y A_f \tag{3.36}$$

in which f_y is the yield strength of the flange and A_f is the area of the compression zone.

3.6 Rotational stiffness of an end-plate splice

The rotational stiffness of an end-plate splice is usually represented as a rotational spring. In Eurocode 3 [1], this rotational spring S_j is the secant stiffness as indicated in Fig. 3.15 (c). For a design moment-rotation characteristic, the definition of S_j applies up to the rotation ϕ_{Xd}, at which $M_{j,Ed}$ first reaches $M_{j,Rd}$, the design moment resistance of the joint. The design rotation capacity, which is the maximum rotation of the design moment characteristic is the limit ϕ_{Cd} in Fig. 3.15 (c). Problem with the Eurocode 3 is that it does not give any design rules on how to determine the maximum rotation capacity for an end-plate connection.

The initial rotational stiffness $S_{j,ini}$ corresponds to the elastic range of the moment-rotation characteristics and it should be taken as presented in the following expression

$$S_{j,ini} = \frac{E z_{eq}^2}{\sum_i \frac{1}{k_i}} \tag{3.37}$$

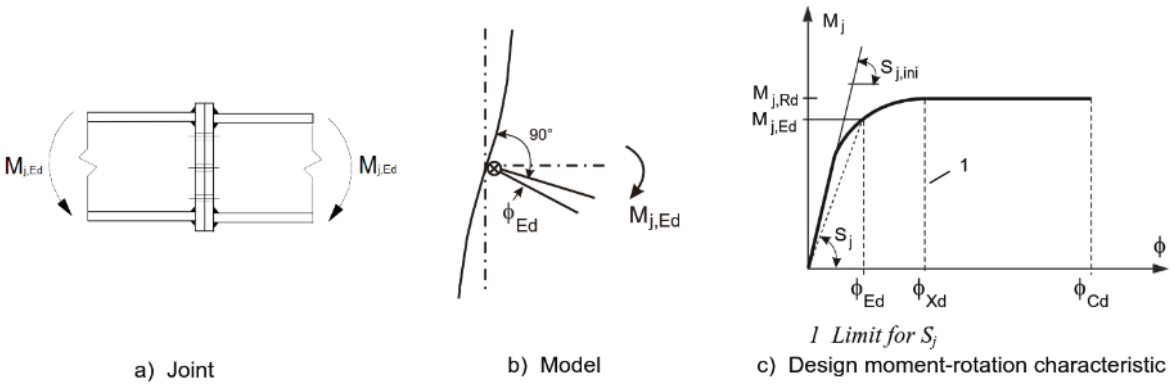

Fig. 3.15 Design moment-rotation characteristics for an end-plate splice according to [1]. $M_{j,Ed}$ is the design bending moment, $M_{j,Rd}$ the design moment resistance, $S_{j,ini}$ the initial rotational stiffness in elastic range and S_j the secant stiffness. ϕ_{Xd} corresponds to the rotation angle at design moment resistance and ϕ_{Cd} to the maximum rotation angle.

in which k_i is the stiffness coefficient for basic joint component *i* and z_{eq} is the lever arm of the basic joint component *i*. The elastic range of the stiffness is considered to reach until two thirds of the design moment resistance.

After the yielding point, the secant stiffness S_j can be calculated by using the initial rotational stiffness and the stiffness ratio μ as presented in the following expression

$$S_j = \frac{S_{j,ini}}{\mu}. \tag{3.38}$$

The stiffness ratio μ should be determined from the following expressions. If the design moment $M_{j,Ed} \leq \frac{2}{3} M_{j,Rd}$ then

$$\mu = 1.0 \tag{3.39}$$

or if $\frac{2}{3} M_{j,Rd} \leq M_{j,Ed} \leq M_{j,Rd}$ then the stiffness ratio μ takes the following form

$$\mu = \left(\frac{1{,}5 M_{j,Ed}}{M_{j,Rd}} \right)^{\Psi} \tag{3.40}$$

in which the coefficient $\Psi = 2{,}7$ in case of bolted end-plate connections. [1]

3.6.1 Spring components of the splice

The design moment-rotation characteristics of an end-plate joint depend on the properties of its basic components. In the case of an end-plate splice, the spring stiffness model only consists of the stiffness of the bolts in tension and the end-plate in bending.

According to Eurocode 3 [1], the stiffness of the end-plate in bending can be expressed with the following expression

$$k_5 = \frac{0.9\, l_{eff} t_p^3}{m^3} \tag{3.41}$$

in which l_{eff} is the smallest of the effective lengths obtained for the particular bolt row, t_p is the end-plate thickness and m should be taken as defined in Fig. 3.11.

The stiffness of the bolts for a single bolt row with two bolts should be taken as

$$k_{10} = \frac{1.6\, A_s}{L_b} \tag{3.42}$$

where A_s is the tensile area of the bolt and L_b is the elongation length of the bolt.

3.6.2 Rotational stiffness in in-plane bending

Eurocode 3 [1] presents a general method for obtaining the rotational stiffness of a bolted end-plate splice. The principle idea is to sum up all the spring components and to take into account the equivalent lever arm of each component. First of all, the effective stiffness coefficient $k_{eff,r}$ for bolt row *r* should be determined as follows

$$k_{eff,r} = \frac{1}{\sum_i \frac{1}{k_{i,r}}} \tag{3.43}$$

in which $k_{i,r}$ is the stiffness coefficient representing the component *i* of the bolt row *r*.

The effective stiffness coefficient $k_{eff,r}$ of each basic spring component can then be implemented into the formula of the equivalent stiffness coefficient k_{eq}. The idea is that all of the individual stiffness coefficient are represented by a single equivalent stiffness coefficient

$$k_{eq} = \frac{\sum_r k_{eff,r}\, h_r}{z_{eq}} \tag{3.44}$$

where $k_{eff,r}$ is the effective stiffness coefficient for bolt row *r* taking into account the stiffness coefficient $k_{i,r}$ of the basic component, h_r is the distance between bolt row *r* and the compression center and z_{eq} is the equivalent lever arm. The equivalent lever arm z_{eq} is determined by the following expression

$$z_{eq} = \frac{\sum_r k_{eff,r}\, h_r^2}{\sum_r k_{eff,r}\, h_r} \tag{3.45}$$

Following the above mentioned procedure, the equivalent lever arm z_{eq} can be determined and then, to obtain the initial rotational stiffness for an end-plate splice, it can be implemented into equation (3.37).

3.6.3 Rotational stiffness in out-of-plane bending

The Eurocode 3 [1] does not provide step-by-step instructions on how to calculate the rotational stiffness in out-of-plane bending. However, as in ultimate bending resistance calculations, the rotational stiffness in out-of-plane bending can be calculated by logically applying the main principles presented in the standard.

Considered that the yield line patterns can be calculated as presented in section 3.5.2, the calculation procedure of the rotational stiffness in out-of-plane bending follows exactly the same routine as described in the previous section. Here, as well as in in-plane bending, the spring components only govern the stiffness of the bolts and the end-plate in bending. The lever arms of each component are determined as the distance between the spring component and the compression force resultant.

3.7 Eurocode based calculation sheet

A Eurocode based calculation sheet is deducted as part of this thesis. The spreadsheet program is based on the Eurocode 3 [1] principles presented in section 3 and it is used to calculate analytically the resistance and the initial stiffness of an individual T-stub and the same characteristics for a flush end-plate splice both in in-plane and in out-of-plane bending. The analytical calculation program only consists of cases with pure bending and with non-preloaded bolts. This limitation is due to the fact that Eurocode 3 does not provide standardized design rules on how to determine the resistance and initial stiffness of joints in case of combined bending and axial loading and in case of preloaded bolts.

Example of an output print of the calculations of an individual T-stub are presented in Appendix 2. The example is performed for a T-stub specimen found in the literature [32,33]. The same T-stub specimen will also be used in the validation of the techniques for finite element modelling in section 4.1.

An output print of the analytical end-plate calculations for a flush end-plate splice are presented in Appendix 3 for in-plane bending and in Appendix 4 for out-of-plane bending. The example analysis presented in the appendices is based on one example joint geometry. In the output print it can be seen that, as presented in subsection 3.4.1, the calculation sheet is programmed to go through all possible failure modes with all possible yield line patterns and then to find the minimum resistance for the external load. The rotational stiffness is calculated as an equivalent rotational spring, consisting of the individual tension components assembled together as presented in subsection 3.6.

4 Finite element modelling

This section is divided into two separate parts: the validation of the chosen finite element methods and the formulation of a full size model of an end-plate splice. In subsection 4.1, the suitable finite element modelling techniques are studied with a simple T-stub specimen, which sufficiently represents the basic issues and phenomena that typically occur with bolted steel joints. The FE model is then validated against the experimental results found in the literature [32,33]. After finding an appropriate approach for finite element modelling of a steel joint, the same techniques are used to develop a finite element model of a full size end-plate splice. The full size FE model will then be used in the parametric study. The FE model of an end-plate splice, the parametric study and the measured variables are presented in sub-sections 4.2-4.4.

4.1 Validation of the finite element model

The finite element techniques of the full size end-plate splice are validated against the experimental results from the tests executed by Bursi and Jaspart [32,33]. The test specimen is presented in Fig. 4.1. The experimental program was done on a T-stub specimen and it has been widely used in research and in validation of finite element modelling of bolted steel connections [24,34]. This experiment is suitable for validation, since the geometry and the material properties, as well as the loading conditions, have been profoundly documented. A simple T-stub is basically a section of the full end-plate splice and that makes it very useful for the validation of the chosen finite element modelling techniques and properties.

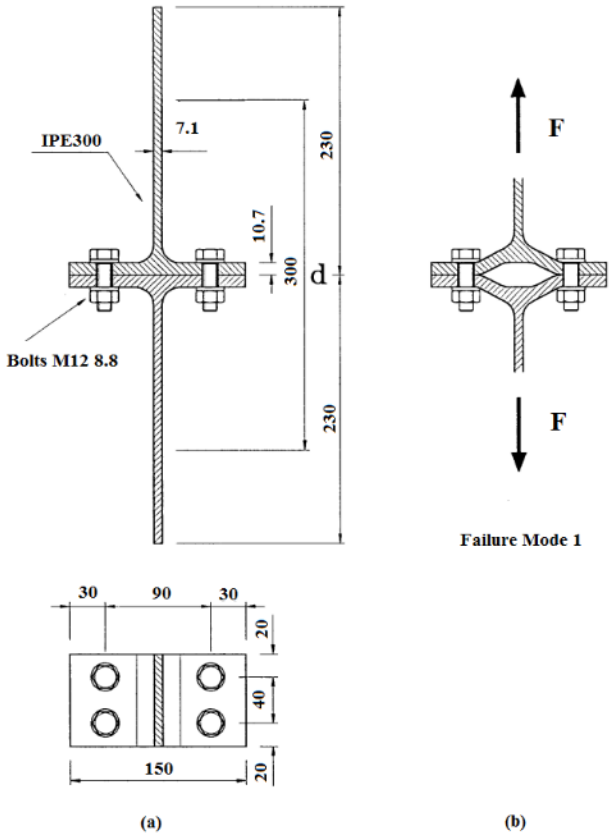

Fig. 4.1 Geometrical properties of the test specimen. [33]

4.1.1 Set up of validation specimen

The experiment [32,33] was executed on a T-stub in which two T-shaped profiles are bolted from the flanges. The T-stub specimen is presented in Fig. 4.1. Originally the experiment was executed using multiple specimens with varying parameters, but for the purposes of this study, only one configuration was chosen. The basic information about the modeled specimen is gathered in Appendix 5. The specimen used for validation consists of two sliced IPE300 profiles, which are bolted using partially-threaded 4 x M12 8.8 bolts.

Strength class 8.8 means that the manufacturer guarantees a yield strength of $f_y = 640\ MPa$ and an ultimate strength of $f_u = 800\ MPa$. However, in [33] the true material properties of bolts, flanges and webs were presented, so to get fully comparative results, the experimental material data needs to be used in the validation model.

For simplicity and to reduce the number of contact surfaces, a double symmetry was used. This means that only one quarter of the specimen is modeled. Using double symmetry significantly reduces the size of the model and makes it easier to vary the model settings and to search for the best practices for the modelling of the bolted end-plate connection. When only one quarter of the specimen is modeled, the total tension force needs to be divided by four.

To reduce the size of the model even more, it would be possible to add a third symmetry plane between the flanges. This way, only one eight of the T-stub specimen would be modeled. This type of three-symmetric modelling is easily justified because of its simplicity, but due to the non-symmetric geometry of the partially-threaded bolts, the behavior of the T-stub is non-symmetric in vertical direction. To account for the non-symmetric geometry of the bolts, a so called Agerskov's expression could be used [35]. Agerskov's expression takes into account the effective length of the threaded bolt shank, so in practice the bolt shank is modeled using only the diameter of the threaded section and the length of the bolt is defined by Agerskov's expression. Without the effective length of the bolt shank, the bolts would be modeled too flexible and the deformations would become much larger than in reality.

Even though additional simplicity could be achieved by using three symmetry planes, the double symmetric design was decided to be used in the T-stub validation. This way, the suitable design practices can be tested with the T-stub model and then applied to the full size end-plate splice model. The design moment resistance and the rotational stiffness of the end-plate splice could be simulated by using the additional symmetry condition between the end-plates and the effective length of the bolts, but by modelling whole bolts and both sides of the connection, the real behavior of the components of the end-plate splice can be more easily seen. Using Agerskov's expression might also bring some uncertainties to the finite element modelling, since in [36], it was proved that Agerskov's analytical expression can lead to stiffened bolt response and according to [34] it is very sensitive to the effective length of the bolt.

For fully accurate finite element results, also the bolt threads should be modeled. There are basically three potential failure mechanism for the bolts: (i) bolt shank failure under tension and bending, (ii) stripping of the bolt threads and (iii) stripping of the nut threads [24,37]. Accurate modelling of the bolt threads would be very time consuming and applying it to a parametric study of a full end-plate connection would be cumbersome. The complex geometry of the bolt threads would also increase the number of elements and the computational time by a considerable amount. In addition, according to [24] the modelling of the bolt and

nut threads would lead to significant uncertainties, since the real material properties of the threads are basically impossible to measure. The method, in which the bolt threads are neglected, while still taking into account the reduced tension area of the threaded portion of the bolts, has been found accurate enough in multiple studies [28,37,38]. This simplification is generally used and it will also be employed in this thesis.

4.1.2 Finite element modelling of the T-stub

Element types
In Ansys finite element software, there are basically two commonly used three dimensional solid element categories which can be used in this type of finite element problems: quadratic tetrahedral and hexahedron structural solids. These element categories are then divided into multiple element types depending on the number of nodes and the degrees of freedom. [39] It is generally known and quite thoroughly studied in [40,41] that in bending dominated problems hexahedron solid elements should be used. In the T-stub behavior, bending is the primary driver for displacement, so hexahedron meshing method was chosen.

Even though hexahedron dominant method was used, some triangle shaped elements were created due to the curved geometry of the web root and the bolt holes. It might be possible to avoid this by more accurate and manually controlled meshing options, but since the idea is to find a suitable procedure for the modelling of the parametric end-plate splice study, some automation in meshing is preferred.

The quadratic solid element types in the T-stub validation model are: a 20-node brick element SOLID 186 and a 10-node tetrahedron element SOLID 187. They are defined by 20 or 10 nodes, each having three degrees of freedom per node. These nodes are formulated so that their degrees of freedom only govern the translation in x, y and z direction so there are no rotational degrees of freedom with these quadratic solid elements. [42] A 10- and 20-node quadratic solid elements are shown in Fig. 4.2.

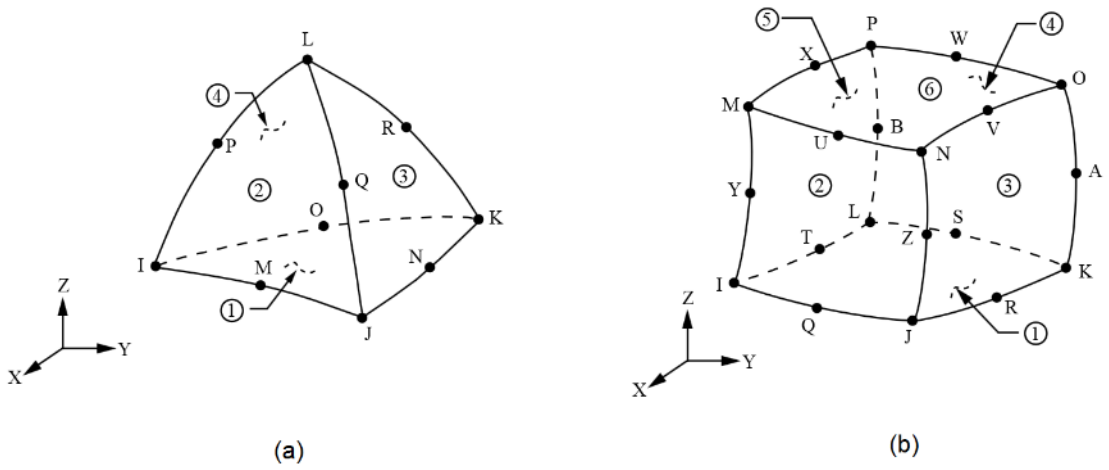

Fig. 4.2 10- and 20-node structural solid element types used in the T-stub model.

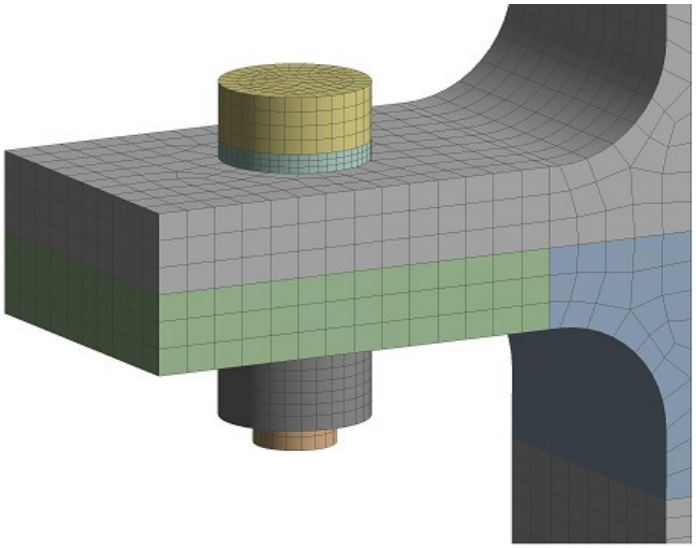

Fig. 4.3 Finite element mesh of the T-stub model.

An example of the mesh is shown in Fig. 4.3 and it can be seen that there are always at least three layers of elements over the thickness of the structural part, which is under bending, as recommended in [43]. Meshing is denser in the flanges and in the bolts, whereas in the webs, there is only one layer of element through the thickness. This is enough, since only axial loading occurs in the webs. According to [44], when quadratic solid elements are used, it could be possible to model a simple structural part by using only one layer of elements, but in this case, when the flanges include holes, more than one layer is preferred.

Contact modelling

In finite element modelling of a bolted connection, it is necessary to determine two types of contacts: frictional and bonded contacts. These contact areas can be modeled by using a 3D interface contact and target element pair: TARGE 170 and CONTA 174. This contact formulation allows the use of Coulomb frictional contact. [39]

The true behavior of touching steel surfaces, which are under compression, needs to be defined by using a frictional contact. Frictional contact allows sliding and it can carry the shear stresses up to a certain magnitude. The friction coefficient in frictional contacts is set to 0.2 and they are formulated by using augmented Lagrange method. For nonlinear frictional contact, it would be also possible to use pure penalty formulation, but augmented Lagrange formulation is recommended for this type of problems. [43] The benefit of the augmented Lagrange method is that the contact formulation is less sensitive to contact stiffness, thus, it is not as dependent on the normal contact stiffness definition made by the user. These formulation methods are both based on penalty calculations and the idea is to find the maximum or the minimum of the potential energy functional as presented in [44]. The penalty based formulation principles are also presented in [45].

Bonded contacts are used whenever a modeled part is attached to another part. Although the bolts could be modeled as one part, here they are modeled in three parts and they are attached to each other by using a bonded contact. This modelling approach allows better control of

the bolt parameters, when bolt size is varied in the parametric analysis of the full end-plate splice. Bonded contacts exist between (i) the bolt shank and bolt head and (ii) bolt shank and the inner surface of the nut. Bonded contacts are defined using multi point constraint (MPC) formulation, which is a linear method of using constraint equations for tying the displacements of the contact surfaces. Bonded contacts formulated by multi point constraint equations do not allow any sliding or separation between the surfaces. [43]

Material modelling

Finite element model of the T-stub can be defined by using two material models: bilinear isotropic hardening and multilinear isotropic hardening. These isotropic hardening models can be used in large strain analysis in static cases and in case of a cyclic loading, kinematic hardening should be used. [43,46] A von Mises yield criterion with isotropic hardening was also used in the simulations presented in [47] and the material models showed good performance in replicating the experimental results.

Bilinear isotropic hardening is very useful in practical design tasks, since the true material properties for structure elements are usually not known to the designer. Using bilinear isotropic hardening requires only the input of Young's modulus E and the tangent modulus E_t of the material. In Eurocode 3 [5], some values for tangent modulus are given. Bilinear material behavior is divided into two segments, in which the slope of the first segment of the stress-strain curve is equivalent to the Young's modulus while the scope of the second segment is the tangent modulus. [43] Bilinear stress-strain curve is shown in Fig. 4.4 (a).

Multilinear isotropic hardening can be used in cases, in which a higher accuracy of material modelling is required. For multilinear material modelling, the true material data of the specimens needs to be available. In Ansys Workbench, the stress strain data needs to be provided in the form of plastic strain and stress. This means that the first point of the curve must be the yield stress and then the plastic strain of the first point is zero. Other points are defined according to the provided material data. [43] Multilinear stress-strain curve is shown in Fig. 4.4 (b).

The material data provided in [33] was in the form of the total strain and stress, so the data had to be converted into plastic strain and stress. This can be simply done by subtracting the elastic strain from the total strain as presented in the following formula

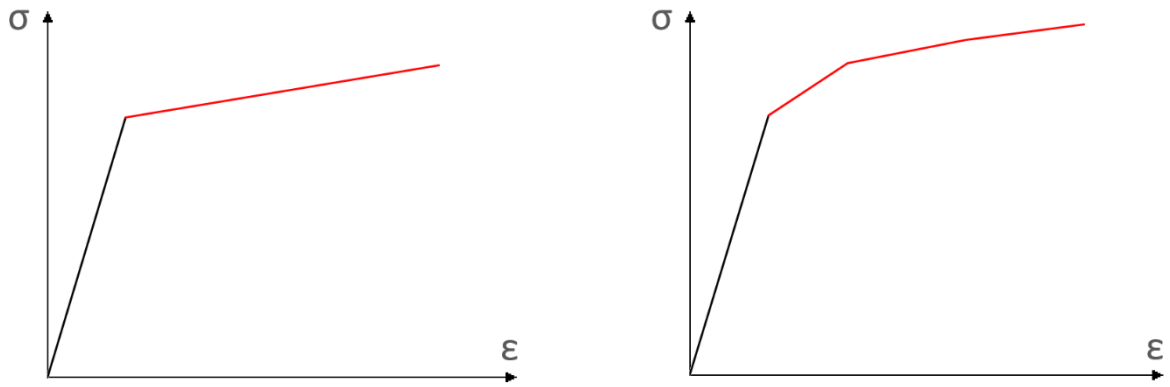

Fig. 4.4 Bilinear and multilinear material models.

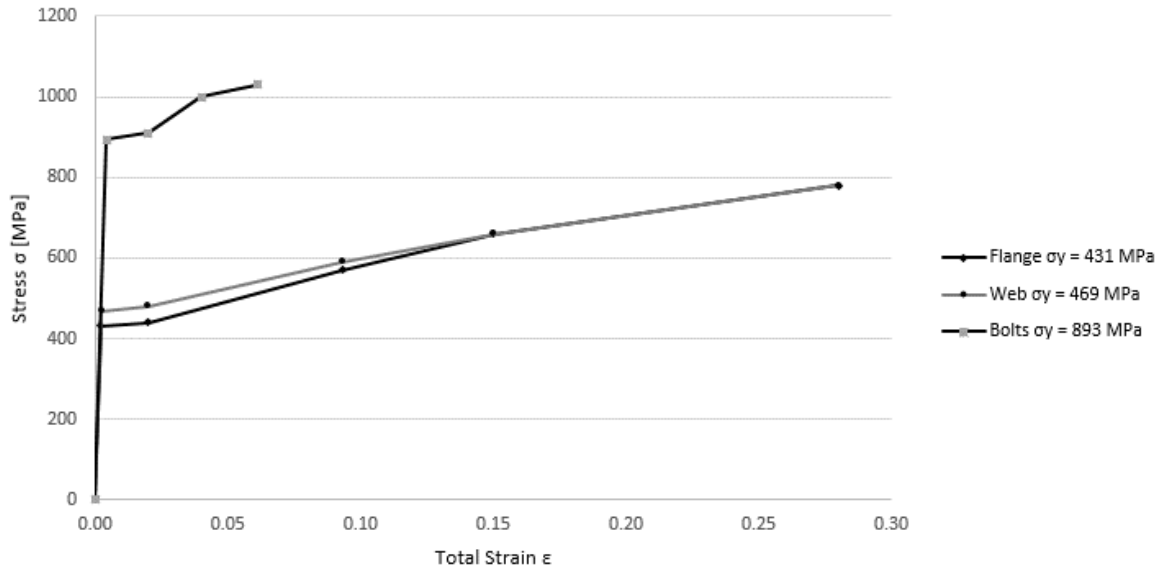

Fig. 4.5 The material data provided in [33]. The material data was gathered with coupon tests for flange, web and bolts separately.

$$\varepsilon_P = \varepsilon_T - \frac{\sigma}{E} \tag{4.1}$$

where ε_P is the plastic strain, $\varepsilon_E = \frac{\sigma}{E}$ is the elastic strain according to Hooke's law and ε_T is the total strain.

For the experiments reported in [33] Bursi and Jaspart provide the material data of the tested specimen. The material data was gathered by experimental tests, which were performed on the flange, web and bolts separately. Provided multilinear material data is presented in Fig. 4.5. A similar simplified multilinear material law was also used in [25] and it was noticed that the multilinear models can reproduce accurately the hardening of the material in similar cases. Although a multilinear material model is used in the validation model, the full size end-plate splice will be modeled by using a bilinear model, since in practical design cases, only the yield strength and the ultimate strength of the material is available.

Analysis options

T-stub analysis in this study have been performed under force control, even though according to [34], a displacement-driven analysis could offer better convergence. In more complex simulations, a displacement-driven analysis might be required, but in this case the convergence was not an issue. A force-driven analysis is also preferred, since it offers more simplicity and post-processing ease.

In Ansys, a nonlinear analysis is organized into three different levels of operation. First of all, each analysis consists of load steps. These load steps are defined explicitly over a time span. Each load step can then be divided into sub steps, so that the external load can be applied more gradually. The lowest level of operations happens within each sub step, in which the program performs equilibrium iterations to obtain a converged solution. [48]

As a default method, Ansys employs the Newton-Raphson approach for solving the nonlinear iterative problems. In this approach, the load is subdivided into a series of load increments. [48] In Newton-Rapson approach, the idea is to find an equilibrium between the proposed equations. In structural problems, this can be, for example, an equilibrium between the internal and external forces or moments. This equilibrium is found through an iterative procedure, in which an out-of-balance load vector is formed within each iteration until the force difference is sufficiently small. To define sufficiently small, a convergence criteria must be introduced. In simplicity, the Newton-Raphson method is about finding the tangent of the function at the calculated point. The convergence criteria needs to be realistic for the particular case. It cannot be too tight so that too much computational effort is used and on the other hand, the criteria can't be too loose to cause inaccurate results. The formation of the out-of-balance force vector, which is also called a force residual, is illustrated in Fig. 4.6. The convergence is obtained when the force residual becomes less than the convergence criteria. [46,49] In the T-stub analysis and with the full end-plate splice analysis, a program controlled value for the force convergence criteria is used.

The time step in the iterative analysis can be defined through manual or automated options in Ansys. The iteration procedure in this T-stub analysis was executed by using the automatic time stepping. It is the recommended load increment setting for non-linear structural problems. [43] Automatic time stepping allows the user to specify initial, minimum and maximum number of sub steps, but instead of always using those constant numbers of steps, the program automatically adjusts the required number of sub steps. If the convergence is not found with the tried number of sub steps, the analysis retreats to the previous converged solution and increases the number of sub steps so that the convergence will be found. [48]

Two different cases were analyzed: one with non-preloaded bolts and another by preloading the bolts before applying the external loading. The analysis with preloaded bolts was divided into two different load steps: first step with preloading of the bolts and the second with external loading. The preloading force used in the T-stub model is $60{,}7\ kN$, the same as in the tests [32] executed by Bursi and Jaspart. With non-preloaded bolts, initial, minimum and maximum load steps were set to 100, 50, and 1000 respectively. With the preloaded bolts, in the preloading step, only 20, 1 and 100 were required for the defined ranges and the second load step was performed with same values as with non-preloaded bolts.

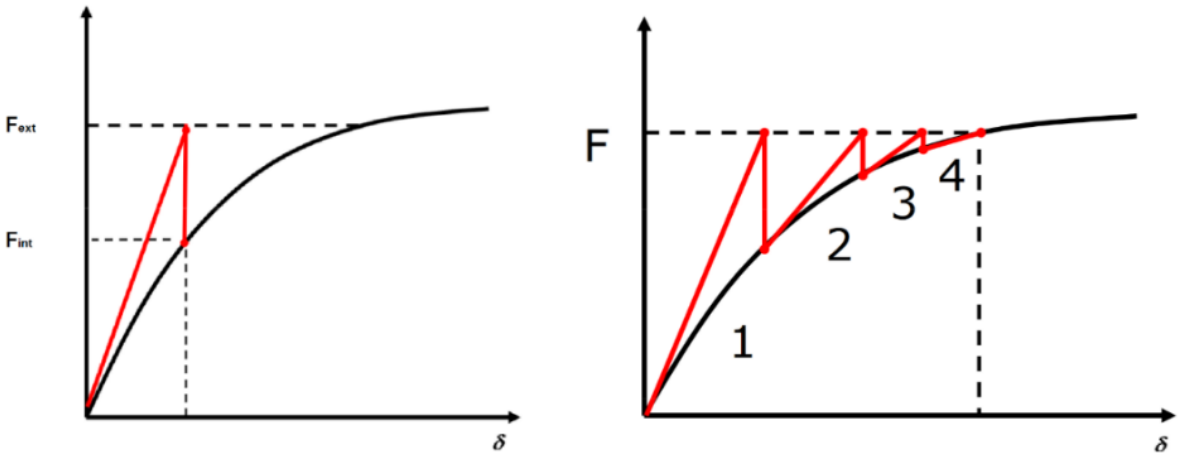

Fig. 4.6 The formation of the force residual in the iterative procedure. Numbers are indicating the equilibrium iterations, F_{int} and F_{ext} represent the internal and external loads respectively and δ is the displacement.

Ansys Mechanical Software offers various ways of applying the preloading of the bolts. An easy way of preloading is just via adjusted displacement of the bolt base, but in this case, since the actual preloading force was given, it can be used in the analysis. In the analysis of the full size end-plate splice, adjustment of the bolt base will be used for preloading, since the actual preloading load is not known in the studied cases.

4.1.3 Results of validation

The comparison of the analytical, numerical and experimental results of the design tension resistance and the axial stiffness of the T-stub specimen are presented in this section. The T-stub is presented in Fig. 4.1. The design tension resistance corresponds to the ultimate capacity of the specimen and the initial axial stiffness is defined as the slope of the force-displacement curve in the elastic zone.

From Fig. 4.7, it can be seen that the finite element models with non-preloaded and preloaded bolts show good performance in replicating the experimental results especially in the elastic range. However, some discrepancies occurred at the onset of yielding. In [33,50], similar discrepancies were discovered and it is claimed that the discrepancies can be explained by the residual stresses, which would determine more gradual plastification in the actual specimen. The residual stresses of the specimen could not be modelled, since the residual stress data was not available.

The Eurocode based analytical prediction of the force-displacement response shows also good performance compared to the experimental and numerical models with non-preloaded bolts. It was possible to use the analytical model for the case with the non-preloaded bolts only so the comparison with preloaded bolts is done only between numerical and experimental results. As seen in Fig. 4.7, the stiffness of the analytical model appears to be smaller than that of the experimental or that of the numerical model. Reason for the reduced stiffness is that the Eurocode based model takes into account the whole elongation length with only the tension area A_s. If the bolt was modeled with the real length of the threaded and unthreaded portion, the analytical force-displacement response would be closer to numerical and experimental results. The design tension resistance of the analytical model is also significantly smaller. Although the response of the analytical model differs quite significantly

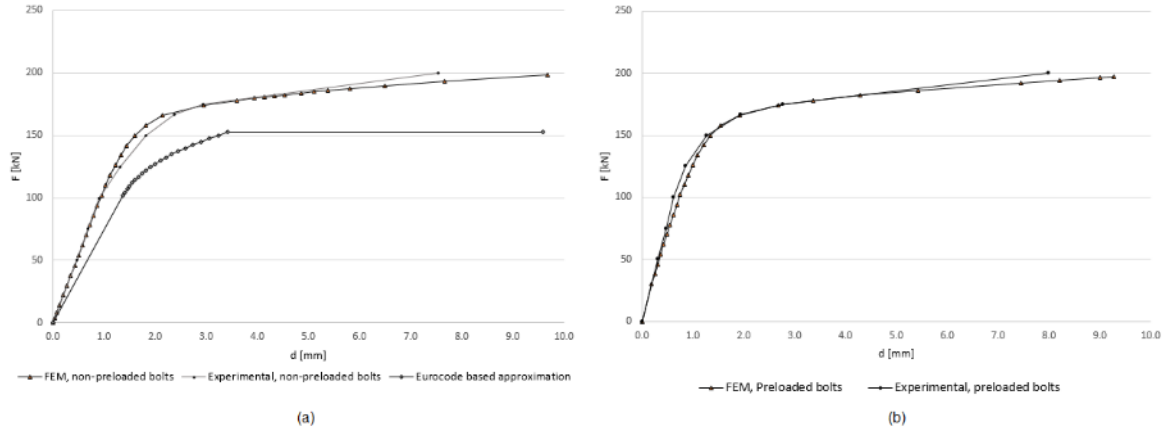

Fig. 4.7 Force-displacement curve of the experimental, numerical and analytical models for (a) non-preloaded and (b) preloaded cases. The axial displacement is measured from the point, in which the force F is acting as shown in Fig. 4.1. F is the external load and d is the corresponding displacement.

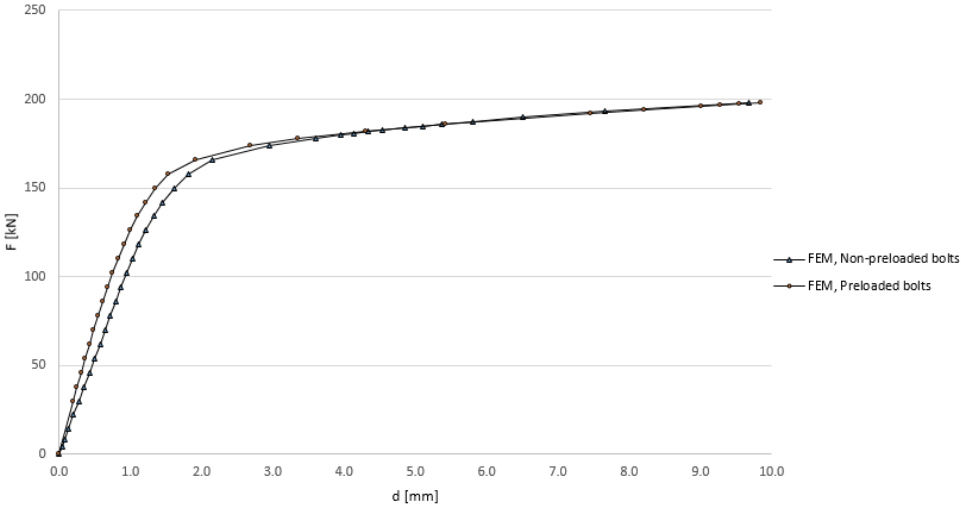

Fig. 4.8 The increase of initial stiffness in load-displacement response when bolts are preloaded. *F* is the external tension load and *d* is the corresponding displacement.

from the other two models, it should be considered that it's only an analytical approximation of the true behavior. In practical cases it is preferred that the design tension resistance defined according to the standard is on the safe side of the true capacity.

Comparison of the force-displacement curves of the model with non-preloaded bolts and with preloaded bolts is shown in Fig. 4.8. In [33,34] it was found that preloading increases the stiffness of the specimen but it doesn't make a significant contribution to the design tension capacity of the T-stub section. As it can be seen, similar results were also detected in this study, since the preloaded bolts provide stiffer force-displacement response.

The mesh dependency was also studied to discover suitable practices for the analysis of the full size end-plate splice. Three different mesh size configuration were used and they are shown in Fig. 4.9. Fig. 4.9 (a) shows a coarse mesh in which only one layer of elements is modeled through the thickness of the flange, (b) is showing a recommended mesh with three layers and (c) is indicating a dense mesh with multiple layers of elements through the thicknesses of the flange.

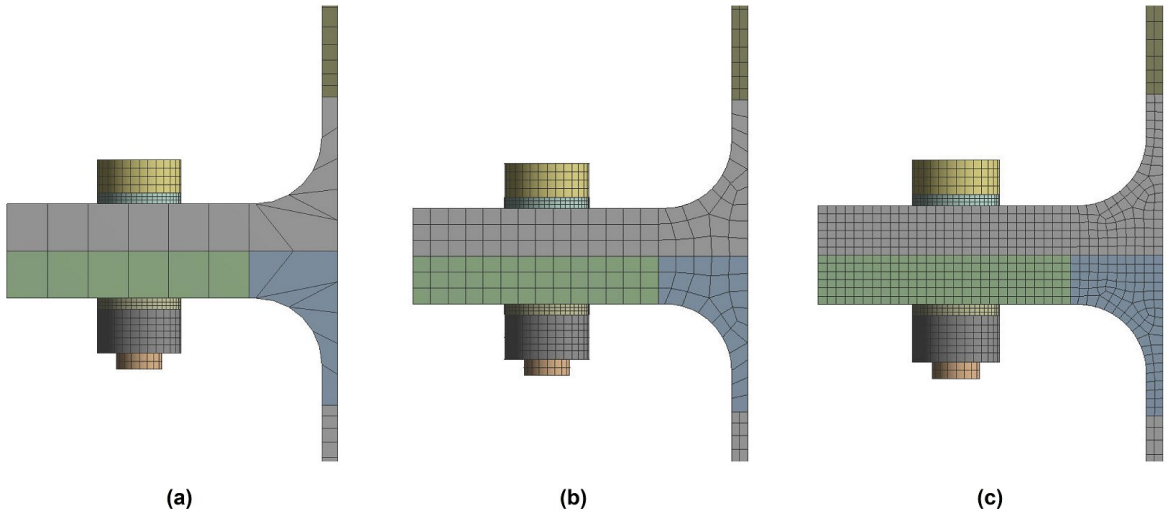

Fig. 4.9 The studied mesh configurations with different element sizes in the flange of the T-stub.

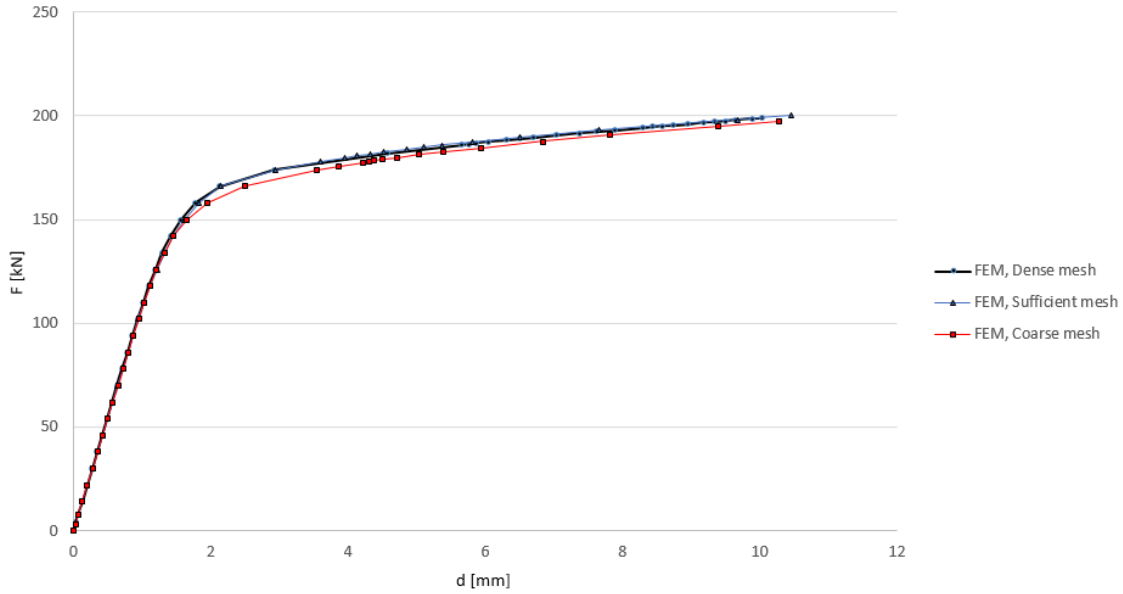

Fig. 4.10 The force-displacement curves obtained with different mesh configurations.

The force-displacement curves of the different mesh configurations are presented in Fig. 4.10. It can be seen, that all three meshing options can reproduce the force-displacement response very accurately in elastic range, but some minor discrepancies occur with the coarse mesh at the on-set of yielding. The maximum error is less than 2 % and it occurs at about $d = 2$ mm. From Fig. 4.10, it can also be seen that the results between the dense and the sufficient mesh configurations do not differ, whereas the computational time with the dense mesh is significantly increased and it would become very time consuming to perform a parametric study of the full end-plate splice with such dense mesh. According to these results, the analysis of the full size end-plate splice should be executed with three layers of elements through the thickness of each structural part which is under bending. However, the number of joint geometries to be studied is very high, so it will be checked if two layers of elements would be enough in the analysis of a full size end-plate splice.

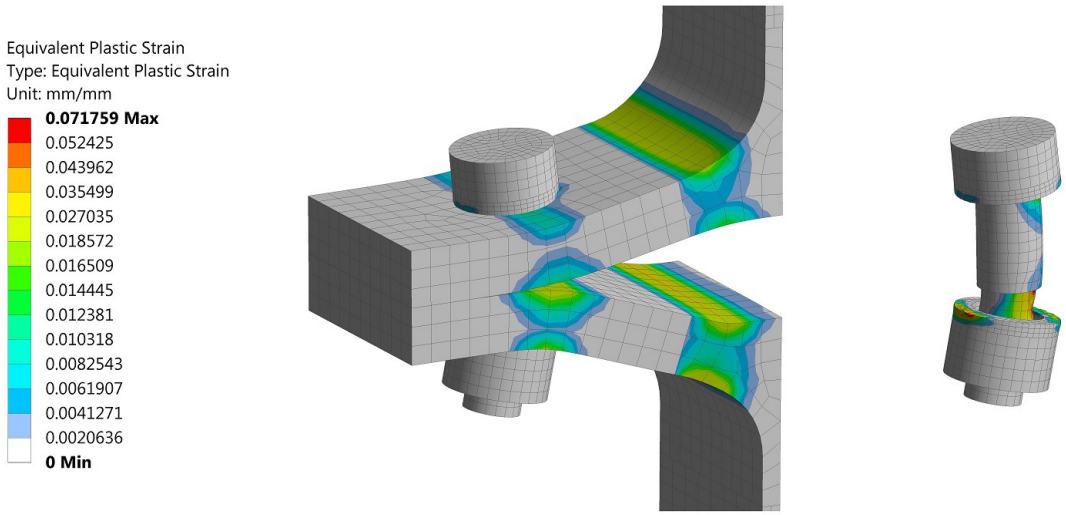

Fig. 4.11 Plastic hinges when the T-stub is loaded to its full design tension resistance. The deformation of the T-stub is exaggerated by factor of 10.

The deformed model of the T-stub and the developed plastic hinges are shown in Fig. 4.11. The complete flange yielding occurs in the studied T-stub, which indicates that the failure mechanism is of type-1 as predicted with expression (3.7). As it can be seen, the plastic hinges are developed exactly to the locations, which can be predicted with the Eurocode based beam patterns. Although the failure mechanism is of type-1, some plastification occurs also in the bolt shanks when the full design tension resistance is reached.

4.2 Finite element model for a flush end-plate splice

The full size finite element model of a flush end-plate splice is presented in this subsection. This model is used in the parametric study presented in subsection 4.3 and the results of this study are presented in section 5. The analysis of the end-plate splice is performed by analyzing a simply supported HEA400 steel beam. The basic geometry and boundary conditions of the model are shown in Fig. 4.12. The finite element model of the full size end-plate splice is built mostly by using the same properties that were found suitable in the analysis of the T-stub specimen in section 4. Although the contacts, elements and loading of the end-plate splice are modeled similarly, some simplifications had to be made to the full end-plate splice model. The basic principles and the loading conditions of the parametric study of the end-plate splice are presented in the following subsections.

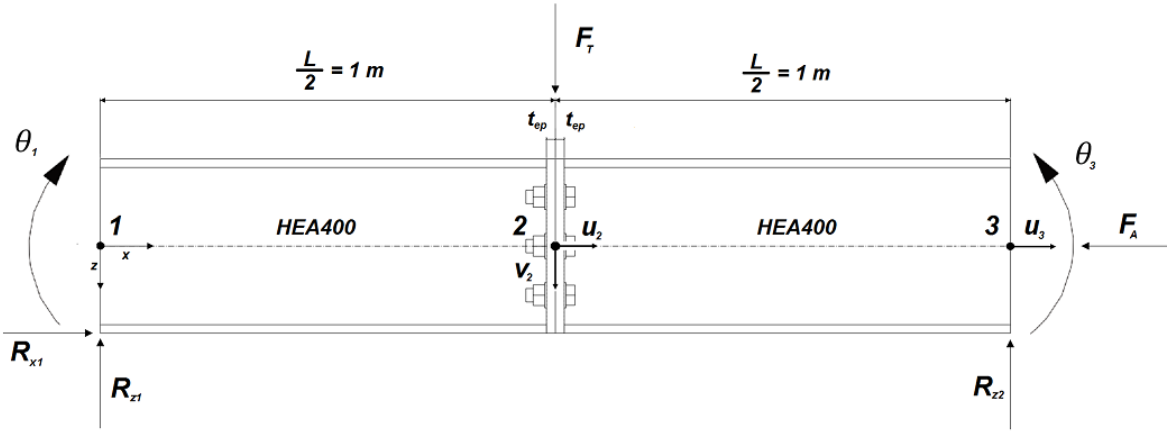

Fig. 4.12 The global degrees of freedom and the boundary conditions of the studied beam geometry. The presented geometry corresponds to in-plane bending case and for out of plane bending the studied case is identical except that it's flipped about x-axis.

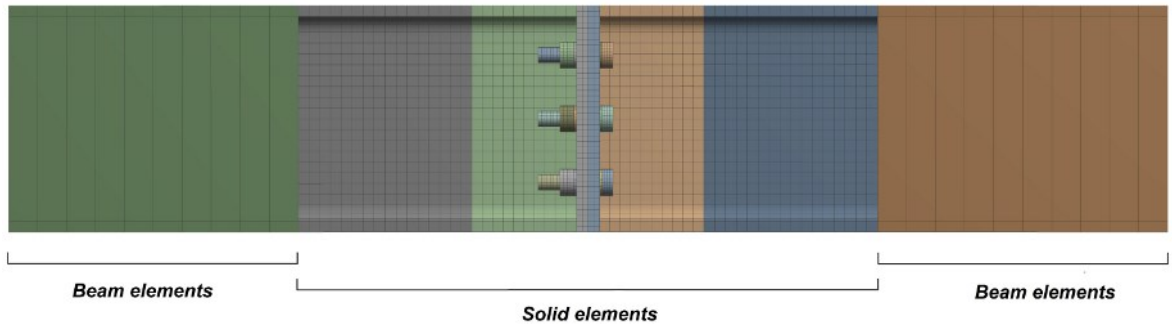

Fig. 4.13 The chosen mesh configuration of the simply supported beam geometry. The ends of the beam members are modeled using ten BEAM 188 elements at each end. The joint geometry and the beam members at the proximity of the joint are modeled using hexahedron and tetrahedral solid elements described in subsection 4.1.2.

4.2.1 Basic principles used in the model

In the analysis of the end-plate splice, solid elements were used to model the connection and the beam parts at its proximity. The chosen elements and the mesh configuration of the studied model is shown in Fig. 4.13. Now, since the behavior of the end-plate splice is studied as part of a beam geometry, the ends of the beam members can be modeled by using beam elements. Beam elements can be used at the ends, since the cross-section remains plain in the areas, which are far from the end-plate splice. The total amount of nodes in the model is significantly reduced, when the ends of the beams are modeled with beam elements. With this element configuration, the analysis efficiency is significantly improved compared to a model which is fully modeled with high order solid elements.

The chosen Ansys beam element is a two noded BEAM 188 element with six degrees of freedom at each node. [42] These degrees of freedom include translation in x, y and z direction as well as rotation about x, y, and z axis. The element geometry is shown in Fig. 4.14. BEAM 188 element is based on Timoshenko beam theory so it includes the shear deformation effects. When the effect of shear deformations are considered in beam-bending analysis, the cross-section originally normal to the neutral axis remains plane, but because of the shear deformations, the cross-section does not stay normal to the neutral axis. [49]

The solid elements used in this model are the same tetrahedron and hexagonal elements as described in subsection 4.1.2. In Fig. 4.13, it can be seen, that the end-plates are modeled by using two layers of elements through the thickness and in other beam parts, only one layer of elements is used. Although in subsection 4.1.3, it was found that only one layer of elements would be enough for accurate results, a denser mesh configuration was decided to be used in the end-plates. This setting is preferred, since the deformation in the end-plates is highly driven by three dimensional bending and a denser mesh is also beneficial for visualizing the yield line patterns.

A bilinear material model is used in the parts, which are modeled with solid elements. The steel grade in beam members and end-plates is S355 and the bolts are of grade 8.8. This means that the yield stress in structural steel is 355 MPa and in the bolts 640 MPa. The two material models are shown in Fig. 4.15. The bilinear material models are obtained by using the values presented in standard EN 1993-1-5 [5] Appendix C. The Young's modulus $E = 210\ GPa$ in the elastic range and the tangent modulus $E_t = 21\ MPa$. An elastic material model is used for the beam elements at the ends of the beam. The elastic material model can be used close to the supports, since the stress levels in these locations are within the elastic range.

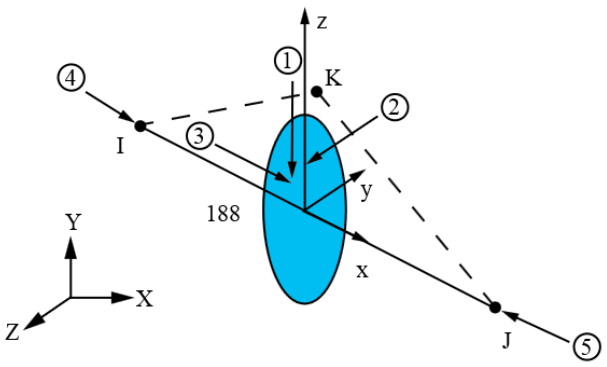

Fig. 4.14 The geometry of Ansys beam element BEAM 188. The element has two nodes and six degrees of freedom: translation in x, y and z direction and rotation about x, y and z axis. [42]

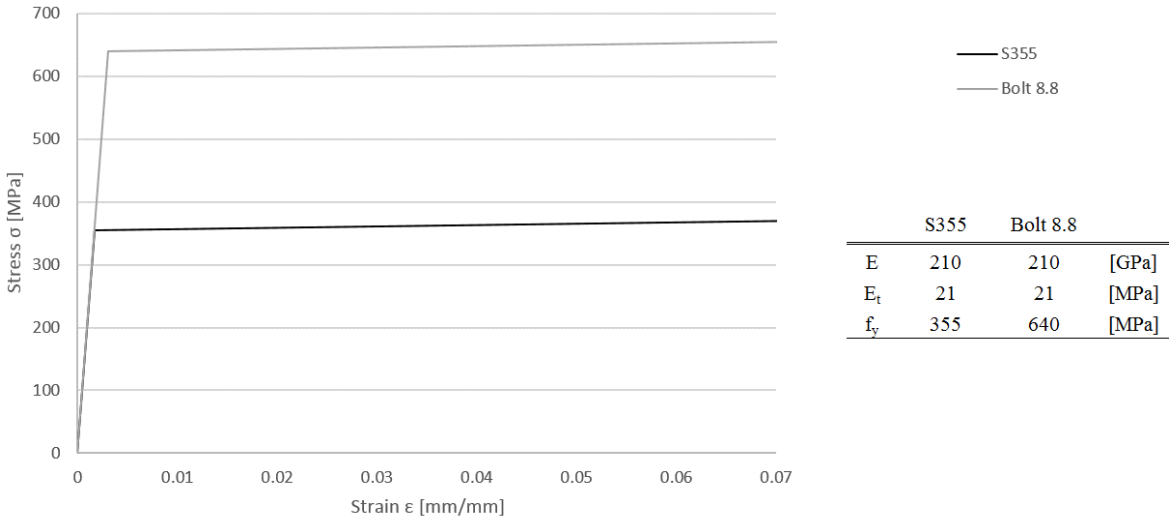

	S355	Bolt 8.8	
E	210	210	[GPa]
E_t	21	21	[MPa]
f_y	355	640	[MPa]

Fig. 4.15 The two material models used in the finite element model of the end-plate splice. *E* is Young's modulus, E_t is the tangent modulus and f_y is the yield stress of the material.

The choice for modelling the structure was verified by performing a simple comparative analysis, in which the response of the beam, which is modeled completely by a dense solid element mesh and with a non-linear material model was compared to a model with chosen element and material configuration as seen in Fig. 4.13. The results from this comparative analysis can be seen in Fig. 4.16. Although there are some minor discrepancies after the yielding point, the initial stiffness is reproduced very accurately and the computational effort is significantly reduced with the chosen configuration. With these results, the chosen mesh and material configurations can be justified for the use in the parametric analysis of the full size end-plate splice.

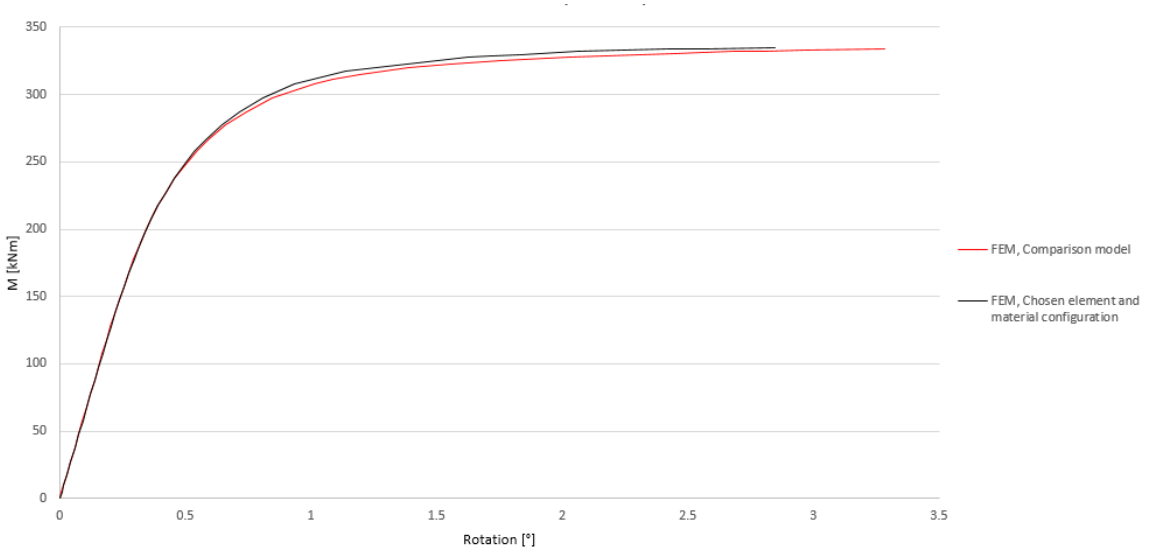

Fig. 4.16 The moment-rotation response of the finite element model with chosen element and material configuration compared to a model, which is completely modeled with solid elements. The chosen element configuration is presented in Fig. 4.13. *M* is the internal moment at the connection and rotation is the corresponding rotation angle in degrees.

4.3 Parametric study

The parametric analysis of a full size end-plate splice is performed to study the effects of the bolt size and the end-plate thickness to the moment-rotation response of a flush end-plate splice. The parametric study of the end-plate splice is done by varying the bolt size and end-plate thickness of the connection. The studied parameters and parametrized configurations are presented in Table 4.1. The studied parameters are kept within practical limits and they are chosen so that different failure mechanisms can be detected. Bolt size is either M24 or M30 and the end-plate thickness is varied between 15-40 mm. Other dimensions in Table 4.1, as well as the cross-sections of the connected beam members, are kept constant in all of the studied cases. The studied parametrizations are referred to by EPS and they are numbered from EPS1 to EPS8.

The lengths of the partially threaded bolts are chosen so that they fulfill the criteria for partially threaded bolts determined in Eurocode 3 [1]. The design criteria defines that the threaded part of the bolt cannot reach further than one third of the plate thickness. With this restriction it is guaranteed that the threaded portion of the bolt is far enough from the shear plane of the connection. The dimension for bolts, nuts and washer plates are determined according to standards [51-53].

Fig. 4.17 shows the loading cases used in the parametric study. The behavior of the end-plate splice is studied both in in-plane and in out-of-plane bending. Also the effect of bolt preloading and additional axial tension and compression forces are studied for each geometrical configuration. The transversal load $F_T = 1000$ kN and the axial load $F_A = 500$ kN. The transversal point load is applied to mid-span of the structure and the axial point load is added centrically to the end of the structure. With eight geometrical parameters and four loading cases and while each joint configuration is studied in both directions, a total of 64 cases are studied.

All of the analysis are performed by using force control, in which the loads are increased gradually starting from zero. Usually only one load step is used, but in cases with preloaded,

Table 4.1 The parametrized models EPS 1-8 and the geometrical parameters of the studied cases. *EPS* refers to end-plate splice. t_{ep} is the end-plate thickness, h_{ep} the end-plate height, b_{ep} the end-plate width, e is the distance from the edge of the plate to the center of the bolt, p the horizontal distance between the bolts and p_1 and p_2 are the vertical distances between the horizontal bolt rows.

	Bolt size	t_{ep} [mm]	h_{ep} [mm]	b_{ep} [mm]	e [mm]	p [mm]	p_1 [mm]	p_2 [mm]
EPS1	M24	15	390	300	85	130	110	110
EPS2	M24	20	390	300	85	130	110	110
EPS3	M24	30	390	300	85	130	110	110
EPS4	M24	40	390	300	85	130	110	110
EPS5	M30	15	390	300	85	130	110	110
EPS6	M30	20	390	300	85	130	110	110
EPS7	M30	30	390	300	85	130	110	110
EPS8	M30	40	390	300	85	130	110	110

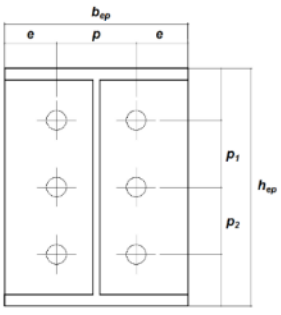

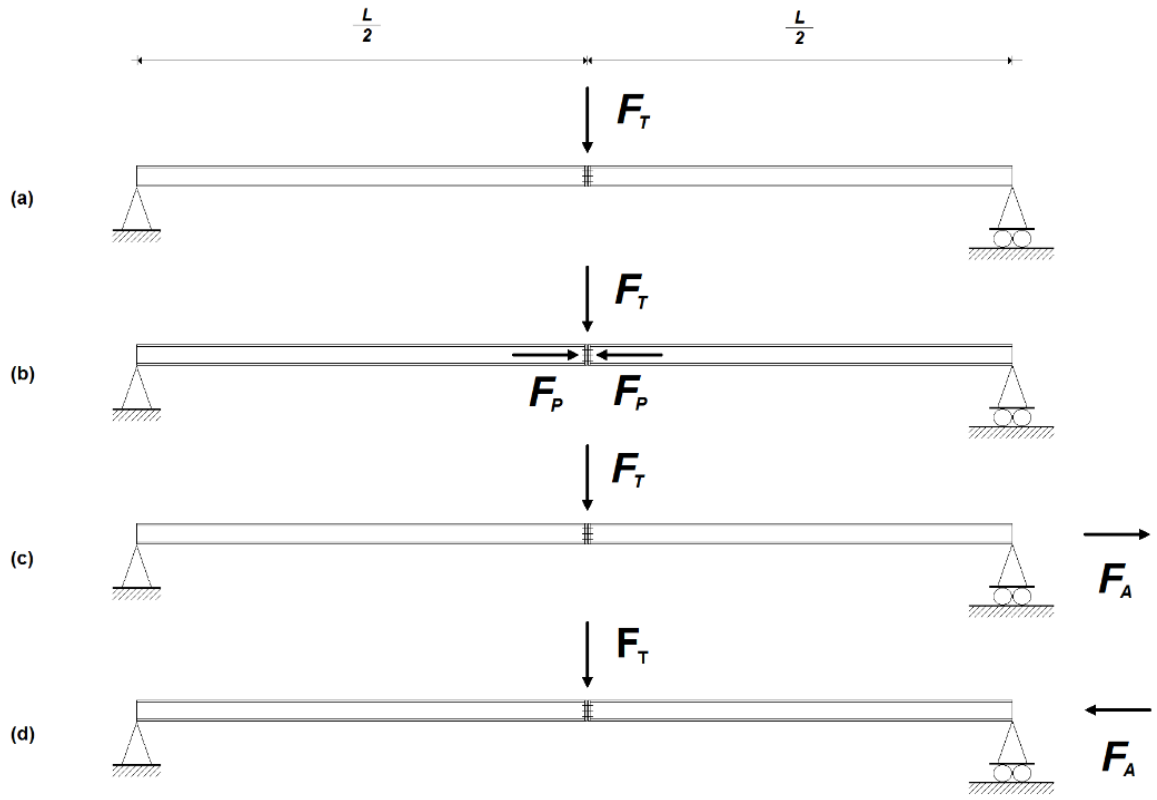

Fig. 4.17 The studied loading cases: (a) pure bending caused by transversal point load in mid-span with non-preloaded bolts, (b) pure bending caused by transversal point load in mid-span with preloaded bolts, combined bending and tension with non-preloaded bolts and (d) combined bending and compression with non-preloaded bolts.

bolt, the analysis is performed in two steps as described in subsection 4.1.2. The bolt pre-loading force is defined according to Eurocode 3 [1] with the following expression

$$F_{p,Cd} = 0.7\frac{f_{ub}A_s}{\gamma_{M7}} \tag{4.2}$$

in which f_{ub} is the ultimate strength of the bolt material, A_s is the tensile area of the bolt and γ_{M7} is the partial safety factor for preload of the bolt. The preloading force for M30 bolts is 285.6 kN and for M24 bolts 179.7 kN.

In the cases with combined bending and axial loading, both forces are ramped proportionally starting from zero. A real life case of this kind of combined bending and axial loading could be a case, in which the axial load is applied excentrically to the end of the structure as presented in Fig. 4.18 (a). Other possibility for applying the load combination would be by using two steps. First by loading the beam axially and then in the second step by applying the transversal loading as shown in Fig. 4.18 (b). This type of loading can occur especially with columns, which are loaded by centric axial loads and then an additional load, for example a lateral wind load, starts to cause the bending of the structure. To see the difference between the two loading scenarios with combined loads, model EPS6 is also analyzed by first loading the structure axially and then by adding the transversal load in the second step.

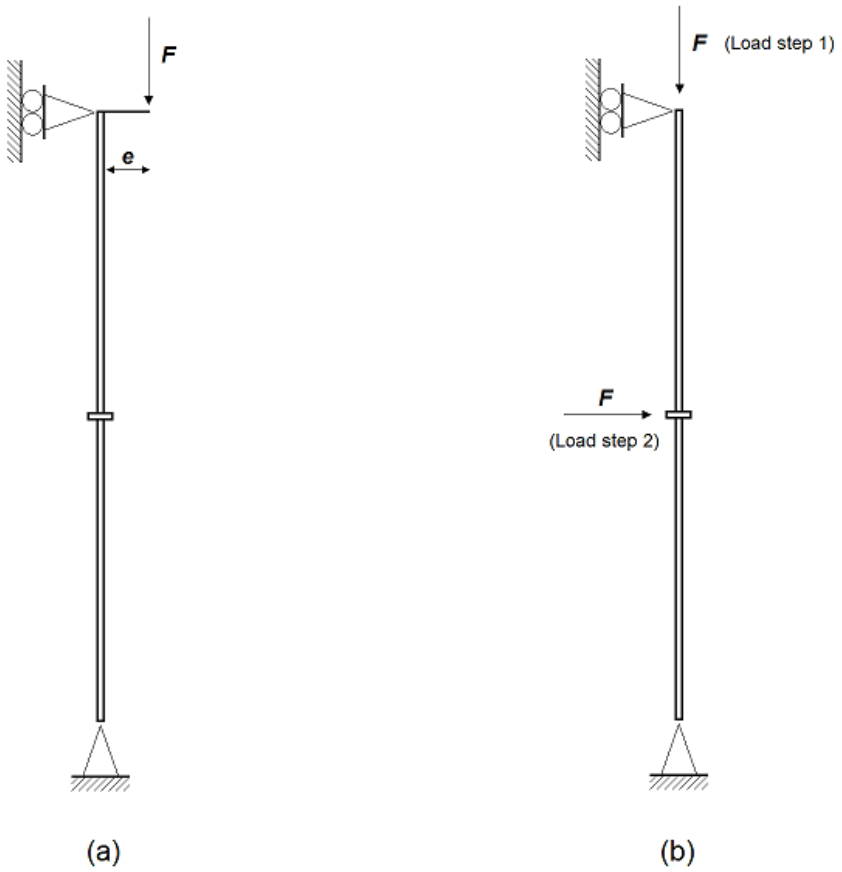

Fig. 4.18 Examples of different loading scenarios for combined bending and axial force in case of columns. (a) is showing the case in which axial force and bending increase proportionally starting from zero and bending is caused by excentric axial loading. (b) is showing a situation when the column is loaded with a central axial force before bending occurs.

4.4 Measured variables

To study the moment-rotation response of a flush end-plate splice, the rotation angle and internal moment of the joint needs to be determined. The determination of the rotation angle of the joint is presented in subsection 4.4.1. To further study the local behavior of the joint and to determine the bending moment resistance of the joint, some limiting criteria have to be determined. The determination of the moment resistance and the rotational stiffness, as well as the ductility and resistance ratios, are presented in subsection 4.4.2.

4.4.1 Determination of rotational angle

The rotation angle of the end-plate splice can be determined by measuring the deflection of the beam at mid-span. Similar method was used in the experimental tests of end-plate splices on tubular members executed by Perttola and Heinisuo [54]. The principal idea is that the beam is loaded so that it stays on the elastic zone and all permanent deformation is caused by the local deformations in the joint. Although the global rotation angle at the mid-span of a simply supported beam is zero, the beam geometry can be considered as two beam members connected with a rotational spring as shown in Fig. 4.19. The total deflection of the spliced beam geometry can be measured from the finite element analysis, but to isolate the

deflection caused by the end-plate splice, the elastic deflection of the beam is subtracted from the total measured deflection as follows

$$\delta_{joint} = \delta_{tot} - \delta_{el} \tag{4.3}$$

in which δ_{joint} is the deflection due to the end-plate splice, δ_{tot} is the total measured deflection from finite element results and δ_{el} is the elastic deflection of the beam geometry without the joint at the mid-span.

The elastic deflection at the mid-span could be calculated with the generally known formula [55]

$$\delta_{el} = \frac{F_T L^3}{48EI} \tag{4.4}$$

in which E is the Young's modulus and I is the moment of inertia. However, in this case the Ansys beam elements BEAM 188 is based on Timoshenko beam theory so the beam element formulation includes the shear deformation effects. Taking into account the shear deformation effects, the total elastic deflection can increase quite significantly with relatively short beams [49]. In this case, the total deflection with shear deformations included is nearly twice as big compared to the analytical result without consideration of the shear deformations effects. To account for this, instead of using the analytic expression (4.4), the elastic deflection of a simply supported HEA400 beam without an end-plate splice was determined with a simple comparative finite element analysis with Ansys. For this comparative finite element model, only Ansys BEAM 188 elements were used. As a result, a linear force-displacement relation was conducted and it can be used for subtracting the elastic deflection from the total deflection at all load magnitudes between zero and the maximum allowed loading. A linear force-displacement relation was also conducted for cases with combined bending and axial loading.

With this assumption and using the geometrical properties presented in Fig. 4.19, the rotation angle caused by the end-plate splice can be calculated with the following trigonometric expression

$$sin\left(\frac{\theta_{joint}}{2}\right) = \frac{\delta_{joint}}{\frac{L}{2}} \tag{4.5}$$

in which θ_{joint} is the rotation angle caused by the local deformations in the end-plate splice. Then by applying the theory of small angles on the trigonometric function $sin\,\theta \approx \theta$, the expression simplifies into

$$\theta_{joint} = \frac{4\delta_{joint}}{L}. \tag{4.6}$$

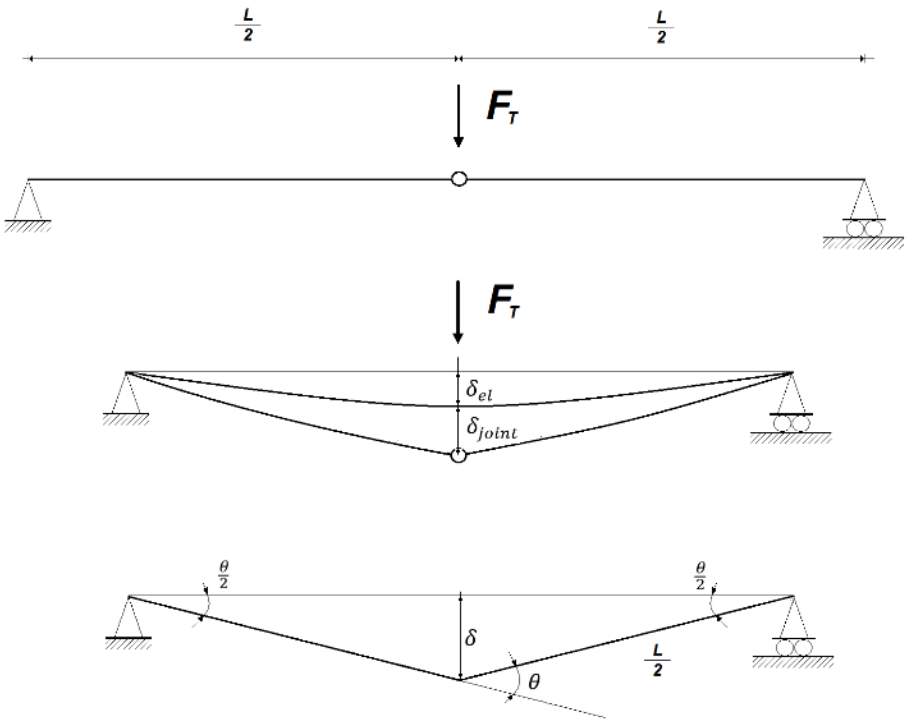

Fig. 4.19 The determination of the rotation angle θ caused by the end-plate splice at the mid-span. F_T is the transversal point load at mid-span, δ_{el} is the elastic deflection of the beam geometry without an end-plate splice and δ_{joint} is the deflection caused by the end-plate splice.

Now, since it is assumed that the deflection of the beam stays in the elastic zone, the elastic limits need to be determined. For the studied beam geometry, the maximum allowed elastic internal moment at mid-span can be calculated with the following expression

$$M_{el} = f_y W_{el} \tag{4.7}$$

in which f_y is the yield strength of the member and W_{el} is the elastic section modulus. [2] For HEA400 cross-section, the elastic internal moment in in-plane bending is $M_{el,y} = 787.6$ kNm and for out-of-plane bending $M_{el,z} = 202.4$ kNm. The limiting transversal point load at mid-span can be calculated with

$$F_{T,el} = \frac{4M_{el}}{L} \tag{4.8}$$

where M_{el} is the elastic bending moment and in all of the studied cases, the length of the beam span is $L = 2$ m. [55] The limiting point loads at mid-span are $F_{el,y} = 1575.1$ kN and $F_{el,z} = 404.9$ kN. To determine the moment-rotation response of the end-plate splice, the corresponding internal moment at mid-span needs to be calculated at each converged solution point. The internal moment in pure bending cases can be calculated by modifying the expression (4.8) into the following form

$$M_{joint} = \frac{F_T L}{4} \tag{4.9}$$

in which M_{joint} is the internal bending moment at mid-span. With combined bending and axial loading, the expression for the internal moment can be derived by using the free body diagram of the simply supported beam geometry. The expression for the internal bending moment in combined bending and axial loading yields

$$M_{joint,A} = \frac{F_T L}{4} \pm F_A \delta_{L/2} \tag{4.10}$$

in which F_T is the transversal point load at mid-span and F_A is the axial point load at the end of the connected beam member, $\delta_{L/2}$ is the total deflection at mid-span. Here, a compressive axial loading is considered to be with a positive sign and a tension point load with a negative sign. With the maximum point loads used in the analysis, the maximum moment that can occur is with combined bending and compressive axial loading. During the analysis of combined bending and compressive axial loading, it is observed that the elastic limit of the beam cross-section is not exceeded. With tensile axial loads, even with maximum loads, the internal moment is still within elastic limits.

4.4.2 Moment resistance and rotational stiffness

The design moment resistance and the initial rotational stiffness are the primary variables for comparing different joint geometries. The moment resistance and the rotational stiffness, as well as the ductility and resistance ratios, are all used in the comparison of different joint geometries in section 5.

The design moment resistance of the end-plate splice can be attained by using a materially nonlinear finite element model. According to Eurocode 3 [5], when a finite element analysis is used for design purposes, the ultimate capacity of the regions subjected to tensile stresses is defined by limiting the values of the principal plastic membrane strains. The recommended value in the standard is 5 %, but this can differ depending on the National Annex.

Usually in finite element analysis of steel connections performed with a bilinear material model, it is found that the complete collapse of the structure usually occurs very soon after the maximum plastic strain exceeds 5 %. This is especially the case, when the tangent modulus is relatively low. The higher the tangent modulus, the stiffer the response in the inelastic zone and the bigger the ultimate capacity. The problem with a bilinear material model is that the strain hardening continues to infinity, so the force-strain curve never reaches an ultimate peak as in experimental tests. Without a specific ultimate resistance point, the only way for defining the capacity of the structure is by limiting the strain or by attaining some other limiting criteria.

In this thesis, all finite element analysis are performed as long as Ansys solver was able to find a converged solution. Although the analysis can be carried further than the plastic strain limit, the ultimate design bending capacity M_{pl} is obtained at a point, in which the plastic strain equals 5 %. The moment-rotation curves presented in this thesis are plotted until the

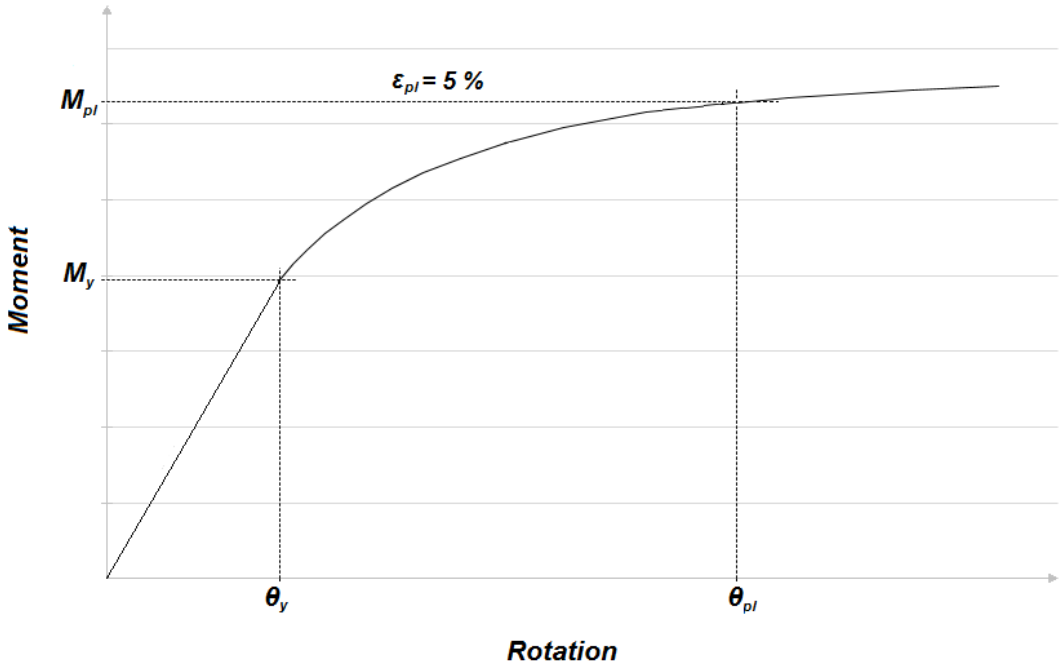

Fig. 4.20 The moment-rotation characteristics obtained by the finite element model. M_{pl} is the design moment resistance obtained at the limit of 5 % plastic strain, M_y is the yield moment and θ_{pl} and θ_y are the corresponding rotation angles.

plastic strain limit is reached. The yield moment M_y is taken as the external moment at a point, in which the first component reaches its elastic limit. The corresponding rotation angles are the ultimate rotation capacity θ_{Rd} and the yield rotation θ_y respectively. These moments and the corresponding rotational angles are presented in Fig. 4.20.

For efficient comparison of the moment-rotation characteristics between different joint geometries, two ratios based on the ductility model conducted by da Silva [56] need to be introduced:

$$Ductility\ ratio = \frac{\theta_{pl}}{\theta_y} \tag{4.11}$$

and

$$Resistance\ ratio = \frac{M_{pl}}{M_y}. \tag{4.12}$$

Ductility ratio of a joint characterizes the ability of the joint to deform after the on-set of yielding. The bigger the ratio, the better the rotational characteristics of the joint. The resistance ratio represents the relative load carrying capacity after the yield point.

In general, high values of ductility ratios represent good ductile behavior and they usually occur with type-1 and type-2 failure mechanisms. Low ductility ratios can be observed with type-3 failure mechanism. The Eurocode based failure mechanisms are presented in subsection 3.2.1. The failure mechanism is determined from the finite element analysis by observing the development of the total strain in each joint component. The limits for elastic strains

can be calculated using Hooke's law. The elastic strain limit for S355 steel is 1,69 ‰ and for the bolt 8.8 the elastic limit is 3,05 ‰. The failure mechanism of type-1 occurs when the elastic limit exceeds only in the end-plates, type-2 occurs when the elastic limit exceeds in the end-plates and bolts simultaneously and type-3, when the elastic limit exceeds only in the bolts.

The initial rotational stiffness of the end-plate splice can be defined from the finite element results as the slope of the moment-rotation curve as follows

$$S_{j,ini} = \frac{M_y}{\theta_y}. \tag{4.13}$$

In the results section, only the initial stiffness obtained with finite element analysis is considered. Although the choice of the tangent modulus has some impact on the design bending capacity, the initial stiffness of the end-plate splice only depends on the linear characteristics of the materials. This makes the initial stiffness obtained with finite element analysis and the analytical Eurocode based initial stiffness comparable, at least concerning the material properties used in both models. It also makes the finite element analysis an efficient tool for determining the joint characteristics, since usually only the linear initial stiffness of the joint is considered in the global analysis of structures [12].

5 Results and discussion

The objective of this thesis is to form a more thorough understanding of the moment-rotation response of a flush end-plate splice and in this section, this behavior is studied by analyzing the results of the parametric study. The moment-rotation response of a flush end-plate splice is studied both in in-plane and in out-of-plane bending. In addition to the pure bending cases, the moment-rotation response is also studied in combined bending and axial loading. Through an extensive finite element analysis, the weaknesses related to the standardized design rules for flush end-plate splices can be identified.

The moment-rotation response in in-plane and in out-of-plain bending is the primary tool for comparing the results of the finite element analysis and the results of the Eurocode based analytical calculations. The comparison between different models is presented in subsection 5.1. The differences in the ductility and rotation capacities between the different joint geometries are presented in subsection 5.2. Although the stiffness and ductility of the joint can be contrarian characteristics in some cases, it is important to acknowledge the ductility even when designing rigid or semi-rigid joints.

Since the parameters of the study are chosen so that the different failure mechanism can occur, the reasons and the specific development of the failure mechanisms are presented and discussed by observing the results of the finite element analysis. The development of failure mechanisms and bolt forces both in in-plane and in out-of-plane bending are studied in subsection 5.3. Especially the development of bolt forces has a significant role in determining the failure mechanism of the semi-rigid joints.

5.1 Moment-rotation response

In the following subsections, the moment-rotation characteristics are presented in both directions. As presented in subsection 4.4.2, although the finite element analysis was performed until Ansys solver was no longer able to converge a solution, the finite element results are plotted until the maximum plastic strain reaches 5 %. Since Eurocode 3 [1] does not provide any guidance on the rotational capacity of an end-plate splice as was discussed in subsection 3.6, the analytical results are plotted so that they fit conveniently to the same diagrams.

5.1.1 Moment-rotation response in in-plane bending

The results of the Eurocode based analytical model and the comparable results of the finite element analysis with non-preloaded bolts are presented in Table 5.1. The results of the finite element analysis of each loading condition are presented in Table 5.2. The values gathered in Table 5.1 and Table 5.2 are obtained as presented in subsection 4.4.2 in Fig. 4.20. All of the percentages shown in these tables are calculated by comparing the particular value to the corresponding value obtained with non-preloaded FE-analysis. The moment-rotation response in in-plane bending for each studied joint geometry and each loading case are shown in Fig. 5.1. The moment-rotation curves visualizing the impact of the thickness of the end-plates is presented in Appendix 6.

In general, with flush end-plate splices, the prediction of the initial stiffness according to Eurocode 3 [1] is significantly higher when compared to the result obtained with finite element analyses with all of the studied joint geometries. In Table 5.1, it can be seen, that with

the Eurocode based model, the initial rotational stiffness is estimated to be 120 % higher than the comparable FE-result on average of the studied joint geometries.

Even though the Eurocode based model over-predicts the initial stiffness in each studied joint configuration, it appears to marginally under-estimate the design moment resistance of the joint. As seen in Table 5.1, the prediction of the design moment resistance is 8 % lower with studied joint geometries on average. In the experiments conducted by Broderick and Thomson [6], similar results were obtained for flush end-plate joints for beam-to-column connections. They found that with some geometries, the Eurocode based prediction over-estimated the initial stiffness by as much as 200 %. The under-estimation of the moment capacities varied between 40-55 %. Although this experiment was performed with relatively thin end-plates that had only two horizontal bolt rows, the experiment in [6] and the results found in this thesis indicate that the standardized analytical model consistently over-estimates the initial stiffness and under-estimates the moment capacity for flush end-plates joints, both with beam-to-column and beam-to-beam connections.

Although there are some significant discrepancies between the finite element and analytical results, as seen in Table 5.1, the Eurocode based model succeeds to predict the correct failure mechanism with all of the studied joint geometries. It is also significant, that by applying the design rule for additional reduction for an individual bolt row as presented in subsection 3.4.1, the analytical model is able to predict that with small bolts, the thickening of the end-plates does not offer a notable increase in design bending resistance. In fact, according to the design code and with M24 bolts, the maximum resistance is obtained already with 20 mm end-plates. With M30 bolts, the maximum capacity is reached with 30 mm end-plates. Without the additional reduction rule, the Eurocode based design moment resistance would be significantly over-estimated.

Table 5.1 The initial stiffness $S_{j,ini}$ and the design moment resistance $M_{pl,Rd}$ obtained with the finite element and the Eurocode (EC) based analytical models in in-plane bending. The results of the finite element model are obtained from the moment-rotation characteristics as presented in subsection 4.4.2. The percentages are calculated by comparing the particular value to the corresponding value obtained with non-preloaded FE-analysis.

	FEM			EC				
	Non-preloaded bolts							
	$S_{j,ini}$ [kNm / °]	$M_{pl,Rd}$ [kNm]	Failure mechanism	$S_{j,ini}$ [kNm / °]		$M_{pl,Rd}$ [kNm]		Failure mechanism
EPS1	439	177	2	845	193 %	167	95 %	2
EPS2	666	198	2	1501	225 %	175	89 %	2
EPS3	985	198	3	2210	224 %	175	89 %	3
EPS4	1117	218	3	2403	215 %	175	81 %	3
EPS5	516	207	1	899	174 %	203	98 %	1
EPS6	725	288	2	1720	237 %	273	95 %	2
EPS7	1121	288	3	2927	261 %	279	97 %	3
EPS8	1371	302	3	3157	230 %	279	92 %	3
AVG					220 %		92 %	

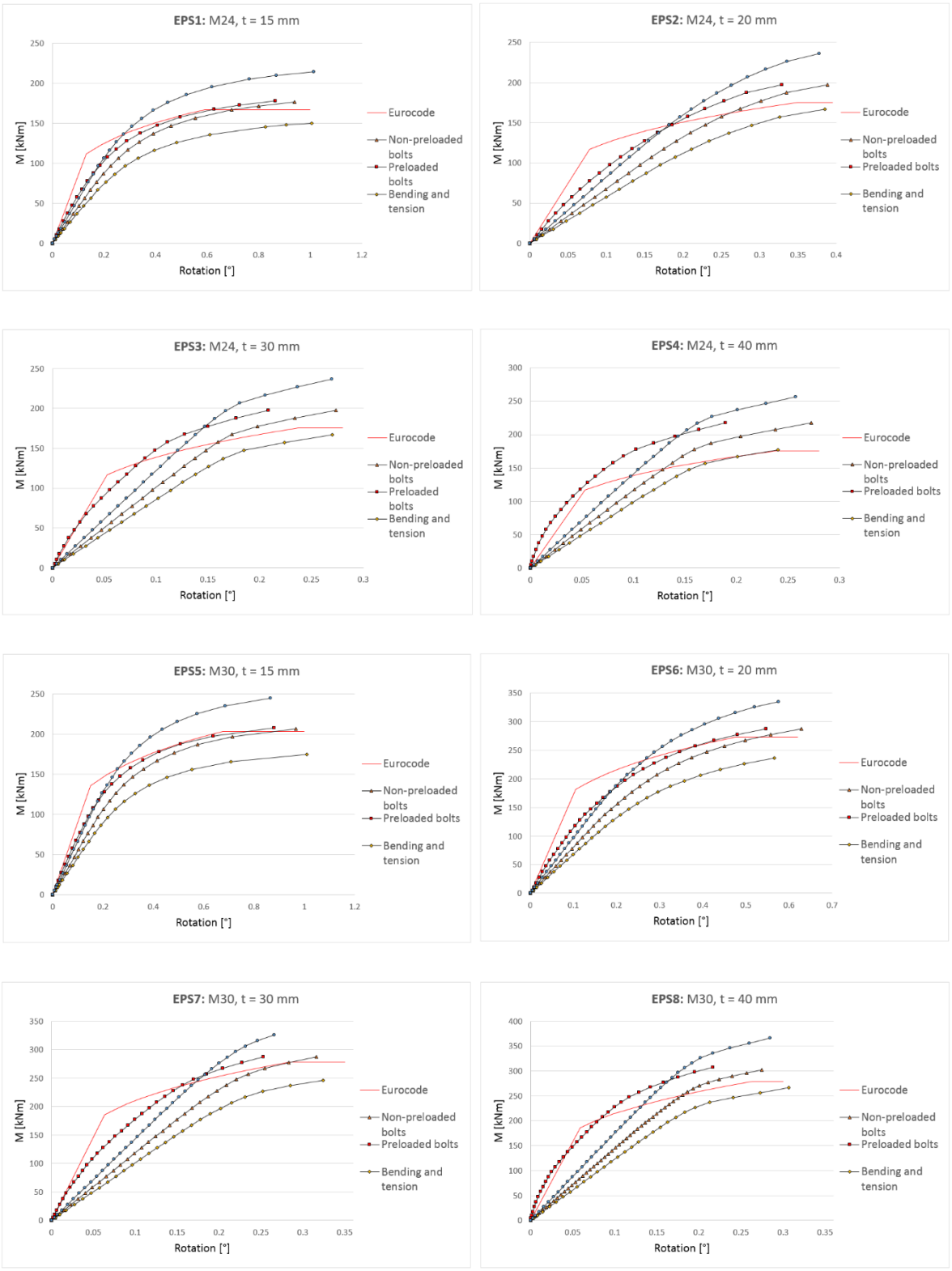

Fig. 5.1 Moment-rotation curves in in-plane bending for parametrizations EPS 1-8. The results are plotted until the maximum plastic strain reaches 5 %. Models 1-4 are with M24 bolts and models 5-8 with M30 bolts. In each diagram, the particular geometry is studied in pure bending with non-preloaded and preloaded bolts. The analysis of combined bending and tension and combined bending and compression are performed with non-preloaded bolts.

In the results of the finite element analysis, it appears that the thickening of the end-plates does not offer any improvement to the moment capacity between thicknesses 20 mm and 30 mm, whereas the effect on the initial stiffness of the joint is almost an additional 50 % with both bolt sizes. Another notable characteristic is that the initial stiffness of the joint is not proportionally increased by the thickening of the end-plates. This is due to the fact, that by thickening the end-plates, the elongation length of the bolts increases significantly and thereby the stiffness of the bolts is considerably reduced.

The finite element results with different loading cases in in-plane bending are presented in Table 5.2. From Table 5.2 and Fig. 5.1 it can be seen, that preloading of the bolts does not give an additional contribution to the design bending resistance, but instead it increases the initial stiffness by 51 % on average with the studied joint geometries. According to obtained values, preloading is more effective with thicker end-plates and with smaller M24 bolts. This indicates, that preloading is most effective when the relative stiffness of the end-plates is significantly higher than that of the bolts. It was found that the initial stiffness of the joint is not enhanced by increasing the preloading values above those values recommended in Eurocode 3 [1].

As seen in Table 5.2 and in Fig. 5.1, the combined loading cases also seem to have a significant impact on the joint characteristics. Due to the limitations in Eurocode 3 [1], the moment-rotation response of an end-plate splice cannot be calculated for combined bending and axial loading. With combined bending and tensile load, the initial stiffness as well as the moment capacity are weakened compared to the pure bending case. As presented in Table 5.2, the tension load decreased the initial stiffness by 15 % and the bending capacity by 16 % on average. By contrast, combined bending and compression has a contrarian impact on the joint behavior. The compressive axial load increased the initial stiffness of the end-plate splice by 23 % on average and the bending capacity by 19 % on average. A similar effect is present with base plate joints of columns [1,57]. Urbonas and Daniunas [9,10] performed finite element analysis on beam-to-beam flush end-plate splices with two horizontal bolt rows and they also found that the tensile axial load deducts both the stiffness and the resistance of the splice whereas the compressive axial load increases them.

Table 5.2 The results of the finite element analysis in in-plane bending in different loading cases. Transversal and axial loads are both ramped gradually starting from zero. The results of the finite element model are obtained from the moment-rotation characteristics as presented in subsection 4.4.2. The percentages are calculated by comparing the particular value to the corresponding value obtained with non-preloaded FE-analysis.

	FEM													
	Non-preloaded bolts		Preloaded bolts				Bending + Tension				Bending + Compression			
	$S_{j,ini}$ [kNm / °]	$M_{pl,Rd}$ [kNm]	$S_{j,ini}$ [kNm / °]		$M_{pl,Rd}$ [kNm]		$S_{j,ini}$ [kNm / °]		$M_{pl,Rd}$ [kNm]		$S_{j,ini}$ [kNm / °]		$M_{pl,Rd}$ [kNm]	
EPS1	439	177	586	134 %	178	101 %	357	81 %	150	85 %	531	121 %	214	121 %
EPS2	666	198	933	140 %	198	100 %	556	84 %	167	84 %	810	122 %	246	125 %
EPS3	985	198	1639	166 %	198	100 %	832	84 %	167	85 %	1202	122 %	237	120 %
EPS4	1117	218	2064	185 %	218	100 %	956	86 %	177	81 %	1377	123 %	256	118 %
EPS5	516	207	685	133 %	208	100 %	451	87 %	175	85 %	643	124 %	244	118 %
EPS6	725	288	1051	145 %	288	100 %	597	82 %	236	82 %	919	127 %	335	117 %
EPS7	1121	288	1694	151 %	288	100 %	977	87 %	246	86 %	1402	125 %	326	113 %
EPS8	1371	302	2114	154 %	308	102 %	1161	85 %	266	88 %	1674	122 %	366	121 %
AVG				151 %		100 %		85 %		84 %		123 %		119 %

5.1.2 Moment-rotation response in out-of-plane bending

The results of the Eurocode based analytical model and the comparable results of the finite element analysis in out-of-plane bending and with non-preloaded bolts are presented in Table 5.3. The results of the finite element analysis of each loading condition are presented in Table 5.4. The values gathered in Table 5.3 and Table 5.4 are obtained as presented in subsection 4.4.2 in Fig. 4.20. The moment-rotation curves in out-of-plane bending for each studied joint geometry and each loading case are shown in Fig. 5.2. The moment-rotation curves visualizing the impact of the thickness of the end-plates is presented in Appendix 7.

As Eurocode 3 [1] only provides clear design rules for end-plate splices in in-plane bending, the analytical model used for out-of-plane bending in this thesis is formed by logically assembling all of the active components. The accuracy of the analytical model in out-of-plane bending compares quite similarly to the in-plane model. As seen in Table 5.3, the initial stiffness is significantly over-estimated with thicker end-plates and the design bending resistance is under-estimated with M24 bolts to some extent. The error of the initial stiffness with 15 mm end-plates is very marginal, but it increases rapidly with thicker end-plates. The under-estimation of the design bending resistance also increases with thicker end-plates and M24 bolts.

Although the bending resistance is under-estimated with M24 bolts, with M30 bolts, the bending resistance is slightly over-estimated, as presented in Table 5.3. Interestingly, with M30 bolts and 15 mm or 20 mm end-plates, the design bending resistance is over-estimated only by 3,5 % on average. With M30 bolts and 30 mm end-plates, the analytical model over-estimates the bending resistance significantly and the prediction for the resistance is even bigger than that of EPS8 with 40 mm end-plates. This is a significant deviation from the other results. This deviation occurs, because the criteria for the additional reduction factor presented in 3.4.1 is not strict enough to work properly with this joint geometry in out-of-plane bending. With the studied joint geometries in out-of-plane bending, the additional reduction factor is only activated with 40 mm plates. This is a clear fault in the model, but the standard does not offer enough information to fix this.

Table 5.3 The initial stiffness $S_{j,ini}$ and design moment resistance $M_{pl,Rd}$ obtained with the finite element and the Eurocode based analytical models in out-of-plane bending. The results of the finite element model are obtained from the moment-rotation characteristics as presented in subsection 4.4.2. The percentages are calculated by comparing the particular value to the corresponding value obtained with non-preloaded FE-analysis.

	FEM			EC				
	Non-preloaded bolts							
	$S_{j,ini}$ [kNm / °]	$M_{pl,Rd}$ [kNm]	Failure mechanism	$S_{j,ini}$ [kNm / °]		$M_{pl,Rd}$ [kNm]		Failure mechanism
EPS1	168	118	2	170	101 %	107	91 %	2
EPS2	236	141	2	354	150 %	125	89 %	2
EPS3	345	154	3	730	212 %	127	83 %	3
EPS4	422	173	3	878	208 %	127	74 %	3
EPS5	195	129	1	245	125 %	135	104 %	1
EPS6	255	177	2	485	190 %	182	103 %	2
EPS7	382	198	3	879	230 %	225	114 %	3
EPS8	482	228	3	972	202 %	203	89 %	3
AVG					177 %		93 %	

As Table 5.1 and Table 5.3 show, the errors of the analytical calculations increase both in in-plane and in out-of-plane bending, when the relative stiffness of the end-plate is high compared to the stiffness of the bolts. Obviously, when the stiffness and resistance of the end-plate is more dominant compared to those of the bolts, the erroneous contribution from the end-plates affects more the analytical results of the whole joint. This indicates, that the errors in stiffness and resistance calculations are caused by erroneous yield line patterns in the end-plates. Although the analytical out-of-plane model has some significant discrepancies compared to the numerical results and although it is not officially determined in the design standards, it can be used in the preliminary design of end-plate splices, regarding that the final design is always verified with other approved design procedures.

The finite element results with different loading cases in out-of-plane bending are presented in Table 5.4. Similarly, as with in-plane bending, the preloading of the bolts increases the initial stiffness of the joint, without giving additional bending capacity. The effect of preloading is more effective with thicker end-plates and on average, the increase is 29 % with the studied joint geometries. Although preloading is beneficial for the joint stiffness also in out-plane bending, it appears that preloading is not as effective in out-of-plane bending as it is with in-plane bending. The effect of the level of preloading was also studied with out-of-plane bending and it was found that already the Eurocode based values are enough to obtain the maximum initial rotational stiffness for the joint.

The impact of combined axial loading and bending was studied also with out-of-plane bending and the results are very similar compared to those of in-plane bending. As illustrated in Fig. 5.2, the tensile axial loading reduces the initial stiffness and the moment resistance of the end-plate splice and the compressive axial loading has a contrarian effect on both values. As presented in Table 5.4, although preloading of the bolts seems to be more effective with thick end-plates, it appears that when the joint is under combined bending and axial tension or compression, the stiffness and the resistance of the joint are more affected with thin end-plates.

Table 5.4 The results of the finite element analysis in out-of-plane bending in different loading cases. Transversal and axial loads are both ramped gradually starting from zero. The results of the finite element model are obtained from the moment-rotation characteristics as presented in subsection 4.4.2. The percentages are calculated by comparing the particular value to the corresponding value obtained with non-preloaded FE-analysis.

	FEM													
	Non-preloaded bolts		Preloaded bolts				Bending + Tension				Bending + Compression			
	$S_{j,ini}$ [kNm / °]	$M_{pl,Rd}$ [kNm]	$S_{j,ini}$ [kNm / °]		$M_{pl,Rd}$ [kNm]		$S_{j,ini}$ [kNm / °]		$M_{pl,Rd}$ [kNm]		$S_{j,ini}$ [kNm / °]		$M_{pl,Rd}$ [kNm]	
EPS1	168	118	205	122 %	120	102 %	150	89 %	108	92 %	179	107 %	130	110 %
EPS2	236	141	298	127 %	141	100 %	216	91 %	133	94 %	266	113 %	158	112 %
EPS3	345	154	469	136 %	154	100 %	314	91 %	140	91 %	379	110 %	168	109 %
EPS4	422	173	601	143 %	173	100 %	379	90 %	140	81 %	466	111 %	187	108 %
EPS5	195	129	242	124 %	133	103 %	176	90 %	120	93 %	218	112 %	143	111 %
EPS6	255	177	307	120 %	188	106 %	238	93 %	172	98 %	292	114 %	191	108 %
EPS7	382	198	501	131 %	188	95 %	349	91 %	185	94 %	421	110 %	209	106 %
EPS8	482	228	623	129 %	228	100 %	442	92 %	215	94 %	531	110 %	239	105 %
AVG				129 %		101 %		91 %		92 %		111 %		109 %

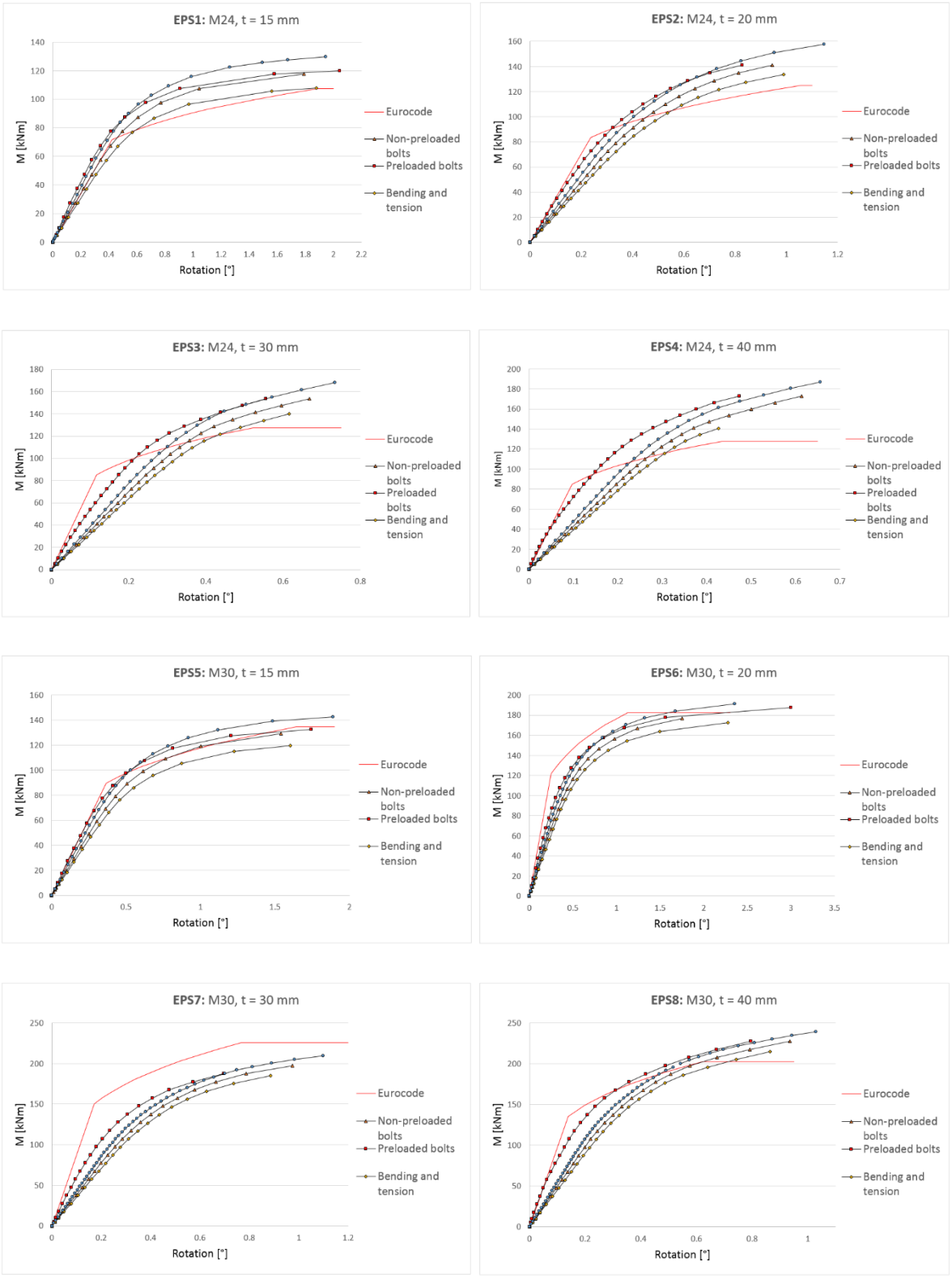

Fig. 5.2 Moment-rotation curves in out-of-plane bending for parametrizations EPS 1-8. The results are plotted until the maximum plastic strain reaches 5 %. Models 1-4 are with M24 bolts and models 5-8 with M30 bolts. In each diagram, the particular geometry is studied in pure bending with non-preloaded and preloaded bolts. The combined bending and tension and combined bending and compression are performed with non-preloaded bolts.

In most of the cases, the elastic part of the rotation characteristics can be easily determined by observing the linear part of the moment-rotation curves. However, with some preloaded cases, the linear part is very short and the joint starts to behave non-linearly already with relatively low bending moments. Such short elastic range can be seen in Fig. 5.2, especially with preloaded EPS4 and EPS8 configurations, which are both with 40 mm end-plates. The narrow elastic response of the joint is due to the fact that because of the thick end-plates, the relative stiffness of the preloaded bolts is very low compared to that of the end-plates.

5.1.3 Effect of the level of axial loading

The level of axial loading was kept constant in all of the studied joint configurations in the previous two subsections. However, to see how the level of axial loading affects to the resistance and stiffness of the joint, another analysis was performed with EPS6 parametrization. In the comparative analysis the axial loading was doubled from 500 kN to 1000 kN both with tensile and compressive loading cases. The transversal and axial loads were both applied simultaneously starting from zero.

The moment-rotation curves of this study are presented in Fig. 5.3. Especially in in-plane bending, the higher level of axial compressive loading increased both the stiffness and the resistance of the joint even more compared to the original axially loaded case. With higher tensile load, both values are decreased to some extent, but the values are not as significantly affected as with higher compressive loading. In out-of-plane bending, the stiffness is slightly increased with the higher compressive load and slightly reduced with higher tensile load. Differently than in in-plane bending, the higher axial loads have no significant effect on the resistance of the joint compared to original axial loading cases in out-of-plane bending. Again, the behavior is similar to that of the base plate joints, as according to Eurocode 3 [1], a more dominant compressive axial force further increases the joint stiffness and by contrast, a more dominant tensile axial force further reduces the joint stiffness.

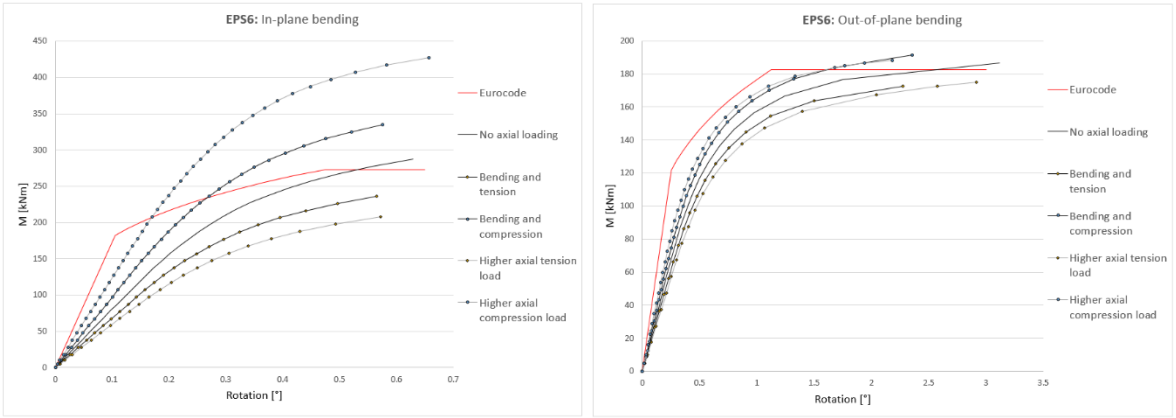

Fig. 5.3 The effect of the level of axial loading with EPS6 joint. Axial loading in these magnified cases is $F_A = 1000$ kN whilst originally it was 500 kN. In comparison, also the original moment-rotation curves with $F_A = 500$ kN and the case without axial loading, as well as the Eurocode based curves, are presented in the same diagrams.

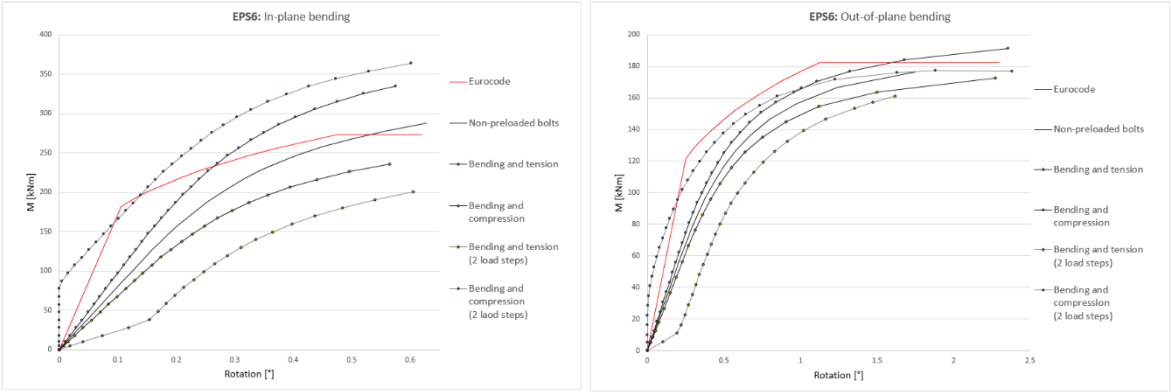

Fig. 5.4 The moment-rotation curves, when the joint is axially loaded before any bending occurs. The axial load in first load step is 500 kN both in tensile and compressive cases. In comparison, also the original moment-rotation curves with and without the axial loading as well as the Eurocode based curves are presented in the same diagrams.

As presented in subsection 4.3, it is possible that the axial and transversal loads are not applied simultaneously, but so that the structure is axially loaded before bending occurs. To see how this affects the joint behavior, a comparative analysis is performed again with EPS6 model. The moment-rotation curves of this comparative study, in which the axial load is applied in the first load step and then kept constant during the second load step, are presented in Fig. 5.4.

Both in in-plane and in out-of-plane bending the differences are clearly visible. When the beam members are loaded with a compressive force before bending, the joint is completely rigid until the bending moment reaches 80 kNm in in-plane bending. In out-of-plane bending, the joint stays completely rigid until the bending moment reaches 35 kNm. As seen in Fig. 5.4, the opposite phenomenon occurs with the tensile axial load and the stiffness of the joint is significantly reduced with low bending moments in both directions. With the two-stepped loading configuration, while the joint is loaded with a compressive axial load, the moment capacity of the joint is increased and on the contrary, the capacity is decreased with a tensile axial load. The differences in the bending moment capacities are bigger in in-plane bending than in out-of-plane bending. In general, when the loads are applied in two steps, the behavior of the joint is significantly affected with relatively low bending moments.

5.1.4 Classification of the studied joint geometries

The Eurocode based classification of steel joints is presented in subsection 2.1. The classification of the studied joint geometries is presented in Table 5.5 for in-plane bending and in Table 5.6 for out-of-plane bending. In both tables, the classification is performed by using the beam span of $L_b = 10$ m and it should be noted, that the shorter the beam span, the higher the criteria for rigid joints. Tables include both the classification by strength and the classification by stiffness.

Although the values of the bending moment capacities of different models deferred to some extent in in-plane bending, as can be seen in Table 5.5, the classification of the joint by strength is the same between the Eurocode based analytical values, numerical results with non-preloaded bolts, numerical results with preloaded bolts and the numerical results with combined bending and tension. This is due to the fact, that the classification limits for the

strength of the joints are really wide. With combined bending and compression, all other joint geometries except EPS1 are classified by strength as *partial strength*. As expected, a *full strength* joint is not achieved with any of the joint geometries, since the criteria for *full strength* joints is relatively difficult to obtain with practical joint geometries.

As can be expected, since there were significant differences in the initial stiffness of different models and loading configurations, also the classification by stiffness varies quite notably. The Eurocode based initial stiffness leads to more rigid classification as can be seen by comparing the classification by Eurocode based values and the values obtained with non-preloaded numerical models in Table 5.5. The classification is the same between Eurocode based values and the preloaded numerical values in all joint geometries except with the joints that are built with 20 mm end-plates. Quite notably, the combined bending and compression leads to almost as stiff classification as preloaded bolts, whereas all joint geometries with combined bending and tension are classified only as *semi-rigid*.

As presented in Table 5.6, the classification of the studied joint geometries in out-of-plane bending is less varied than in in-plane bending. All joint geometries in out-of-plane bending, according to the Eurocode based values and the numerical values in all loading conditions are classified by strength as *partial strength*. The classification by stiffness for all joint configurations is *rigid* with 30 mm and 40 mm end-plates. A notable factor in Table 5.6 is that the classification by stiffness is the same based on Eurocode values, the preloaded numerical results and the numerical results with combined bending and compression. The classification by stiffness is the same in pure bending and in combined bending and tension with non-preloaded bolts.

Although the moment capacities and the stiffness of the joint geometries are significantly lower in out-of-plane bending than in in-plane bending, it appears that the jointed structure is not as strongly affected by the joint assembly in out-plane bending as it is in in-plane bending. This is due to the fact that the difference between the stiffness of the beam in-plane and out-of-plane bending is higher in value than the difference between the stiffness of the joint between the two directions.

Table 5.5 The classification of the studied joint geometries in in-plane bending and with a beam span of $L_b = 10$ m. The table includes both the classification by strength and the classification by stiffness according to Eurocode 3 [1].

	EC		Non-preloaded bolts		Preloaded bolts		Bending + Tension		Bending + Compression	
	Classification		Classification		Classification		Classification		Classification	
	by strenght	by stiffness	by strenght	by stiffness	by strenght	by stiffness	by strenght	by stiffness	by strenght	by stiffness
EPS1	Pinned	Semi-rigid	Pinned	Semi-rigid	Pinned	Semi-rigid	Pinned	Semi-rigid	Pinned	Semi-rigid
EPS2	Pinned	Rigid	Pinned	Semi-rigid	Pinned	Semi-rigid	Pinned	Semi-rigid	Partial strenght	Semi-rigid
EPS3	Pinned	Rigid	Pinned	Semi-rigid	Pinned	Rigid	Pinned	Semi-rigid	Partial strenght	Semi-rigid
EPS4	Pinned	Rigid	Pinned	Semi-rigid	Pinned	Rigid	Pinned	Semi-rigid	Partial strenght	Rigid
EPS5	Pinned	Semi-rigid	Pinned	Semi-rigid	Pinned	Semi-rigid	Pinned	Semi-rigid	Partial strenght	Semi-rigid
EPS6	Partial strenght	Rigid	Partial strenght	Semi-rigid	Partial strenght	Semi-rigid	Partial strenght	Semi-rigid	Partial strenght	Semi-rigid
EPS7	Partial strenght	Rigid	Partial strenght	Semi-rigid	Partial strenght	Rigid	Partial strenght	Semi-rigid	Partial strenght	Rigid
EPS8	Partial strenght	Rigid	Partial strenght	Rigid	Partial strenght	Rigid	Partial strenght	Semi-rigid	Partial strenght	Rigid

The results above show that although an end-plate splice for HEA400 profile and with M24 bolts can achieve relatively high values for the stiffness, the strength of the joint is not sufficient. Also due to the relatively low strength of the bolts, the ductility of the joints with M24 bolts is rather low. Due to the very flexible end-plates of EPS5, it is also classified by strength as *pinned.* Now since the joint is connecting rather heavy members, the bolts and other geometrical parameters should be chosen accordingly. To maximize the ductility, strength and stiffness as well as to suitability in different loading conditions, the EPS6 model would be the preferable choice of the studied joint geometries. However, if it would be certain that the designed structure would always stay on the elastic zone and if the stiffness of the joint would be prioritized, then EPS7 or EPS8 could be chosen.

As seen in the previous subsection, by loading the structure axially before the bending moment, the initial stiffness and the capacity of the joints are strongly affected. This means that the classification of the joint geometries would be totally different than those presented in Table 5.5 and Table 5.6. However, in this thesis such loading conditions were only studied with EPS6 joint configuration and, thus, not as comprehensive classification tables can be conducted. According to the moment-rotation curves in the previous subsection, the assumption would be that by loading the structure axially before the bending moment, the classification would go towards the more rigid ones with combined bending and compression and towards more flexible ones with combined bending and tension.

By observing the joint classifications in Table 5.5 and Table 5.6 it seems that the rigid classification can only be obtained, when the determining failure mechanism is of type-3. The failure mechanisms are presented in subsection 3.2.1. This is a hypothesis presented in the guide for moment-resisting joints [12] and it makes the design of moment-resisting joints rather difficult. The problem is that usually a fragile failure mechanism should be avoided, but on the other hand the stiffness of the joint should be maximized to guarantee the stability of the structure.

Table 5.6 The classification of the studied joint geometries in out-of-plane bending and with a beam span of $L_b = 10$ m. The table includes both the classification by strength and the classification by stiffness according to Eurocode 3 [1].

	EC		Non-preloaded bolts		Preloaded bolts		Bending + Tension		Bending + Compression	
	Classification		Classification		Classification		Classification		Classification	
	by strenght	by stiffness	by strenght	by stiffness	by strenght	by stiffness	by strenght	by stiffness	by strenght	by stiffness
EPS1	Partial strenght	Semi-rigid	Partial strenght	Semi-rigid	Partial strenght	Semi-rigid	Partial strenght	Semi-rigid	Partial strenght	Semi-rigid
EPS2	Partial strenght	Rigid	Partial strenght	Semi-rigid	Partial strenght	Rigid	Partial strenght	Semi-rigid	Partial strenght	Rigid
EPS3	Partial strenght	Rigid	Partial strenght	Rigid	Partial strenght	Rigid	Partial strenght	Rigid	Partial strenght	Rigid
EPS4	Partial strenght	Rigid	Partial strenght	Rigid	Partial strenght	Rigid	Partial strenght	Rigid	Partial strenght	Rigid
EPS5	Partial strenght	Semi-rigid	Partial strenght	Semi-rigid	Partial strenght	Semi-rigid	Partial strenght	Semi-rigid	Partial strenght	Semi-rigid
EPS6	Partial strenght	Rigid	Partial strenght	Rigid	Partial strenght	Rigid	Partial strenght	Semi-rigid	Partial strenght	Rigid
EPS7	Partial strenght	Rigid	Partial strenght	Rigid	Partial strenght	Rigid	Partial strenght	Rigid	Partial strenght	Rigid
EPS8	Partial strenght	Rigid	Partial strenght	Rigid	Partial strenght	Rigid	Partial strenght	Rigid	Partial strenght	Rigid

5.2 Behavior in inelastic zone

The behavior of the joint geometries in the inelastic zone is studied by calculating the ductility and resistance ratios for each joint geometry. The ductility and the resistance ratios of the studied joint geometries are presented is subsection 5.2.1. The inelastic zone, as well as the ductility and resistance ratios are defined in subsection 4.4.2. As discussed is section 3, the Eurocode 3 does not provide clear design rules for determining the ultimate rotation capacity of a flush end-plate splice. Therefore, the rotation capacities of each joint geometry are studied in this section in all of the loading cases. The criteria for the ultimate rotation capacity is determined in subsection 4.4.2.

5.2.1 Ductility and resistance ratios

The ductility and resistance ratios of the studied cases are presented in Table 5.7 for in-plane bending and in Table 5.8 for out-of-plane bending. The effects of the loading conditions on the ductility and on the resistance ratios of the joints are visualized in Fig. 5.5 for in-plane bending and in Fig. 5.6 for out-of-plane bending.

From the tables and the diagrams, it can be seen that preloading of the bolts increases the ductility of the joints both in in-plane and in out-of-plane bending. As seen in subsections 5.1.1 and 5.1.2, with preloaded bolts, the yield rotations are relatively low when compared to the cases with non-preloaded bolts. This means that the range from the yield rotation to the ultimate rotation is relatively long, which can explain the large increases in the ductility ratios of preloaded cases. As seen in Table 5.7, preloading of the bolts also increases the resistance ratios of the joints in in-plane bending. However, as presented in Table 5.8, preloading decreases the resistance ratio by 6 % on average in out-of-plane bending.

The additional axial load has only minor changes to the ratios in in-plane bending, as tensile load slightly decreases and compressive load slightly increases both ratios. In out-of-plane bending, the axial load has more influence as the tensile load decreases the average ductility ratio by almost 10 % on average and the compressive load increases the average ductility ratio by as much as 26 %, as presented in Table 5.8.

An important aspect to notice from Table 5.7 and Table 5.8, is that the thickening of the end-plates significantly decreases both the ductility and the resistance ratios. For example, in in-plane bending with M24 bolts, the ductility ratio is reduced to about 1/3 of the original, when the end-plate is changed from 15 mm to 40 mm. In out-of-plane bending, the reduction of the ductility is not as significant, but it is still very disadvantageous for the ductile behavior of the joint.

Fig. 5.5 The ductility and the resistance ratios of the studied joint geometries in in-plane bending. The ratios are calculated as presented in subsection 4.4.2.

Table 5.7 The ductility and resistance ratios of the studied joint geometries in in-plane bending. Percentages are calculated by comparing the particular value to that of the same joint geometry with non-preloaded bolts.

	Non-preloaded bolts		Preloaded bolts				Bending + Tension				Bending + Compression			
	Ductility Ratio	Resistance Ratio	Ductility Ratio		Resistance Ratio		Ductility Ratio		Resistance Ratio		Ductility Ratio		Resistance Ratio	
EPS1	4.76	2.04	7.50	158 %	2.63	129 %	4.15	87 %	1.74	85 %	5.07	106 %	2.02	99 %
EPS2	2.03	1.55	3.15	155 %	2.03	131 %	1.83	90 %	1.42	92 %	2.40	119 %	1.67	108 %
EPS3	1.71	1.25	2.91	170 %	1.68	134 %	1.64	96 %	1.22	97 %	1.83	107 %	1.34	107 %
EPS4	1.71	1.23	2.65	155 %	1.47	120 %	1.56	91 %	1.20	98 %	1.80	105 %	1.30	106 %
EPS5	4.28	1.77	6.18	144 %	2.13	120 %	5.27	123 %	2.02	114 %	4.40	103 %	1.94	109 %
EPS6	2.31	1.46	3.89	169 %	1.95	134 %	1.91	83 %	1.33	92 %	2.56	111 %	1.62	111 %
EPS7	1.43	1.16	2.17	151 %	1.46	125 %	1.61	112 %	1.25	108 %	1.45	102 %	1.27	109 %
EPS8	1.42	1.14	1.85	130 %	1.24	109 %	1.57	110 %	1.17	103 %	1.55	109 %	1.19	105 %
AVG				154 %		125 %		99 %		99 %		108 %		107 %

Fig. 5.6 The ductility and resistance ratios of the studied joint geometries in out-of-plane bending. The ratios are calculated as presented in subsection 4.4.2.

Table 5.8 The ductility and resistance ratios of the studied joint geometries in out-of-plane bending. Percentages are calculated by comparing the particular value to that of the same joint geometry with non-preloaded bolts.

	Non-preloaded bolts		Preloaded bolts				Bending + Tension				Bending + Compression			
	Ductility Ratio	Resistance Ratio	Ductility Ratio		Resistance Ratio		Ductility Ratio		Resistance Ratio		Ductility Ratio		Resistance Ratio	
EPS1	5.22	2.04	7.30	140 %	2.09	102 %	4.93	94 %	1.89	92 %	4.50	86 %	1.67	82 %
EPS2	2.83	1.79	3.13	111 %	1.79	100 %	2.95	105 %	1.85	103 %	4.08	144 %	2.11	118 %
EPS3	2.52	1.68	2.67	106 %	1.58	94 %	2.13	84 %	1.54	92 %	2.84	113 %	1.71	102 %
EPS4	2.35	1.57	2.44	104 %	1.48	95 %	1.40	60 %	1.21	77 %	2.77	118 %	1.69	108 %
EPS5	5.09	2.18	7.35	144 %	2.30	105 %	5.02	99 %	2.12	97 %	6.64	131 %	2.30	105 %
EPS6	4.63	1.83	8.57	185 %	1.74	95 %	6.29	136 %	2.00	109 %	7.88	170 %	2.19	120 %
EPS7	3.81	2.03	2.97	78 %	1.60	79 %	3.19	84 %	1.91	94 %	4.68	123 %	2.12	105 %
EPS8	3.84	1.94	3.36	87 %	1.54	80 %	3.26	85 %	1.84	95 %	4.73	123 %	2.07	107 %
AVG				119 %		94 %		93 %		95 %		126 %		106 %

5.2.2 Rotation capacity

The ultimate rotations capacities of the studied joint geometries are presented in Table 5.9 for in-plane bending and in Table 5.10 for out-of-plane bending. In general, the rotation capacities in out-of-plane bending are higher than in in-plane bending. In in-plane bending as well as in out-of-plane bending, the ultimate rotation capacities are consistently in line with the ductility ratios when it comes to the influence of the end-plate thickness. The thickening of the end-plates decreases the rotation capacities, as in in-plane bending with all joint geometries, the ultimate rotation capacity is dropped to 1/3 when the end-plates are changed from 15 mm to 40 mm. Similar drop occurs also in out-of-plane bending with M24 bolts, but with M30 bolts, the drop is not as significant. This is again due to the fact that the joint behavior is more ductile when the relative stiffness and strength of the bolts is high compared to those of the end-plates. Another aspect which is in line with the ductility of the joints is that the rotation capacities with M30 bolts are higher than the rotation capacities with M24 bolts.

As was seen in Table 5.7, although preloaded bolts increased the ductility ratio in all of the studied joint configurations, it was noticed here, that the ultimate rotation capacities are actually reduced with preloaded bolts in in-plane bending. Table 5.9 shows that the average reduction of the rotation capacity is 18 % in in-plane bending. The different behavior of the out-of-plane bending can be seen in Table 5.10, as the reduction happened only with thick end-plates, as with thin end-plates, the rotation capacity is significantly increased with preloaded bolts. In cases with high ductility ratios and where significant reduction of rotation capacity occurred by preloading of the bolts, the phenomenon can be explained by relatively low yield rotations. The additional axial forces do not significantly affect the ultimate rotation capacities in in-plane bending. In out-of-plane bending, the situation is the same for cases loaded with bending and tension. However, as presented in Table 5.10, the compressive axial force increases the average rotational capacity by 16 % on average in out-of-plane bending.

Table 5.9 Ultimate rotation capacities θ_{pl} of the studied joint geometries in in-plane bending. The ultimate rotation capacities are defined as presented in subsection 4.4.2 and they are presented in degrees.

	Non-preloaded bolts	Preloaded bolts		Bending + Tension		Bending + Compression	
	θ_{pl} [°]	θ_{pl} [°]		θ_{pl} [°]		θ_{pl} [°]	
EPS1	0.94	0.86	92 %	1.01	107 %	1.01	108 %
EPS2	0.39	0.33	85 %	0.39	99 %	0.44	113 %
EPS3	0.27	0.21	76 %	0.27	99 %	0.27	99 %
EPS4	0.27	0.19	70 %	0.24	88 %	0.26	94 %
EPS5	0.97	0.88	91 %	1.01	104 %	0.86	89 %
EPS6	0.63	0.55	87 %	0.57	90 %	0.58	92 %
EPS7	0.32	0.25	80 %	0.32	103 %	0.27	84 %
EPS8	0.27	0.22	79 %	0.31	112 %	0.28	104 %
AVG			82 %		100 %		98 %

Table 5.10 Ultimate rotation capacities θ_{pl} of the studied joint geometries in out-of-plane bending. The ultimate rotation capacities are defined as presented in subsection 4.4.2 and they are presented in degrees.

	Non-preloaded bolts	Preloaded bolts		Bending + Tension		Bending + Compression	
	θ_{pl} [°]	θ_{pl} [°]		θ_{pl} [°]		θ_{pl} [°]	
EPS1	1.79	2.04	114 %	1.88	105 %	1.95	109 %
EPS2	0.94	0.83	88 %	0.99	105 %	1.15	121 %
EPS3	0.67	0.56	83 %	0.62	92 %	0.73	110 %
EPS4	0.61	0.47	77 %	0.43	70 %	0.66	107 %
EPS5	1.54	1.74	113 %	1.60	104 %	1.89	123 %
EPS6	1.75	3.00	171 %	2.27	130 %	2.35	134 %
EPS7	0.97	0.70	72 %	0.89	91 %	1.10	113 %
EPS8	0.94	0.79	85 %	0.86	92 %	1.03	110 %
AVG			100 %		99 %		116 %

5.3 Development of failure mechanisms

The development of the different failure mechanisms in in-plane and in out-of-plane bending are explained by using non-preloaded EPS5, EPS6 and EPS8 models as examples. The different parametrizations (EPS) of the parametric study are presented in Table 4.1. All of the example models in this section are built with M30 bolts and with EPS5 the end-plate thickness is 15 mm, with EPS6 20 mm and with EPS8 40 mm. Because of the different end-plate thicknesses, these models can be used for explaining the differences between the development of the three typical failure mechanisms predicted by Eurocode 3 [1]. The typical failure mechanisms were defined in subsection 3.2.1.

5.3.1 Development of failure mechanisms in in-plane bending

According to Eurocode 3 and as seen in Table 5.5, in in-plane bending EPS5 is classified by strength as *pinned* and by stiffness as *semi-rigid*. As seen in Table 5.1, the Eurocode prediction and the numerically attained failure mechanism for EPS5 is of type-1, so the failure is ductile and it is driven by the yielding of the end-plates. The Eurocode based classification for EPS6 model is *partial strength* by strength and *semi-rigid* by stiffness. The failure with EPS6 model is of type-2, so it occurs with the simultaneous yielding of the end-plates and the bolts. The most fragile failure mechanism occurs with EPS8 model and the Eurocode based classification both by strength and by stiffness is the same as with EPS6 model. The failure mechanism with EPS8 is of type-3 according to both Eurocode 3 and the numerical results.

The chosen joint geometries are suitable for visual observations on the development of the joint failure. By observing the development of the plastic strain in EPS5 and EPS8, it becomes clear that the failure is driven by end-plate yielding with EPS5 model and by bolt fracture with EPS8 model. Fig. 5.7 shows the plastic strain of the bolts with the three models. The deformation in this figure is exaggerated by a factor of 10. From the side view on the left it can be seen, that with EPS5 model, the elongation of the bolts is minimal whereas with EPS8 model, the elongation of the lowest bolt row is significant.

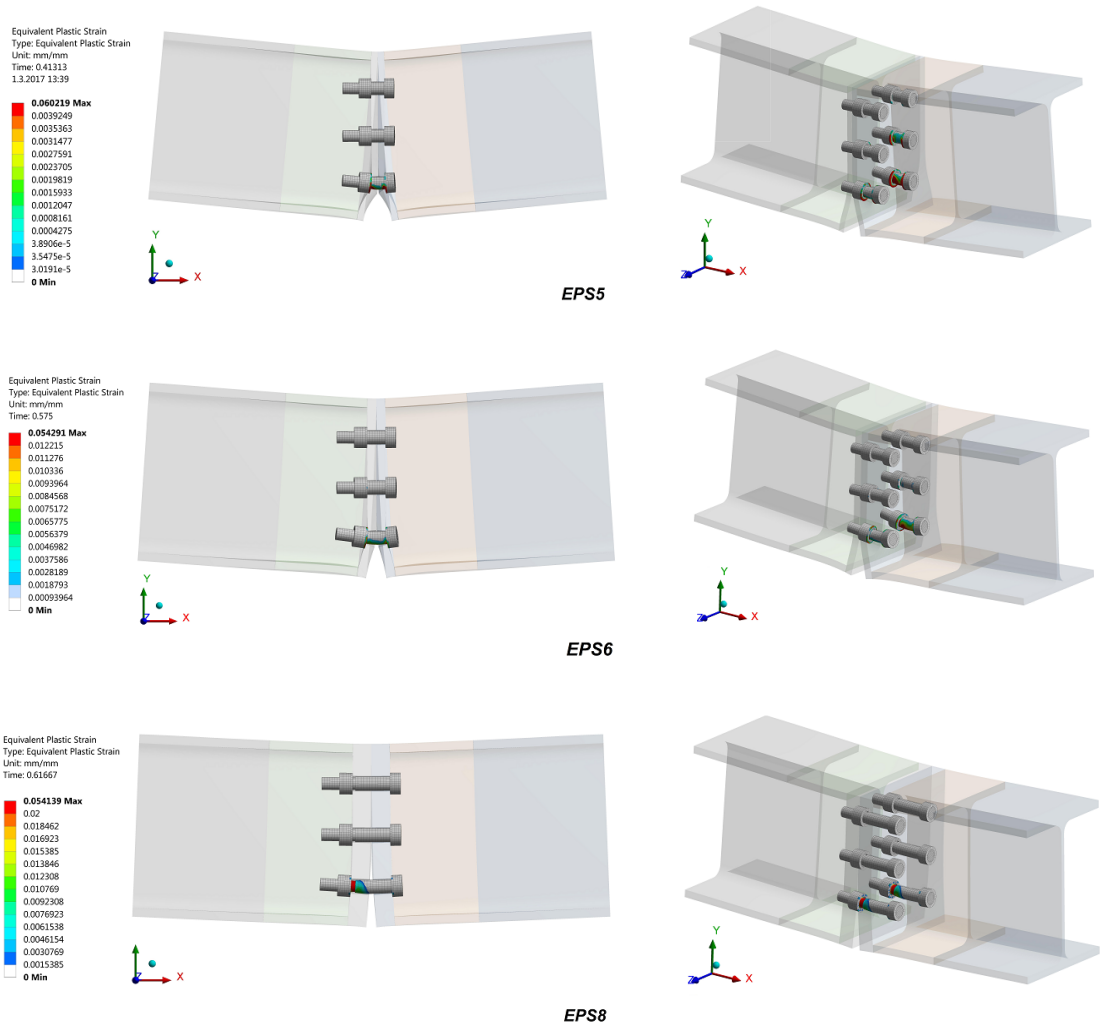

Fig. 5.7 The plastic strain of the bolts in EPS5, EPS6 and EPS8 models when the joints are loaded to the bending moment capacity in in-plane bending. The deformation is exaggerated by a factor of 10 to visualize the different deformation patterns.

Since the bolt elongation is very small with EPS5 model, the separation of the end-plates is minimal along the vertical bolt lines. With EPS8 model, the deformation of the end-plates is small and the deformation of the whole joint is mostly driven by the elongation of the bolts in the lowest bolt row. Fig. 5.7 also shows that when the EPS8 joint reaches its capacity, only one bolt row is truly plastified. Here, with EPS6, it can be seen that the failure is something between the two contrarian modes, since at the same time with the end-plate plastification, especially the lowest bolts undergo some significant elongation.

Different failure mechanisms, especially the different behavior of the end-plates causes some differences to the distribution of bolt forces. In Fig. 5.8, the distribution of the bolt forces is shown for models EPS5, EPS6 and EPS8. Bolts of different models are marked with different colors. Due to the varying lever arms of each bolt row, the bolt forces differ quite significantly from each other. However, not all of the bolt force differences can be explained by different lever arms. The magnitudes of the bolt forces are highly affected by two factors: one is the development of internal prying forces as presented in subsection 3.2.1 and the other is the ability of the joint to deform locally, so that the bolt forces are more evenly distributed between the different bolt rows.

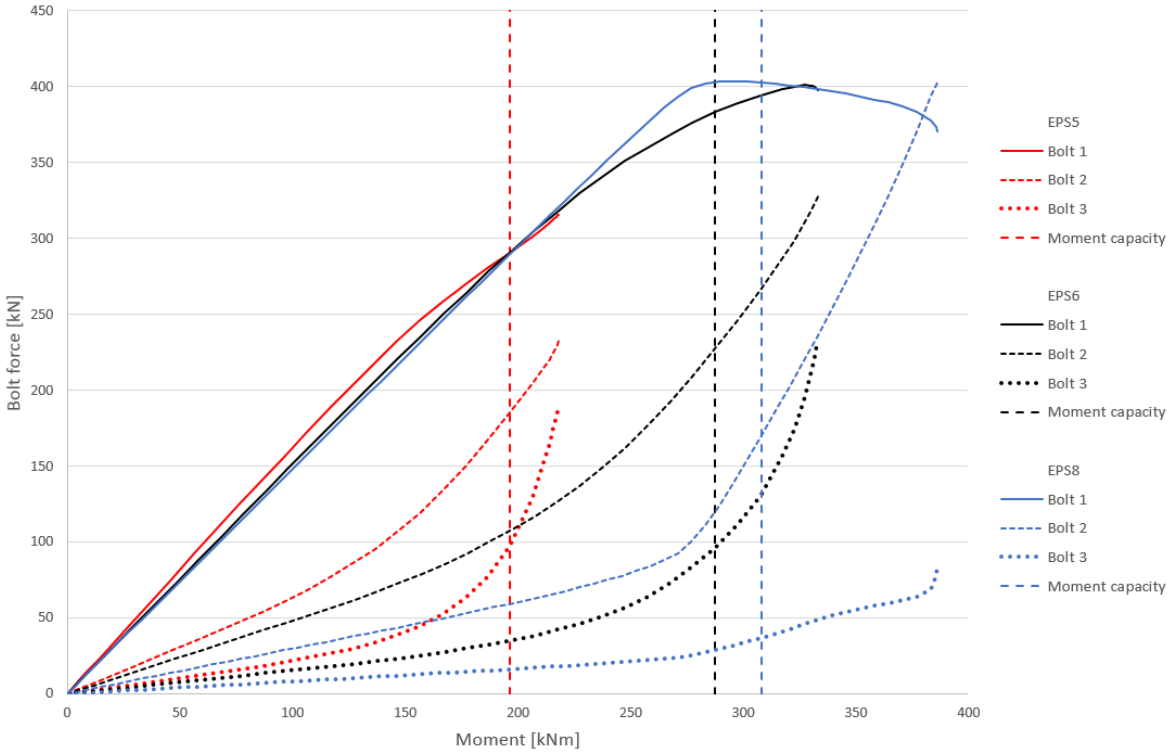

Fig. 5.8 The distribution of the bolt forces in EPS5, EPS6 and EPS8 models when the joints are loaded to the moment capacity in in-plane bending. Bolts 1, 2 and 3 refer to the bolts in vertical bolt rows and bolt row 1 is the furthest from the center of compression. The vertical dashed lines are indicating the bending moment capacities of each joint configuration.

More easily detectable feature is the prying force action. In Fig. 5.8 it can be seen, that the thinner the end-plates, the bigger the bolt forces are at the same bending moment. This phenomenon is especially clear with bolts 2 and 3. For example, when the bending moment $M_{Ed} = 100$ kNm, the bolt force in bolt 2 with EPS5 (dashed red line) is approximately 30 % higher than the same bolt force of EPS6 model (dashed black line). This is due to the fact that the failure mechanism of EPS5 is of type-1, which means that the failure is developed by the maximum internal prying forces as was defined in subsection 3.2.1. The prying action and the distribution of internal forces and moments of the T-stub of EPS5 are presented in Fig 5.9. With EPS6, the type-2 mechanism means that only some internal prying action occurs, so the bolt forces are smaller than with EPS5. As presented in subsection 3.2.1, with type-3 failure mechanism, there are no prying forces, so the smallest bolt forces of these three models occur with EPS8 model (blue lines). Again, by comparing the bolt force in bolt 2 of EPS6 (dashed black line) and the bolt force in bolt 2 of EPS8 (dashed blue line), it is noticed that the bolt force in EPS6 is approximately 40 % higher than that of EPS8 at $M_{Ed} = 100$ kNm.

Another important detail can be detected by comparing the bolt forces of an individual joint configuration. EPS8 with very thick end-plates is suitable for explaining this phenomenon, since by comparing the bolt forces of EPS8 model, it is noticed that the bolt force in bolt 1 (solid blue line) is notably higher than in bolt 3 (dotted blue line). The relative difference is significantly higher than the same difference with EPS5 (solid and dotted red lines), thus, the difference cannot be completely explained by the different lever arms.

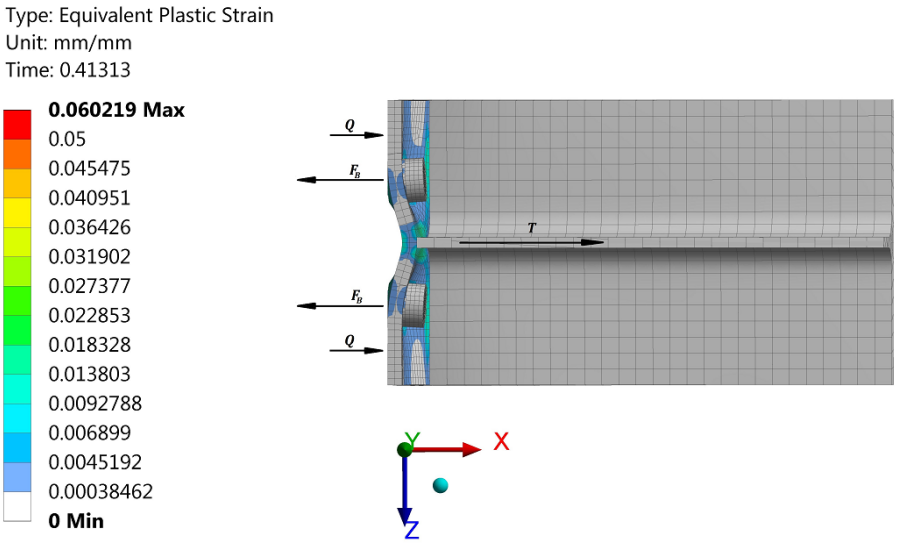

Fig. 5.9 The distribution of internal forces and moments in the T-stub flange of EPS5 in in-plane bending as presented in subsection 3.2.1. Plastic strain visualizes the locations of the plastic hinges. Q is the prying force, F_B is the bolt force and T is the tension force resultant for an individual T-stub.

The high difference between the bolt forces indicates that due to small local deformations in the end-plates, the EPS8 model fails to distribute the bolt forces to all bolts, but instead the redistribution of bolt forces occurs when the loading approaches the maximum capacity of the joint. The plastification of a single bolt row was also visualized in Fig. 5.7. In Fig. 5.8, the discontinuities of the bolt force curves of EPS8 model (solid and dashed blue lines) at about $M_{Ed} = 280$ kN represent the redistribution of bolt forces. A sudden redistribution of loads usually indicates that a complete fracture of an individual component occurred and it is not favorable for steel joints. A complete fracture of an individual component may cause an additional dynamic load for the joint and thereby a complete collapse of the structure.

The ductile behavior of the EPS5 model is clearly visible in Fig. 5.7, as the curves of the bolt forces (red lines) develop smoothly without any sudden discontinuities. Especially, since the bolt forces in bolt row 1 (solid red line) develop almost linearly until the bending capacity, it indicates that the most heavily loaded bolt is not even close to a fracture. Also EPS6 model seems to behave in a ductile manner, since all bolt force curves are smooth (black lines) without any discontinuities before the bending capacity. The first discontinuity with EPS6 model occurs when bolt 1 (solid black line) fractures at $M_{Ed} = 340$ kN, which is about 20 % above the maximum bending capacity. This is acceptable, since the fragile behavior of EPS6 joint occurs after the design capacity.

In Fig. 5.10, the different failure mechanisms are visualized by slicing the joints along bolt row 2 and illustrating the development of the plastic strain. With EPS5, it can be seen that the fully developed plastic hinges are formed at the root of the beam web as well as along the horizontal and vertical bolt lines. Especially on the left hand side, the four plastic hinges are clearly visible, which is characteristic to the ductile type-1 failure. The reason for the strong prying action is also clearly visible, since due to the plastic hinges, the end-plates get widely separated between the vertical bolt lines. With EPS6 model, instead of four, only two

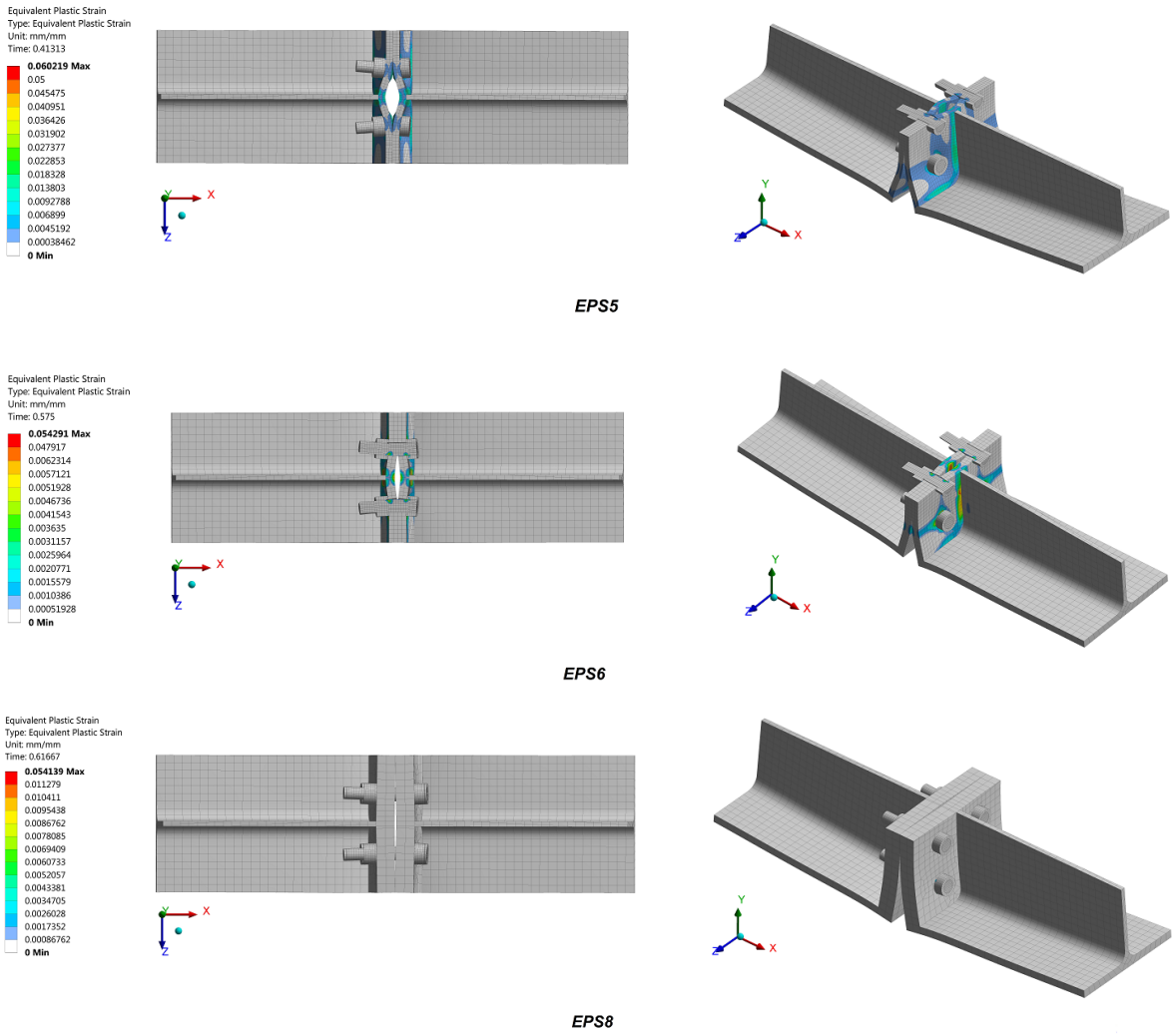

Fig. 5.10 The development of plastic hinges in in-plane bending, when the joints are loaded to the moment capacities. Due to the fully developed plastic hinges, great prying forces occur with EPS5 and EPS6 models. With EPS8, the vertical edges of the end-plates get separated, so there are no internal prying forces. The deformations are exaggerated by a factor of 10 for EPS5 and EPS6 and by a factor of 20 for EPS8.

plastic hinges are formed at the root of the beam web. The fragile failure mechanism of EPS8 model can also be verified by observing Fig. 5.10, since no plastic hinges are formed and the vertical edges of the end-plates get separated. The separation of the edges guarantees that there are no internal prying forces. The development of the plastic hinges and thereby the failure mechanism of these three models corresponds very closely to those presented in Fig. 3.5 in the theory section.

The plastic strains in the end-plates of EPS5, EPS6 and EPS8 models are shown in Fig. 5.11. The development of the yield line patterns appears to be similar to those predicted by Eurocode 3 [1] and presented subsection 3.4.1. The yield line pattern with EPS5 and EPS6

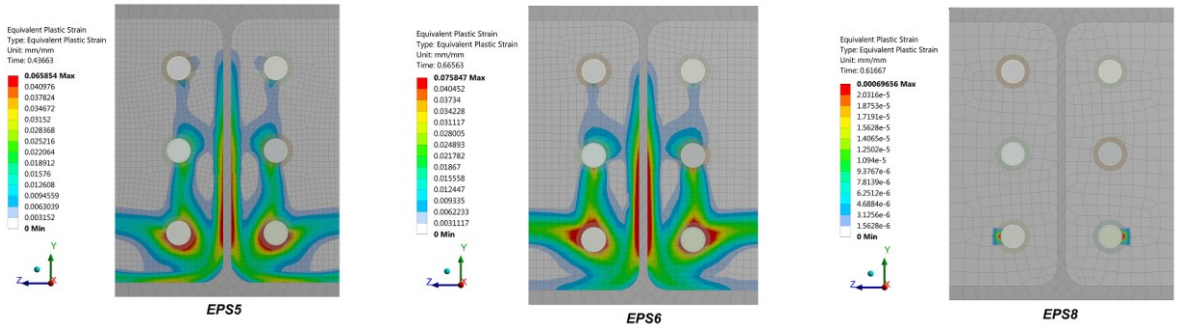

Fig. 5.11 The yield line patterns of EPS5, EPS6 and EPS8 joint configurations at a final converged solution point in in-plane bending. EPS5 and EPS6 have significant plastic strains in the end-plates whereas the end-plates of EPS8 stay on elastic zone.

indicate that the end-plates yield as a group of bolt rows and with non-circular patterns. The yield line patterns for EPS8 cannot be verified, since the end-plates stay on the elastic zone until the failure of the joint.

5.3.2 Development of failure mechanisms in out-of-plane bending

For the observation of the different failure mechanisms in out-of-plane bending, the same non-preloaded EPS5, EPS6 and EPS8 parametrizations are used as examples. As seen in Table 5.6, the Eurocode based classification by stiffness for EPS5 parametrization is *semi-rigid* and for EPS6 and EPS8 the classification is *rigid*. The classification by strength for all three example configurations is *partial strength*. Similarly, as in in-plane bending, the failure mechanism is of type-1 for EPS5, type-2 for EPS6 and type-3 for EPS8. The failure mechanisms of each joint geometry in out-of-plane bending can be seen in Table 5.3.

Fig. 5.12 is showing the plastic strain of the bolts in EPS5, EPS6 and EPS8 when the joints are loaded to the moment capacity in out-of-plane bending. The deformation in this figure is exaggerated by a factor of 10. By observing the development of the plastic strain in the bolts in the three different models, it becomes clear that with EPS5, the failure is driven by end-plate yielding and with EPS8, by the bolt fracture. From the side view on the left it can be seen, that similarly, as with in-plane bending, the elongation of the bolts is minimal with EPS5 model, whereas with EPS8 model, the lowest bolts get highly elongated.

As the bolt elongation is very small with EPS5 model, the separation of the end-plates is minimal along the vertical bolt lines. With EPS8 model, the deformation of the end-plates is small and the deformation of the whole joint is mostly driven by the elongation of the bolts in the lowest bolt row. Fig. 5.7 also shows that when the EPS8 joint reaches its moment capacity, only the two corner bolts are heavily plastified. Here, with EPS6, it can be seen that the failure is between the two opposite modes, since at the same time with the end-plate plastification, especially the lowest corner bolts undergo some significant elongation.

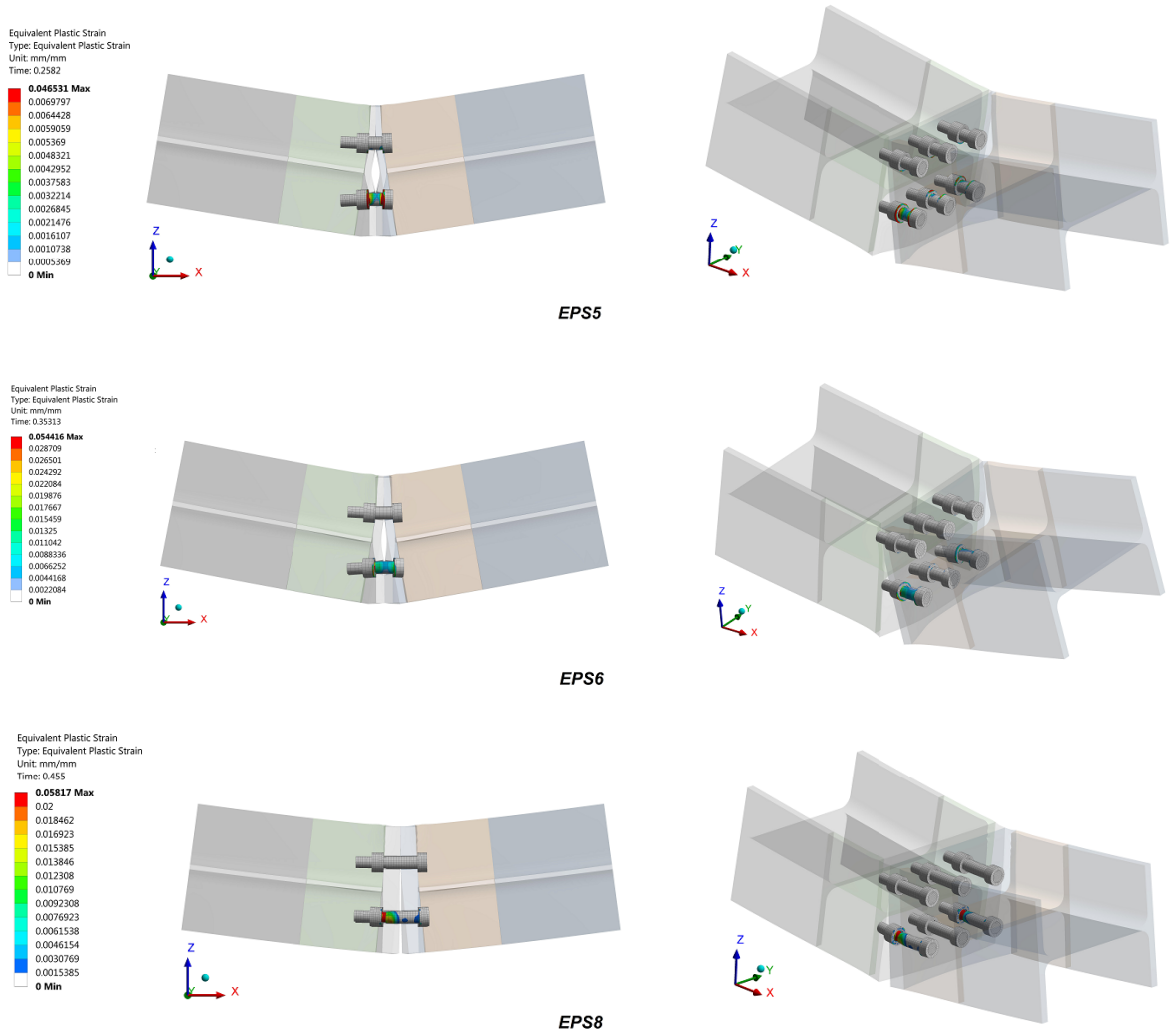

Fig. 5.12 The plastic strain of the bolts in EPS5, EPS6 and EPS8 models when the joints are loaded to the bending moment capacity in out-of-plane bending. The deformation of the joints is exaggerated by a factor of 10 to visualize the different deformation patterns.

Similarly, as in in-plane bending, the different failure mechanisms, especially the different behavior of the end-plates, causes some differences to the distribution of bolt forces also in out-of-plane bending. In Fig. 5.13 the distribution of the bolt forces is shown for models EPS5, EPS6 and EPS8. Bolt force curves of different models are marked with different colors and here the same bolts 1, 2 and 3 as in in-plane bending are considered. In out-of-plane bending, the three bolts are all in the same bolt row with the same lever arm. Also in out-of-plane bending, the magnitudes of the bolt forces are highly affected by the two factors: the development of internal prying forces and the ability of the joint to deform locally, so that the bolt forces get more evenly distributed between the two bolt rows.

Again, by observing Fig. 5.13 and by taking an example at $M_{Ed} = 100$ kNm, it can be noticed, that the bolt forces of EPS5 model (red lines) are significantly higher compared to those of EPS6 (black lines) or EPS8 (blue lines). In in-plane bending, as well as in out-of-plane bending, the differences in the bolt forces are caused by the level of prying forces with

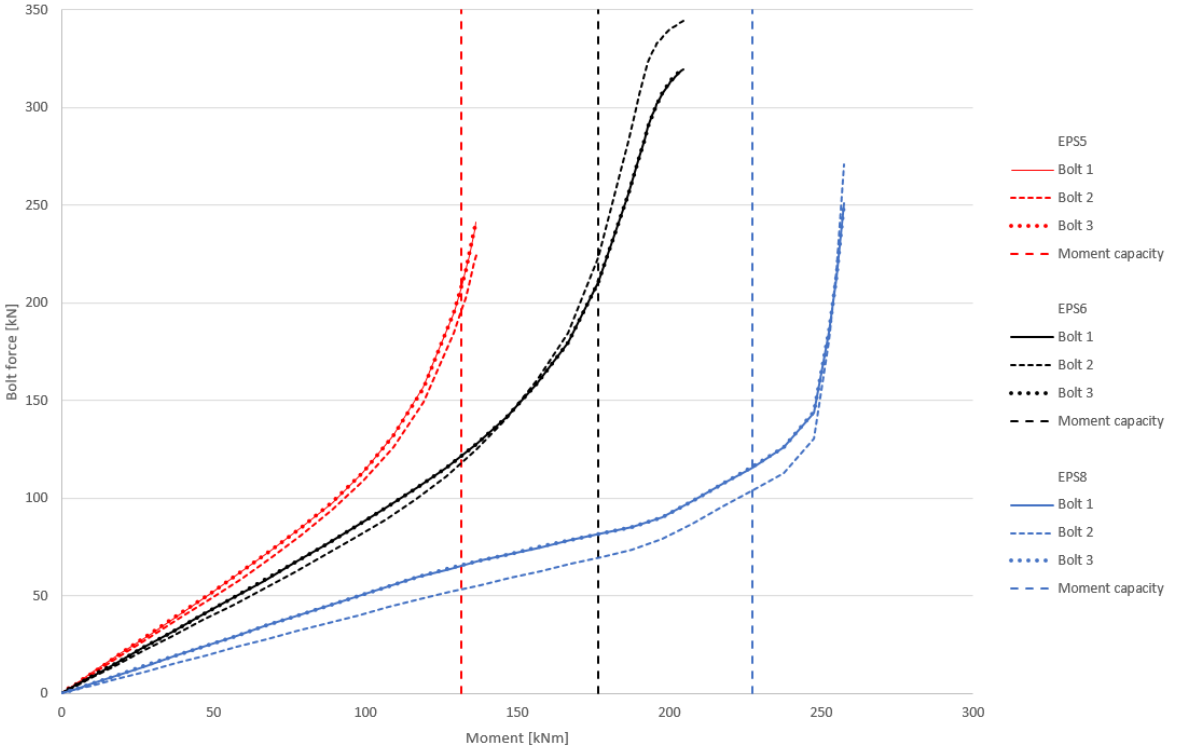

Fig. 5.13 The distribution of the bolt forces with EPS5, EPS6 and EPS8 models in out-of-plane bending. Bolts 1, 2 and 3 refer to the bolts in the furthest bolt row from the center of compression. This means that in out-of-plane bending, the lever arm is the same for each bolt. The vertical dashed lines are indicating the bending moment capacities of each joint configuration.

different failure mechanisms. EPS5 model with type-1 mechanism develops the maximum prying forces and thereby the maximum bolt forces. The prying action with EPS5 is presented in Fig. 5.14. Significant prying forces occur also in type-2 failure mechanism with EPS6, so the bolt forces are only marginally smaller than with EPS5. No prying forces are developed with the thick end-plates of EPS8, so the bolt forces are significantly smaller than those of EPS5 and EPS6 models.

In out-of-plane bending, according to basic mechanics, the three bolt forces considered should be equal, since the lever arm is the same for each bolt. However, similarly, as in in-plane bending, the local deformations of the end-plates determine how efficiently the bolt forces are distributed between the bolts. In Fig. 5.13 it can be seen, that with the thin end-plates of EPS5 and EPS6 models, such local deformation occurs in the end-plates, so that although the corner bolt 1 (solid red and black lines) and bolt 3 (dotted red and black lines) are slightly more heavily loaded than the center bolt 2 (dashed red and black lines), the differences between these bolt forces are still marginal. With EPS8, the thick end-plates prevent most of the local deformation in the end-plates, so the corner bolt 1 and corner bolt 3 (solid and dotted blue lines) are significantly more heavily loaded than the center bolt 2 (dashed blue line). With EPS8 model, it appears that also some redistribution of forces occurs at about $M_{Ed} = 200$ kN, which is before the ultimate capacity of the joint. The redistribution of the bolt forces indicates that a complete fracture of an individual component occurred and after such point, the capacity of the joint is uncertain.

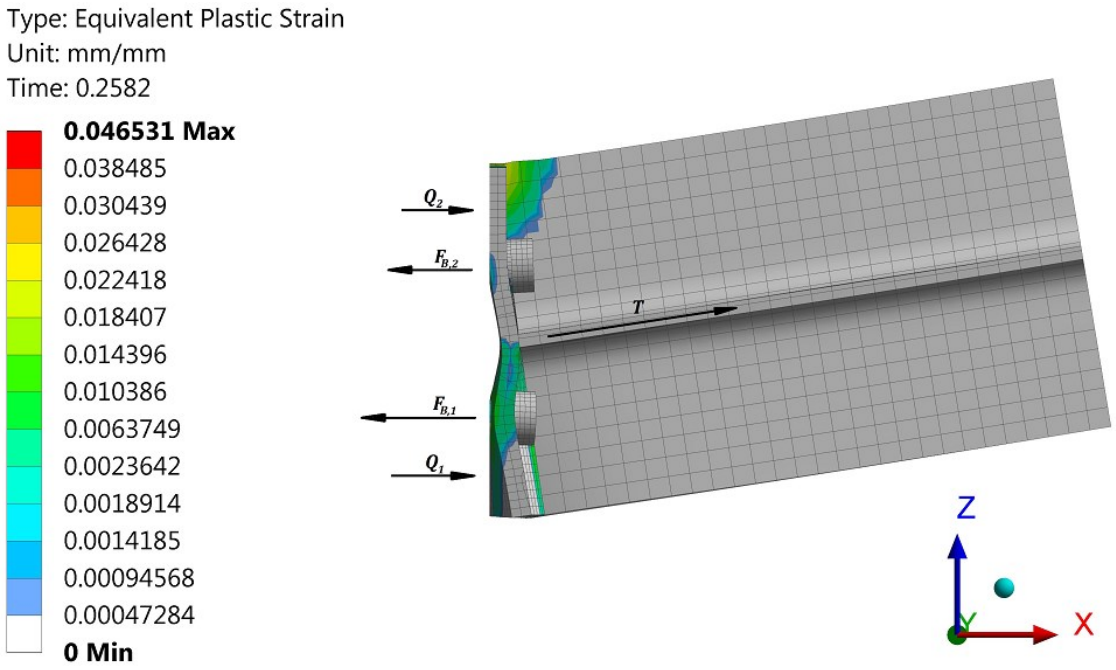

Fig. 5.14 The distribution of internal forces and moments in the T-stub flange of EPS5 in out-of-plane bending as presented in subsection 3.2.1. Plastic strain visualizes the locations of the plastic hinges. Q is the prying force, F_B is the bolt force and T is the tension force resultant for an individual T-stub.

In Fig. 5.15, the different failure mechanisms are visualized by slicing the joint configurations along bolt row 3 and illustrating the development of the plastic strain. With EPS5, it can be seen that the fully developed plastic hinges are formed at the root of the beam web as well as along the horizontal and vertical bolt lines on both sides of the beam web. The formation of the plastic hinges corresponds to the ductile type-1 failure. The reason for the strong prying action is also clearly visible, since due to the plastic hinges, the end-plates get widely separated between the vertical bolt lines.

As Fig. 5.15 illustrates, with EPS6 model, it appears that the two plastic hinges are developed in the tension side of the beam web, which corresponds to type-1 failure. However, on the compression side of the beam web, although the bolts are in tension, the two plastic hinges are not fully developed. This indicates that the failure mechanism on the compression side of the web, is of type-2. The different failure mechanism of the opposite sides of the beam web are not predicted by the analytical model, which can explain the differences in the stiffness and ultimate resistance calculations.

In Fig. 5.15, similarly, as in in-plane bending, the fragile failure mechanism of EPS8 model can also be verified in out-of-plane bending, since no plastic hinges are formed and the vertical edges of the end-plates get separated in the tension side of the beam web. The separation of the edges guarantees that the prying forces are nonexistent.

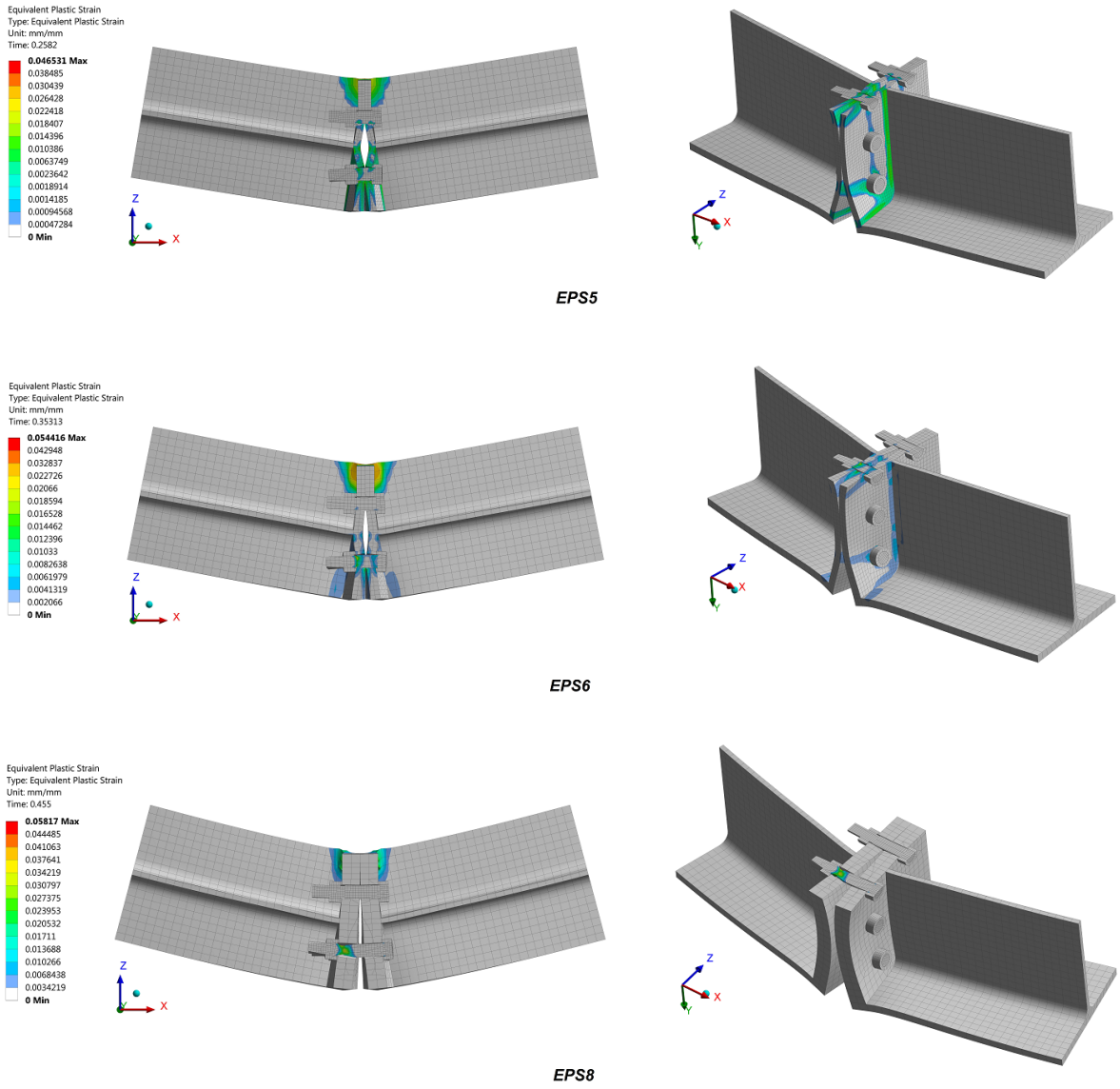

Fig. 5.15 The development of plastic hinges in out-of-plane bending, when the joints are loaded to the moment capacities. Due to the fully developed plastic hinges, great prying forces occur with EPS5 and EPS6 models. With EPS8, the vertical edges of the end-plates get separated on the tension side, so there are no internal prying forces. The deformations are exaggerated by a factor of 10 for EPS5 and EPS6 and by a factor of 20 for EPS8.

The plastic strains in the end-plates of EPS5, EPS6 and EPS8 models are shown in Fig. 5.16. The development of the yield line patterns appears to be similar to those predicted by Eurocode 3 [1] and presented in subsection 3.5.2. The yield line patterns with EPS5 and EPS6 indicate that the end-plates yield as a group of bolt rows and with non-circular patterns on the tension side of the beam web. On the compression side, the end-plates yield as an individual bolt row and with the beam pattern. The yield line patterns for EPS8 model seem to be of the same form, although the patterns cannot be fully determined, since the end-plates stay on the elastic zone.

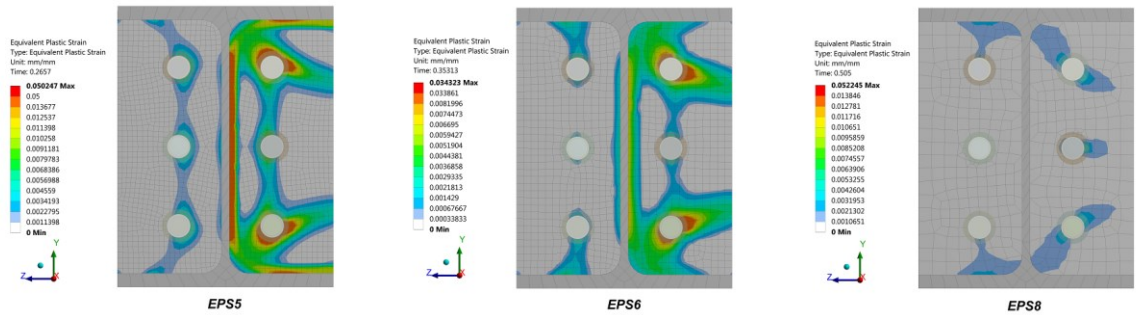

Fig. 5.16 The yield line patterns of EPS5, EPS6 and EPS8 joint configurations at bending moment capacity in out-of-plane bending. EPS5 and EPS6 have significant plastic strains in the end-plates whereas the end-plates of EPS8 stay on elastic zone.

5.4 Summary

In the parametric study, it was found that the Eurocode based analytical model highly over-estimates the initial stiffness and under-estimates the ultimate bending capacity of a flush end-plate splice both in in-plane and in out-of-plane bending. The discrepancies between the analytical and numerical results appeared to magnify with thicker end-plates. This indicates that the errors of the analytical calculations of a flush end-plate splice are increased when the relative stiffness and the resistance of the end-plates are higher compared to those of the bolts.

Through the analysis of combined bending and axial loading, it was found that the axial loading has a significant contribution to the moment-rotation response of a flush end-plate splice. With combined bending and tension, the stiffness and the resistance of the joint are significantly reduced and with combined bending and compression, both values are increased to some extent. The impact of the axial load appeared to be more effective in in-plane bending. Although the majority of the analysis were performed so that bending and axial loading were applied gradually starting from zero, to see the difference, another analysis with two load steps was also performed with one individual joint geometry.

With this type of loading condition, when the connected structure is axially loaded before bending occurs, it was found that the joint behavior is even further affected. With such loading conditions, especially with low bending moments and under combined bending and compression, the example joint is classified by stiffness as rigid, both in in-plane and in out-of-plane bending. With combined bending and tension, the classification by stiffness is pinned in both directions. Some comparative analyses were also conducted with varying levels of axial loading and it was found that the initial stiffness and the ultimate capacity of the joints are very sensitive to the levels of axial loading in both directions.

Although there are some significant discrepancies in the moment-rotation responses conducted with the Eurocode based model and with the finite element model, it was found that the failure mechanisms of different joint geometries are predicted correctly with standardized models. In subsection 5.3, it was also found that with an extensive finite element analysis, the development of the Eurocode based failure mechanisms can be accurately studied and through the analysis of the bolt force and plastic hinge development, the different failure mechanism can be easily identified.

6 Conclusions

The principal objective of this thesis was to achieve a more thorough understanding of the behavior of a flush end-plate splice under pure bending and under combined bending and axial loading. In the preliminary studies, it was found that a beam-to-column flush end-plate joint is widely researched and significant amount of literature concerning both the resistance and the stiffness of this type of joint is available. However, only little documented research was found concerning a flush end-plate splice for I-cross-sectioned beams and columns. Especially the understanding of the behavior in out-of-plane bending was limited. Although the design programs for end-plate splices in in-plane bending are included in some steel design software, the out-of-plane bending is always excluded due to the limitations in the design code. Historically, the behavior of an end-plate splice in out-of-plane bending is probably considered of lesser importance, since beams and columns with I-sections are more often loaded about the primary bending axis of the cross-section. However, especially in industrial steel frames, the structures can be under bending in both directions separately or simultaneously.

A Eurocode based analytical calculation sheet was formed as part of this thesis in in-plane bending and by applying the same principles and by logically assembling the active components in out-of-plane bending, a similar analytical model was conducted also for out-of-plane bending. To verify the accuracy of the two models for flush end-plate splices, a comparative finite element analysis was performed. The finite element analysis was performed as a parametric study by varying the bolt size and the end-plate thickness of the connection. The finite element modelling techniques were validated by performing a comparative analysis on an individual T-stub specimen and by comparing the finite element results to the experimental results found in the literature.

Through the parametric study, it was found that the Eurocode based analytical model highly over-estimates the initial stiffness and under-estimates the ultimate bending capacity of a flush end-plate splice both in in-plane and in out-of-plane bending. The results indicated, that the errors of the Eurocode based calculations of a flush end-plate splice are increased, when the relative stiffness and resistance of the end-plates are higher compared to those of the bolts. Although the analytical out-of-plane model is not accurate with all of the studied joint configurations and even though it is not officially approved, it can be used for the preliminary design of a flush end-plate splice, provided that the stiffness and the resistance of the final design is verified with some other approved design procedure.

All of the studied joint geometries were also analyzed in combined bending and axial loading. In the analysis of the combined loading cases, it was found that a flush end-plate splice behaves similarly as a base plate joint. As presented in section 5, with combined bending and tension, the stiffness and the resistance of the joints are significantly reduced. With combined bending and compression, both values are increased to some extent. It was also noticed, that the stiffness and the resistance of a flush end-plate splice are very sensitive to the level of axial loading.

By comparing Table 5.5 and Table 5.6, it can be noticed, that the criteria for a rigid joint is achieved with more joint configurations in out-of-plane bending than in in-plane bending. This is due to a fact that the bending stiffness of the connected members is significantly lower about the weak axis. This can indicate that splicing structural members with flush end-

plate splices is not as substantial in out-of-plane bending and that the spliced structure is less affected concerning the global behavior in out-of-plane bending.

In the design of the moment-resisting joints, the intent is to maximize the rigidity of the joints and preferably to avoid the design of joints with fragile failure mechanisms. However, within the studied joint geometries, it was found that the rigid classification can only be obtained, when the determining failure mechanism is of type-3 (fragile failure mechanism). This makes the design of moment-resisting end-plate splices difficult, since the final design is always a compromise balancing between the multiple design criteria.

Even though most of the results obtained with the parametric study in this thesis are consistent and can be explained through the analysis of the different failure mechanisms, it needs to be taken into consideration that although more than 60 configurations with different geometries and loading conditions were analyzed, the total number of the varied parameters is still relatively low. The low amount of varied parameters makes it impossible to obtain generally applicable conclusions for a flush end-plate splice. For more thorough understanding of a flush end-plate splice, the behavior would have to be studied with connected members with varying cross-sections and by varying the edge dimensions of the bolts. Another considerable factor, which could be varied in a more extensive parametric study, is the total number of the bolts, which in this thesis was kept constant.

In this thesis, the behavior of a flush end-plate splice was always studied individually either in in-plane or in out-of-plane bending. However, the loading conditions are hardly ever that simple and usually when the structure is under bending about its weak axis, it is also simultaneously under the strong axis bending. This type of biaxial bending causes complicated three dimensional behavior in the end-plates and it is very disadvantageous for the corner bolts under tension. Biaxial bending occurs rather usually with industrial steel frames and to handle the complexity of the problem, some conservative methods exist. Conservative design methods usually lead to increased use of materials so further understanding of the behavior of these types of steel joints can enhance the total cost effectiveness.

As noticed, due to the complexity of the three dimensional behavior, the moment-rotation response of a flush end-plate splice is difficult to predict with the analytical component method. However, the materially and geometrically nonlinear finite element modelling was found suitable for the analysis of end-plate splices and according to the study of an individual T-stub specimen, the finite element modelling techniques were found to yield reliable results. With the finite element analysis, the capacity of the structures can be determined quite accurately and cost efficiently, since in some cases, the simulations can replace the experiments. Although finite element modelling is rather time consuming, the total cost of construction is usually reduced by the optimal design obtained with the accurate results of finite element modelling.

References

[1] EN 1993-1-8, 2005: Design of steel structures, Part 1-8: Design of Joints. CEN Brussels, Belgium.

[2] EN 1993-1-1, 2005: Design of steel structures, Part 1-1: General rules and rules for buildings. CEN Brussels, Belgium.

[3] EN 1993-1-2, 2005: Design of steel structures, Part 1-2: General rules. Structural fire design. CEN Brussels, Belgium.

[4] EN 1993-1-3, 2006: Design of steel structures, Part 1-3: General rules. Supplementary rules for cold-formed members and sheeting. CEN Brussels, Belgium.

[5] EN 1993-1-5, 2006: Design of steel structures, Part 1-5: Plated structural elements.

[6] Broderick BM, Thomson AW. The response of flush end-plate joints under earthquake loading. Journal of Constructional Steel Research, 2002. 58. 1161-1175. 0143-974X.

[7] Gil B, Bijlaard F, Bayo E. T-stub behavior under out-of-plane bending. II: Parametric study and analytical characterization. Eng Struct, 2015. 98. 241-250.

[8] Gil B, Goñi R. T-stub behaviour under out-of-plane bending. I: Experimental research and finite element modelling. Eng Struct, 2015. 98. 230-240. 0141-0296.

[9] Daniūnas A, Urbonas K. Analysis of the steel frames with the semi-rigid beam-to-beam and beam-to-column knee joints under bending and axial forces. Eng Struct, 2008. 30. 3114-3118. 0141-0296.

[10] Urbonas K, Daniūnas A. Behaviour of semi-rigid steel beam-to-beam joints under bending and axial forces. Journal of Constructional Steel Research, 2006. 62. 1244-1249. 0143-974X.

[11] Mohamadi-shooreh MR, Mofid M. Prediction of the yielding moment of flush endplate splice connections using finite element modeling. Sci Iranica, 2013. 20. 270-277. 1026-3098.

[12] Joints in Steel Construction - Moment resisting joints to Eurocode 3. UK: The British Constructional Steel Association Limited and The Steel Construction Institute; 2013. 978-1-85-942209-0.

[13] Simão PD, Girão Coelho AM, Bijlaard FSK. Influence of splices on the buckling of columns. Int J Non-Linear Mech, 2012. 47. 806-822. 0020-7462.

[14] Girão Coelho AM, Simão PD, Bijlaard FSK. Stability design criteria for steel column splices. Journal of Constructional Steel Research, 2010. 66. 1261-1277. 0143-974X.

[15] Girão Coelho AM, Simão PD, Bijlaard FSK. Stability design criteria for steel column splices. Journal of Constructional Steel Research, 2010. 66. 1261-1277. 0143-974X.

[16] Snijder HH, Hoenderkamp JCD. Influence of end plate splices on the load carrying capacity of columns. Journal of Constructional Steel Research, 2008. 64. 845-853. 0143-974X.

[17] Dunkerley S. On the whirling and vibrations of shafts. 1984. Volume 185. ISSN 1364-503X.

[18] Zoetemeijer P. Design method for the tension side of statically loaded, bolted beam-to-column connections. Heron, 1974. 20.

[19] JP Jaspart. Éude de la semi-rigiditè des noeuds poutre-colonne et son influence sur la resistance et la stabilite des ossatures en acier. Liège: University of Liège; 1991.

[20] Weynand K, Jaspart J, Steenhuis M. The stiffness model of revised annex j of eurocode 3. In: Bjorhovde R, Colson A, Zandonini R, editors. Connections in Steel Structures III Oxford: Pergamon; 1996. p. 441-452.

[21] Yee YL, Melchers RE. Moment-rotation curves for bolted connections. J Struct Eng, 1986. 112. 615-635.

[22] JP Jaspart. Contributions to recent advances in the field of steel joints – column bases and further configurations for beam-to-column joints and beam splices. Liège: University of Liège; 1997.

[23] Packer JA ML. A limit state design method for the tension region of bolted beam-to-column connections. The Structural Engineer, 1977. 446-458.

[24] Francavilla AB, Latour M, Piluso V, Rizzano G. Simplified finite element analysis of bolted T-stub connection components. Eng Struct, 2015. 100. 656-664.

[25] F.S.K. Bijlaard, A.M. Gresnigt, G.J. van der Vegte, editor. Characterization of the nonlinear behavior of single bolted t-stub connections. Connection in steel structures V Amsterdam: Delft University of Technology; 2004.

[26] Loureiro A, Gutiérrez R, Reinosa JM, Moreno A. Axial stiffness prediction of non-preloaded T-stubs: An analytical frame approach. Journal of Constructional Steel Research, 2010. 66. 1516-1522. 0143-974X.

[27] Ribeiro J, Santiago A, Rigueiro C, da Silva LS. Analytical model for the response of T-stub joint component under impact loading. Journal of Constructional Steel Research, 2015. 106. 23-34. 0143-974X.

[28] Latour M, Rizzano G, Santiago A, Simoes D. Experimental analysis and mechanical modeling of T-stubs with four bolts per row. J Constr Steel Res, 2014. 101. 158-174.

[29] Simões da Silva L, Santiago A, Vila Real P. Post-limit stiffness and ductility of end-plate beam-to-column steel joints. Comput Struct, 2002. 80. 515-531. 0045-7949.

[30] A component method model for semi-rigid end-plate beam-to-column joints including the axial versus bending moment interaction. 5th International Conference on Advances in Steel Structures, ICASS 2007; 2007. 481-486.

[31] M.Heinisuo VL, E.Lehtimäki, editor. Enlargement of the component method into 3D. Proceedings of Nordic steel conference; September 2-4; Malmö, Sweden; 2009.

[32] Bursi OS, Jaspart JP. Benchmarks for Finite Element Modelling of Bolted Steel Connections. J Constr Steel Res, 1997. 43. 17-42.

[33] Bursi OS, Jaspart JP. Basic issues in the finite element simulation of extended end plate connections. Comput Struct, 1998. 69. 361-382.

[34] Gantes CJ, Lemonis ME. Influence of equivalent bolt length in finite element modeling of T-stub steel connections. Comput Struct, 2003. 81. 595-604.

[35] Agerskov H. High-strength bolted connections subject to prying. ASCE J Struct Div, 1976. 102. 161-175.

[36] Wanzek T GN. Numerical aspects for the simulation of end plate connections. Virdi KS, 1999.

[37] Swanson JA, Kokan DS, Leon RT. Advanced finite element modeling of bolted T-stub connection components. J Constr Steel Res, 2002. 58. 1015-1031.

[38] Hu JW, Kim DK, Leon RT, Choi E. Analytical studies of full-scale steel T-stub connections using delicate 3D finite element methods. ISIJ Int, 2011. 51. 619-629.

[39] Ansys I. Ansys: List of element types. 2015; Available at: http://www.ansys.stuba.sk/html/elem_55/chapter3/ES3-1.htm. Accessed 09/01, 2017.

[40] E.Wang TN, R.Rauch. Back to Elements - Tetrahedra vs. Hexahedra. CAD-FEM GmbH, Munich, Germany .

[41] Benzley SE, Perry E, Merkley K, Clark B. A Comparison of All Hexagonal and All Tetrahedral Finite Element Meshes for Elastic and Elasto-plastic Analysis. Brigham Young University, Provo, Utah .

[42] Ansys I. Ansys Scarcnet: List of element types. 2015; Available at: https://www.sharcnet.ca/Software/Ansys/16.2.3/en-us/help/ans_elem/. Accessed 01/09, 2017.

[43] Ansys I. Ansys Mechanical User's Guide. 2013 November 2013;Release 15.0.

[44] Cook RD, Malkus DS, Plesha ME editors. Concepts and applications of finite element analysis. 3rd ed. New York: Wiley, 1989. 630 sivua. 0-471-50319-3; 0-471-84788-7.

[45] Zienkiewicz OC, Taylor RL editors. The finite element method. 5th ed. Oxford ; Boston: Butterworth-Heinemann, 2000. verkkoaineisto (pdf). 1591243009;.

[46] Crisfield MA editor. Non-linear finite element analysis of solids and structures. Volume 1, Essentials. Chichester: Wiley, 1991. 345 sivua. 0-471-92956-5; 0-471-97059-X.

[47] Herrera RA, Bravo M, Gómez G, Aedo G. Performance of built-up T-stubs for Double T moment connections. Journal of Constructional Steel Research, 2013. 88. 289-295. 0143-974X.

[48] Ansys I. Ansys Mechanical APDL: Structural Analysis Guide. 2013;Release 15.0.

[49] Bathe K editor. Finite element procedures in engineering analysis. Englewood Cliffs NJ: Prentice-Hall, 1982. 735 sivua. 0-13-317305-4.

[50] Bursi OS, Jaspart JP. Calibration of a Finite Element Model for Isolated Bolted End-Plate Steel Connections. J Constr Steel Res, 1997. 44. 225-262.

[51] SFS-EN ISO 4014, 2011: Hexagon Head Bolts. Product Grades A and B. CEN Brussels, Belgium.

[52] SFS-EN ISO 4032, 2012: Hexagon Regular Nuts. Product Grades A and B. CEN Brussels, Belgium.

[53] SFS-EN ISO 7089, 2001: Plain Washers. Normal Series. Product Grade A. CEN Brussels, Belgium.

[54] Perttola H. HM, editor. Experimental study on flanged joints of tubular members under biaxial bending. 7th International Workshop on Connections in Steel Structures; May 30 - June 2, 2012; Timisoara, Romania: European Convention for Constructional Steelwork; 2012.

[55] Santaoja K. Rasitusopin käsikirja lujuusopin lukijoille. Espoo: Sasata; 2011.

[56] Simões da Silva L, Girão Coelho A. A ductility model for steel connections. Journal of Constructional Steel Research, 2001. 57. 45-70. 0143-974X.

[57] Laine V. Teräsrungon liitosten jouston huomioon ottaminen integroidussa suunnittelujärjestelmässä (Development of semi-rigid behaviour of structural connections in an integrated design system). Master's Thesis, Tampere University of Technology, Tampere, 2008. (In Finnish).

List of appendices

Appendix 1. Basic joint components

Component			Reference to application rules		
			Design Resistance	Stiffness coefficient	Rotation capacity
1	Column web panel in shear	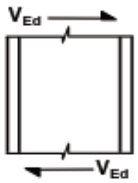	6.2.6.1	6.3.2	6.4.2 and 6.4.3
2	Column web In transverse compression	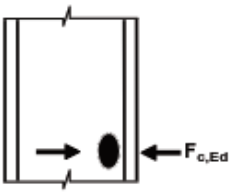	6.2.6.2	6.3.2	6.4.2 and 6.4.3
3	Column web in transverse tension	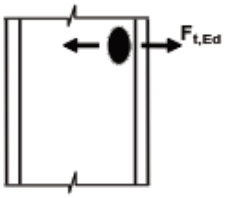	6.2.6.3	6.3.2	6.4.2 and 6.4.3
4	Column flange in bending	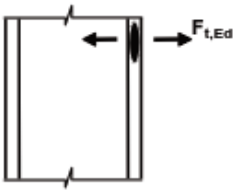	6.2.6.4	6.3.2	6.4.2 and 6.4.3
5	End-plate in bending	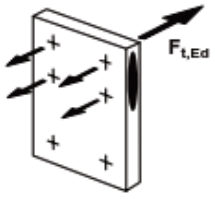	6.2.6.5	6.3.2	6.4.2
6	Flange cleat in bending	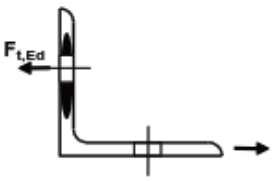	6.2.6.6	6.3.2	6.4.2

Component			Reference to application rules		
			Design Resistance	Stiffness coefficient	Rotation capacity
7	Beam or column flange and web in compression	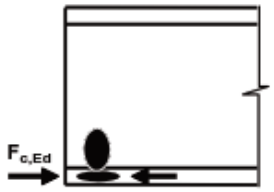	6.2.6.7	6.3.2	*)
8	Beam web in tension	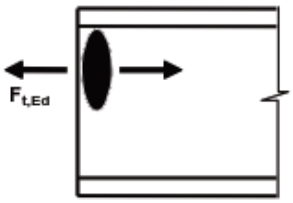	6.2.6.8	6.3.2	*)
9	Plate in tension or compression	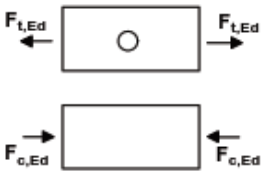	in tension: - EN 1993-1-1 in compression: - EN 1993-1-1	6.3.2	*)
10	Bolts in tension	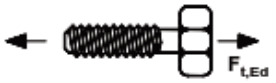	With column flange: - 6.2.6.4 with end-plate: - 6.2.6.5 with flange cleat: - 6.2.6.6	6.3.2	6.4.7
11	Bolts in shear	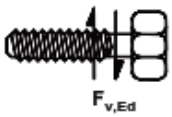	3.6	6.3.2	6.4.2
12	Bolts in bearing (on beam flange, column flange, end-plate or cleat)	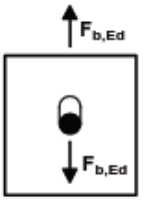	3.6	6.3.2	*)
*) No information available in this part.					

Component			Reference to application rules		
			Design Resistance	Stiffness coefficient	Rotation capacity
13	Concrete in compression including grout		6.2.6.9	6.3.2	*)
14	Base plate in bending under compression		6.2.6.10	6.3.2	*)
15	Base plate in bending under tension		6.2.6.11	6.3.2	*)
16	Anchor bolts in tension		6.2.6.12	6.3.2	*)
17	Anchor bolts in shear		6.2.2	*)	*)
18	Anchor bolts in bearing		6.2.2	*)	*)
19	Welds		4	6.3.2	*)
20	Haunched beam	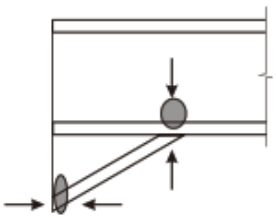	6.2.6.7	6.3.2	*)
*) No information available in this part.					

Appendix 2. Resistance and stiffness of an individual T-stub

T-stub: Resistance and initial stiffness			
f_y	431	[MPa]	Yield strength of material
b	150	[mm]	Width of T-stub specimen
h	300	[mm]	
t_w	7.1	[mm]	Web thickness
t_f	10.7	[mm]	Flange thickness
r	15	[mm]	Fillet radius
e	30	[mm]	Edge distance
m	29.45	[mm]	Distance defined in EN 1993-1-8
p	0	[mm]	Bolt distance
d_w	19	[mm]	Washer diameter
e_w	4.75	[mm]	Factor $e_w = d_w / 4$
h_n	10	[mm]	Nut height
h_h	7.5	[mm]	Bolt head height
t_{washer}	2.5	[mm]	Washer thickness
n	30	[mm]	Edge distance
$b_{eff,1}$	30	[mm]	Beam pattern, EN 1993-1-8; Table 6.4
$b_{eff,2}$	30	[mm]	Beam pattern, EN 1993-1-8; Table 6.4

Resistance of an individual T-stub			
$M_{pl,1,Rd}$	493	[Nm]	Part of a group, EN 1993-1-8; Table 6.4
$M_{pl,2,Rd}$	493	[Nm]	Part of a group, EN 1993-1-8; Table 6.4
$F_{1,pl,Rd}$	153.2	[kN]	Part of a group, EN 1993-1-8; Table 6.4
$F_{2,pl,Rd}$	152.5	[kN]	Part of a group, EN 1993-1-8; Table 6.4
$F_{3,pl,Rd}$	236.5	[kN]	Bolt fracture, EN 1993-1-8; Table 6.4
$F_{pl,Rd}$	152.5	[kN]	Design tension resistance
$2/3\ F_{pl,Rd}$	101.7	[kN]	Elastic design tension resistance
Initial stiffness of an individual T-stub			
E	2.1E+11	[N/m^2]	Young's modulus
K_f	362591	[kN/m]	Flange stiffness
K_b	805826	[kN/m]	Bolt stiffness
K	73999	[kN/m]	Initial stiffness

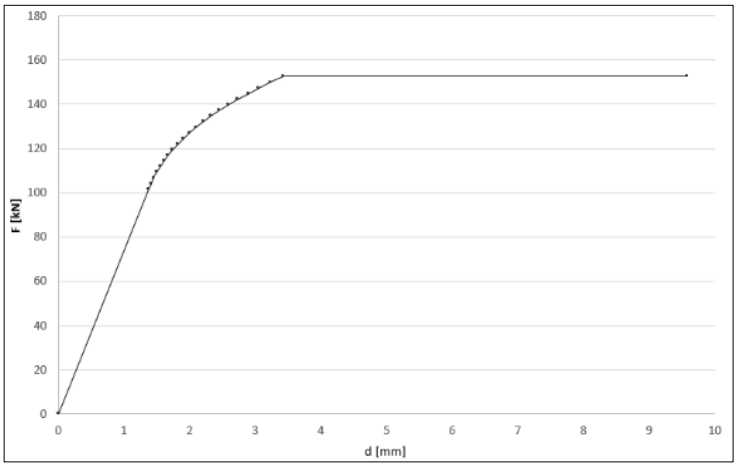

Appendix 3. In-plane bending

Design of beam-to-beam connection			
Loading conditions: EPS1			
N_{Ed}	0	[kN]	
$M_{ed,y}$	100	[kNm]	Bendign moment in in-plane bending
$M_{ed,z}$	100	[kNm]	Bending moment in out-of-plane bending
Geometric properties: HEA400			
h	390	[mm]	Height of beam section
b	300	[mm]	Width of beam section
t_w	11	[mm]	Thickness of the web
t_f	19	[mm]	Thickness of the flange
r	0	[mm]	Radius of beam section fillet
A	15272	[mm^2]	Cross-sectional area of the beam section
I_y	432599491	[mm^4]	Moment of inertia of the beam section in in-plane bending (fillets excluded)
I_z	85539043	[mm^4]	Moment of inertia of the beam section in out-of-plane beding (fillets excluded)
$W_{el,y}$	2218458.9	[mm^3]	Elastic section modulus of the beam section in in-plane bending (fillets excluded)
$W_{el,z}$	570260.28	[mm^3]	Elastic section modulus of the beam section in out-of-plane bending (fillets excl.)
f_y	355	[N/mm^2]	Yield strenght of material, S355
Lenghts of members			
l_1	1	[m]	Lower member
l_2	1	[m]	Upper member
End-plate dimensions and material			
b_p	300	[mm]	Plate height
h_p	390	[mm]	Plate width
t_p	15	[mm]	Plate thickness
f_y	355	[N/mm^2]	Yield strenght of material, S355
Welds			
a_w	6.35	[mm]	Weld of web
a_f	10	[mm]	**Weld of flange**
Bolts			
Class	8.8		
f_y	640	[N/mm^2]	Yield strenght of material
f_u	800	[N/mm^2]	Ultimate strenght of material
d	24	[mm]	Diameter
d_w	36	[mm]	Washer diameter
t_w	4	[mm]	Washer thickness
h_n	19	[mm]	Bolt nut height
h_h	15	[mm]	Bolt head height
A	452.4	[mm^2]	Area of the bolt shank
A_s	353	[mm^2]	Tensilie area of the bolt shank
$F_{t,Rd}$	203.3	[kN]	Design tension resistance of the bolt
$F_{v,Rd}$	173.7	[kN]	Design shear resistance of the bolt
n_h	2		Nb of vertical bolt rows
n_v	3		Nb of horizontal bolt rows
h_1	85	[mm]	Distance from the plate edge to the center of the bolt
e_h	130	[mm]	Horizontal displacement of the bolts
e_v	110	[mm]	Vertical displacement of the bolts
e_1	85	[mm]	Vertical edge distance
e_2	85	[mm]	Horizonal edge distance
Partial safety factors			
γ_{M0}	1		Partial safety factor for resistance of cross-sections whatever the class is
γ_{M2}	1.25		Partial safety factor for resistance of cross-sections in tension to fracture

Beam resistances - In-plane bending				
Compression				
A	15272	[mm^2]		
$N_{c,Rd}$	5421.6	[kN]	Design resistance of the section for compression	[kaava]
Bending				
$W_{pl,Rd}$	2455436	[mm^3]		
$M_{pl,Rd}$	871.7	[kNm]	Design resistance for bending	[kaava]
Flange and web in compression				
$M_{pl,Rd}$	871.7	[kNm]	Design resistance for bending	
h_f	371	[mm]	Distance between the centroids of flanges	
$F_{c,f,Rd}$	2349.5	[kN]	Resistance of the compressed flange	

Geometrical parameters of the connection	
α_1	6.74
α_2	6.1

Bolt rows considered individually

Nr	m	m_x	e	e_x	p	$l_{eff,cp}$	$l_{eff,nc}$	Mode 1 $l_{eff,1}$	Mode 2 $l_{eff,2}$
1	52.3		85	85	110	328.7	352.6	328.7	352.6
2	52.3		85	85	110	328.7	315.5	315.5	315.5
3	52.3		85	85	110	328.7	315.5	315.5	315.5

Bolt rows considered as part of a group

Group	m	m_x	e	e_x	p	$l_{eff,cp,g}$	$l_{eff,nc,g}$	Mode 1 $\Sigma l_{eff,1,g}$	Mode 2 $\Sigma l_{eff,2,g}$
1+2	52.3		85	85	110	494.4	359.9	359.9	359.9
2+3	52.3		85	85	110	494.4	322.8	322.8	322.8
1+2+3	52.3		85	85	110	768.7	572.6	572.6	572.6

Bolt elongation lenght			
w	4	[mm]	Washer thickness
h_n	19	[mm]	Nut height
t_p	30	[mm]	Thickness of bolted material
L_b	55	[mm]	2 x washer
L_b^*	366.2	[mm]	
e_w	9	[mm]	

Connection resistance for compression			
$F_{j,Rd}$	5421.6	[kN]	Connection resistance for compression

Connection resistance for bending			
$F_{t,Rd}$	203.3	[kN]	Design tension resistance of the bolt

End plate resistance for bending								
Bolt rows considered individually - Alternative method								
					Mode 1	**Mode 2**	**Mode 3**	
	$l_{eff,1}$	$l_{eff,2}$	$M_{pl,1,Rd}$	$M_{pl,2,Rd}$	$F_{T,1,Rd}$	$F_{T,2,Rd}$	$F_{T,3,Rd}$	n
Bolt row 1	328.7	352.6	6563.9	7041.2	573.4	345.6	406.7	65.4
Bolt row 2	315.5	315.5	6300.4	6300.4	550.4	333.0	406.7	65.4
Bolt row 3	315.5	315.5	6300.4	6300.4	550.4	333.0	406.7	65.4

Bolt rows considered as part of a group - Alternative method								
Group	$l_{eff,1}$	$l_{eff,2}$	$M_{pl,1,Rd}$	$M_{pl,2,Rd}$	$F_{T,1,Rd}$	$F_{T,2,Rd}$	$F_{T,3,Rd}$	n
1+2	359.9	359.9	7185.8	7185.8	627.7	573.9	813.3	65.4
2+3	322.8	322.8	6445.0	6445.0	563.0	561.3	813.3	65.4
1+2+3	572.6	572.6	11434.3	11434.3	998.8	872.0	1220.0	65.4

Beam web in tension			
	$b_{eff,t,wb}$	$F_{t,wb,Rd}$	6.2.6.8 (1)
Bolt row 1	328.7	1283.6	
Bolt row 2	315.5	1232.1	
Bolt row 3	315.5	1232.1	
Group 1+2	359.9	1405.2	
Group 2+3	322.8	1260.4	
Group 1+2+3	572.6	2236.0	

Beam flange and web in compression			
$M_{c,Rd}$	871.7	[kNm]	
$F_{c,fb,Rd}$	2349.5	[kN]	6.2.6.7

Component assembly for bending moment In-plane bending				
Compression				
Beam flange in compression	$F_{cf,Rd}$	2349.5	[kN]	
Compresssion resistance	**$F_{c,Rd}$**	**2349.5**	**[kN]**	
Bolts				
Bolts in tension	$F_{t,Rd}$	203.3	[kN]	
Bolt row 1				
End-plate in bending:	$F_{t1,Rd}$	345.6	[kN]	
Beam web in tension	$F_{t1,wb,Rd}$	1283.6	[kN]	
Tension resistance	**$F_{t1,Rd}$**	**345.6**	**[kN]**	
Lever arm	**h_1**	**295.5**	**[mm]**	
Bolt row 2				
End plate in bending:	$F_{t2,Rd}$	333.0	[kN]	
End-plate in bending:	$F_{t(1+2),Rd} - F_{t1,Rd}$	228.4	[kN]	
Beam web in tension	$F_{t2,wb,Rd}$	1232.1	[kN]	
Additional reduction needed:	**No**	228.4	[kN]	
Tension resistance	**$F_{t2,Rd}$**	**228.4**	**[kN]**	
Lever arm	**h_2**	**185.5**	**[mm]**	
Bolt row 3				
End plate in bending:	$F_{t3,Rd}$	333.0	[kN]	
End-plate in bending:	$F_{t(2+3),Rd} - F_{t2,Rd}$	333.0	[kN]	
End-plate in bending:	$F_{t(1+2+3),Rd} - F_{t1,Rd} - F_{t2,Rd}$	298.1	[kN]	
Beam web in tension	$F_{t3,wb,Rd}$	1232.1	[kN]	
Additional reduction needed:	**No**	298.1	[kN]	
Tension resistance	**$F_{t3,Rd}$**	**298.1**	**[kN]**	
Lever arm	**h_3**	**75.5**	**[mm]**	
Design resistance for bending				
$M_{pl,Rd}$		**167.0**	**[kNm]**	
$M_{j,Rd}$	(top of column)	871.7	[kNm]	
$M_{j,Rd}$	(within column lenght)	1743.4	[kNm]	
Classfication by strenght:	**PINNED**			

Rotational stiffness In-plane bending		
Young's modulus		
E	2.1E+11	[GPa]
Bolts		
k_{10}	10.3	[mm]
Bolt row 1		
k_5	5.3	[mm]
$k_{eff,j}$	2.1	[mm]
$k_{eff,j}h_j$	622.5	[mm^2]
$k_{eff,j}h_j^2$	183941.8	[mm^3]
Bolt row 2		
k_5	2.3	[mm]
$k_{eff,j}$	1.0	[mm]
$k_{eff,j}h_j$	194.4	[mm^2]
$k_{eff,j}h_j^2$	36052.2	[mm^3]
Bolt row 3		
k_5	4.5	[mm]
$k_{eff,j}$	1.9	[mm]
$k_{eff,j}h_j$	139.7	[mm^2]
$k_{eff,j}h_j^2$	10546.1	[mm^3]
Rotational stiffness		
z_{eq}	241.0	[mm]
k_{eq}	4.0	[mm]
$S_{j,ini}$	**845.0**	**[kNm/°]**
Limit for rigid:	1268.4	[kNm/°]
Limit for pinned:	79.3	[kNm/°]
Classification by stiffness:		**SEMI-RIGID**

Appendix 4. Out-of-plane bending

Beam resistances - Out-of-plane bending			
Compression			
A	15272	[mm^2]	Design compressive resistance of the section
$N_{c,Rd}$	5421.6	[kN]	
Bending			
$W_{pl,Rd}$	865648	[mm^3]	Design resistance for bending
$M_{pl,Rd}$	307.3	[kNm]	
Flange and web in compression			Design resistance for bending
$M_{pl,Rd}$	307.3	[kNm]	
h_f	200	[mm]	Distance between compression and tension resultants
$F_{c,f,Rd}$	1536.5	[kN]	Resistance of compressed parts of flanges

Geometrical parameters of the connection	
α_1	6.74
α_2	6.1

Bolt rows considered individually

Nr	m	m_x	e	e_x	p	$l_{eff,cp}$	$l_{eff,nc}$	Mode 1 $l_{eff,1}$	Mode 2 $l_{eff,2}$
1	52.3		85	85	110	328.7	315.5	315.5	315.5
2	52.3		85	85	110	328.7	315.5	315.5	315.5
3	52.3		85	85	110	328.7	315.5	315.5	315.5

Bolt rows considered as part of a group

Group	m	m_x	e	e_x	p	$l_{eff,cp,g}$	$l_{eff,nc,g}$	Mode 1 $\Sigma l_{eff,1,g}$	Mode 2 $\Sigma l_{eff,2,g}$
1+2	52.3		85	85	110				
2+3	52.3		85	85	110				
1+2+3	52.3		85	85	110	768.7	535.5	535.5	535.5

Bolt elongation lenght			
w	4	[mm]	Washer thickness
h_n	19	[mm]	Nut height
t_p	30	[mm]	Thickness of bolted material
L_b	55	[mm]	2 x washer
L_b^*	366.2337	[mm]	
e_w	9	[mm]	

Connection resistance for compression			
$F_{j,Rd}$	5421.6	[kN]	Connection resistance for compression

Connection resistance for bending			
$F_{t,Rd}$	203.3	[kN]	Design tension resistance of the bolt

End plate resistance for bending								
Bolt rows considered individually - Alternative method								
					Mode 1	**Mode 2**	**Mode 3**	
	$l_{eff,1}$	$l_{eff,2}$	$M_{pl,1,Rd}$	$M_{pl,2,Rd}$	$F_{T,1,Rd}$	$F_{T,2,Rd}$	$F_{T,3,Rd}$	n
Bolt row 1	315.5	315.5	6300.4	6300.4	275.2	166.5	203.3	65.4
Bolt row 2	315.5	315.5	6300.4	6300.4	275.2	166.5	203.3	65.4
Bolt row 3	315.5	315.5	6300.4	6300.4	275.2	166.5	203.3	65.4

Bolt rows considered as part of a group - Alternative method								
Group	$l_{eff,1}$	$l_{eff,2}$	$M_{pl,1,Rd}$	$M_{pl,2,Rd}$	$F_{T,1,Rd}$	$F_{T,2,Rd}$	$F_{T,3,Rd}$	n
1+2								65.4
2+3								65.4
1+2+3	535.5	535.5	10693.5	10693.5	467.1	429.7	1220.0	65.4

Component assembly for bending moment Out-of-plane bending			
Compression			
Beam flanges in compression	$F_{cf,Rd}$		[kN]
Compression resistance	**$F_{c,Rd}$**		**[kN]**
Bolts			
Bolts in tension	$F_{t,Rd}$	203.3	[kN]
Bolt row 1 (vertical bolt row, tension side)			
End-plate in bending	$3F_{t1,Rd}$	499.5	[kN]
End-plate in bending	$F_{t(1+2+3),Rd}$	429.7	[kN]
Tension resistance	**$F_{t1,Rd}$**	**429.7**	**[kN]**
Lever arm	**h_1**	**190**	**[mm]**
Bolt row 2 (vertical bolt row, comp. si		**EC**	
End-plate in bending	$F_{t1,Rd}$	499.5	[kNm]
End-plate in bending	$F_{t(1+2+3),Rd}$	429.7	[kNm]
Additional reduction needed:	**No**	429.7	[kNm]
Tension resistance	**$F_{t1,Rd}$**	**429.7**	**[kNm]**
Lever arm	**h_2**	**60**	**[mm]**
Design resistance for bending		**EC**	
$M_{pl,Rd}$		**107.4**	**[kNm]**
$M_{j,Rd}$	(top of column)	307.3	[kNm]
$M_{j,Rd}$	(within column lenght)	614.6	[kNm]
Classfication by strenght:	**Partial strenght**		

Rotational stiffness Out-of-plane bending		
Young's modulus		
E	2.1E+11	[GPa]
Bolts		
k_{10}	15.4	[mm]
Bolt row 1 (vertical bolt row, tension side)		
k_5	3.8	[mm]
$k_{eff,j}$	1.2	[mm]
$k_{eff,j}h_j$	221.7	[mm^2]
$k_{eff,j}h_j^2$	42116.0	[mm^3]
Bolt row 2 (vertical bolt row,	**EC**	
k_5	3.8	[mm]
$k_{eff,j}$	1.2	[mm]
$k_{eff,j}h_j$	70.0	[mm^2]
$k_{eff,j}h_j^2$	4199.9	[mm^3]
Rotational stiffness	**EC**	
z_{eq}	158.8	[mm]
k_{eq}	1.8	[mm]
$S_{j,ini}$	**169.8**	**[kNm/°]**
Limit for rigid:	250.8	[kNm/°]
Limit for pinned:	15.7	[kNm/°]
Classification by stiffness:		**SEMI-RIGID**

Appendix 5. Information about the T-stub validation model

Bolts	
Bolt size	M12
Bolt class	8.8
Number of bolts	4

Geometry			
T-stub width	b	80	[mm]
Web Length	l_w	115	[mm]
Web thickness	t_w	7,1	[mm]
Flange width	b_f	150	[mm]
Flange thickness	t_f	10,7	[mm]
Fillet radius	r	15	[mm]

Contacts	
Frictional contact	MPC
Bonded	Augmented Lagrange

Element types	
Solid	SOLID 186, SOLID 187
Contact	CONTA 174
Target	TARGE 170

Analysis settings		
	Non-preloaded	Preloaded
Number of steps	1	2
Step end time	1 s.	2 s.
Auto time stepping	On	On
Define by	Substeps	Substeps
Initial substeps	100	100
Minimum substeps	50	50
Maximum substeps	100	100
Solver type	Direct	Direct
Weak springs	Off	Off
Large deflection	On	On
Inertia relief	Off	Off

Appendix 6. Moment-rotation curves in in-plane bending

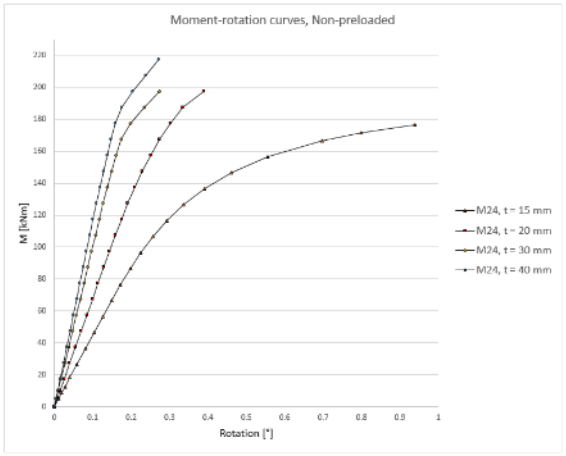

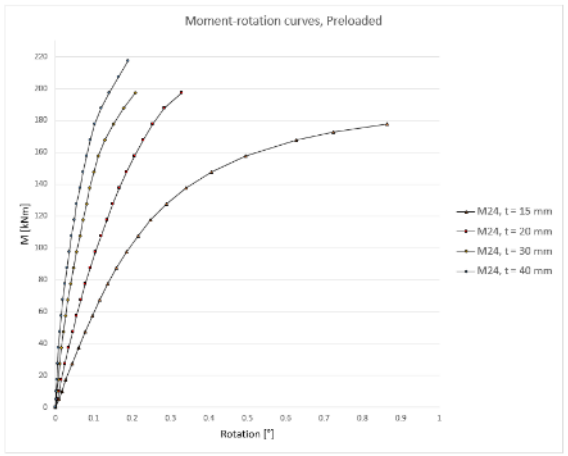

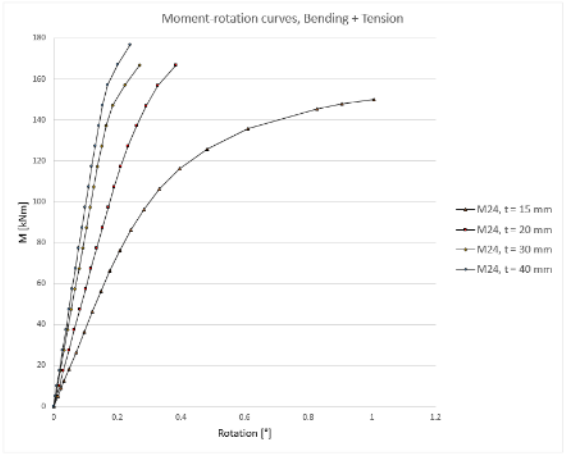

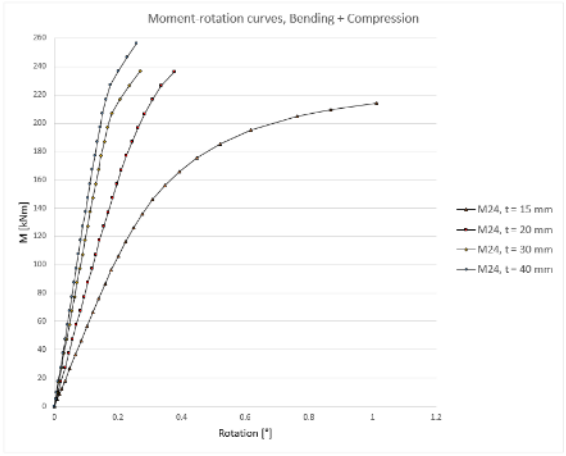

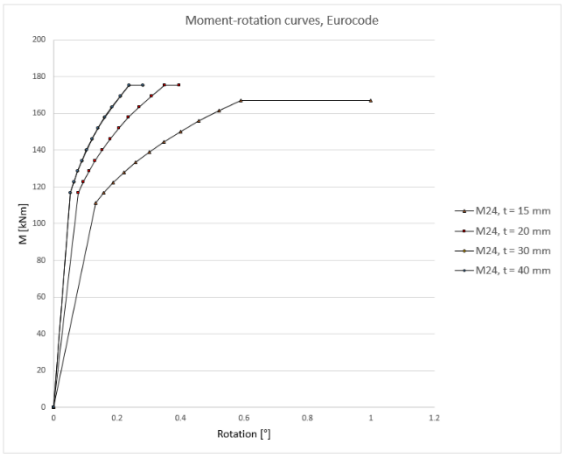

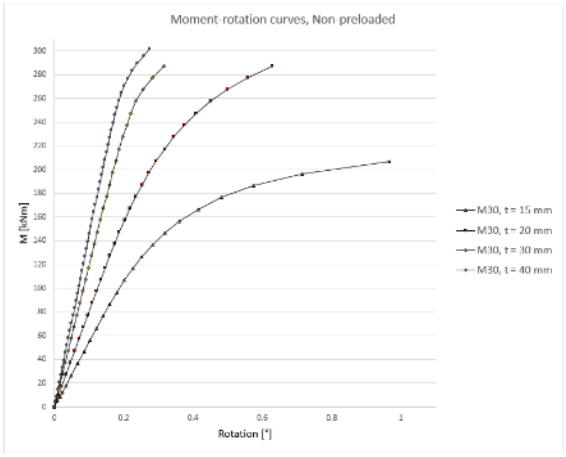
Moment-rotation curves, Non-preloaded
M [kNm]
Rotation [°]
M30, t = 15 mm
M30, t = 20 mm
M30, t = 30 mm
M30, t = 40 mm

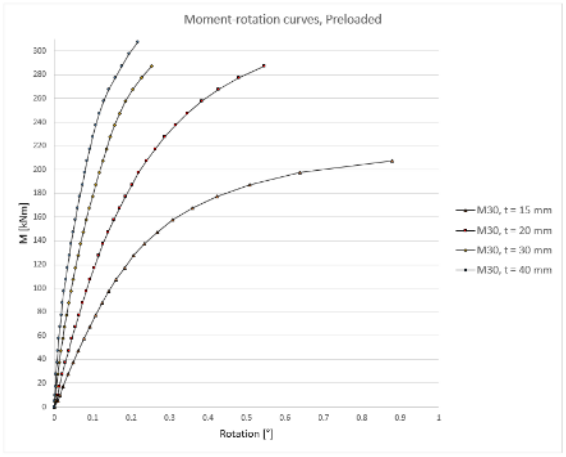
Moment-rotation curves, Preloaded
M [kNm]
Rotation [°]
M30, t = 15 mm
M30, t = 20 mm
M30, t = 30 mm
M30, t = 40 mm

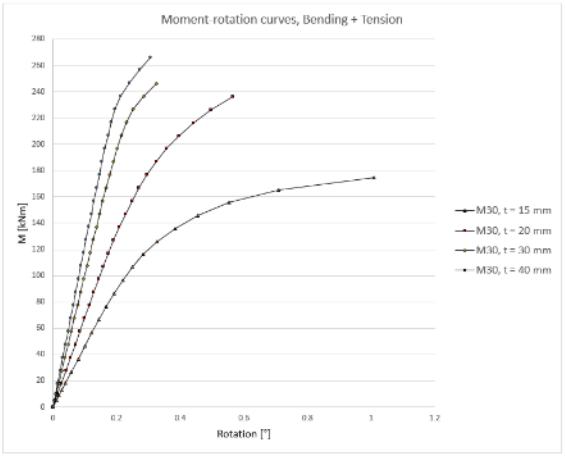
Moment-rotation curves, Bending + Tension
M [kNm]
Rotation [°]
M30, t = 15 mm
M30, t = 20 mm
M30, t = 30 mm
M30, t = 40 mm

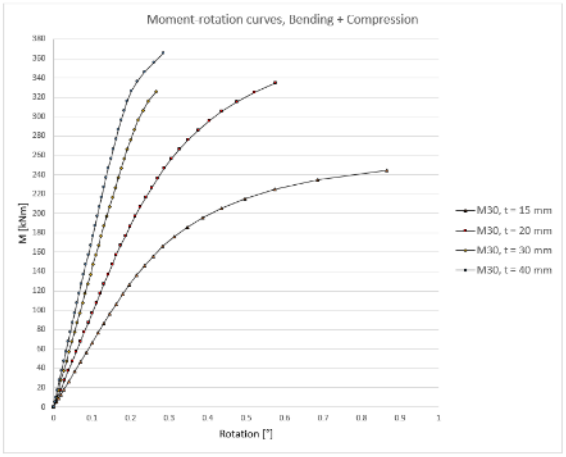
Moment-rotation curves, Bending + Compression
M [kNm]
Rotation [°]
M30, t = 15 mm
M30, t = 20 mm
M30, t = 30 mm
M30, t = 40 mm

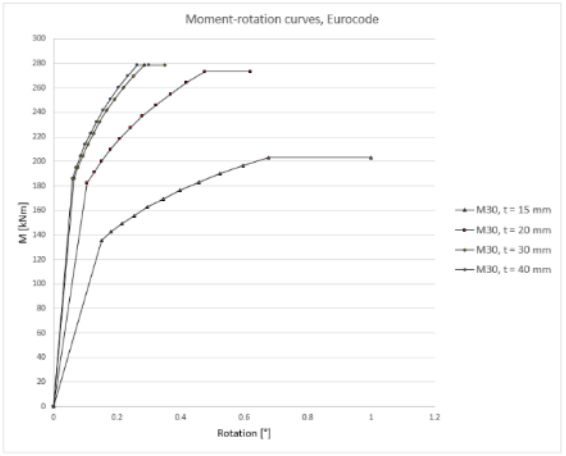
Moment-rotation curves, Eurocode
M [kNm]
Rotation [°]
M30, t = 15 mm
M30, t = 20 mm
M30, t = 30 mm
M30, t = 40 mm

Appendix 7. Moment-rotation curves in out-of-plane bending

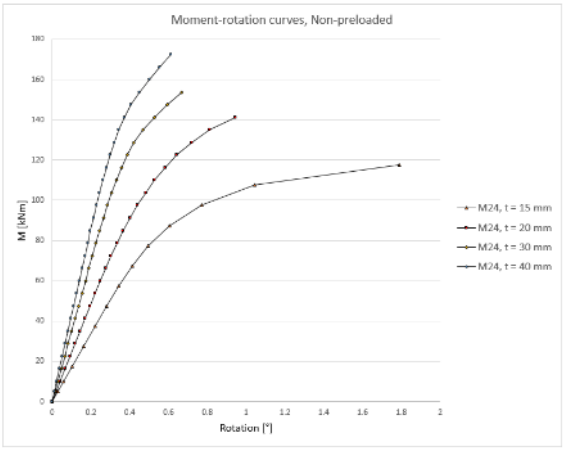

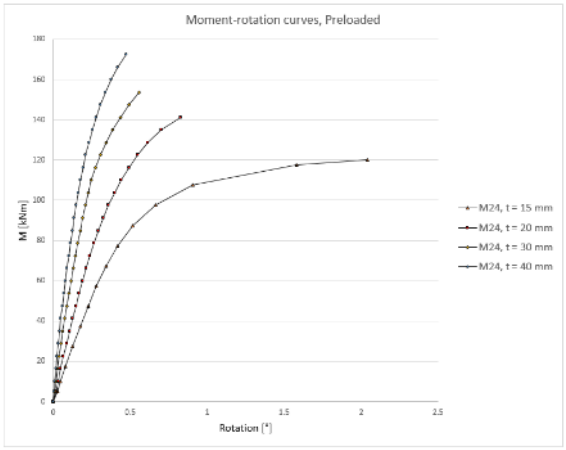

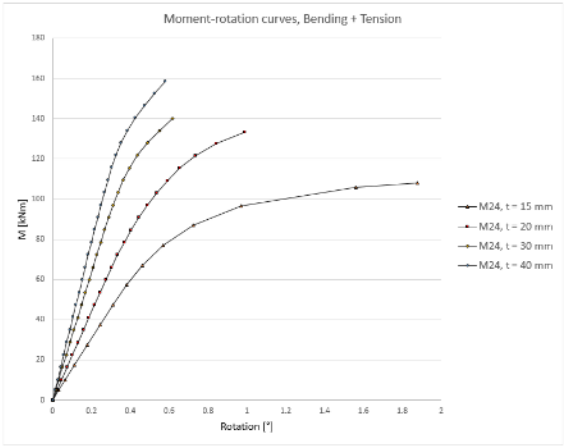

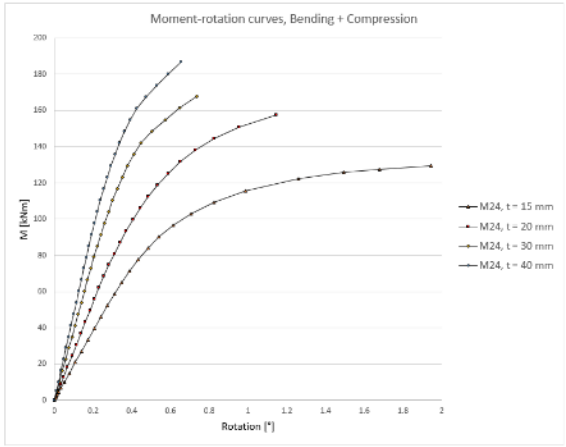

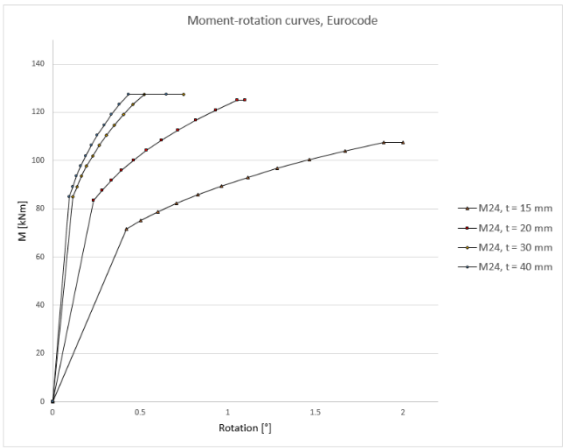

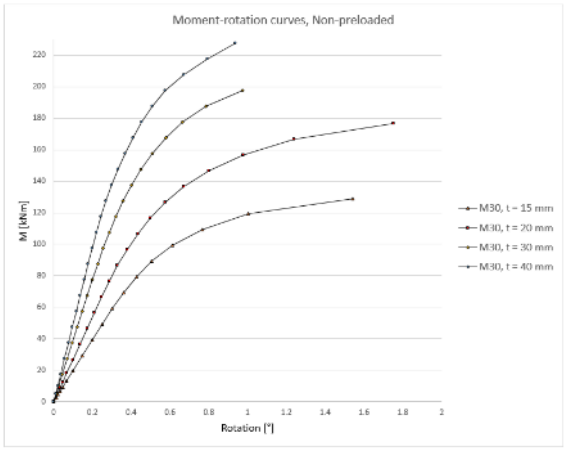
Moment-rotation curves, Non-preloaded
M [kNm]
Rotation [°]
M30, t = 15 mm
M30, t = 20 mm
M30, t = 30 mm
M30, t = 40 mm

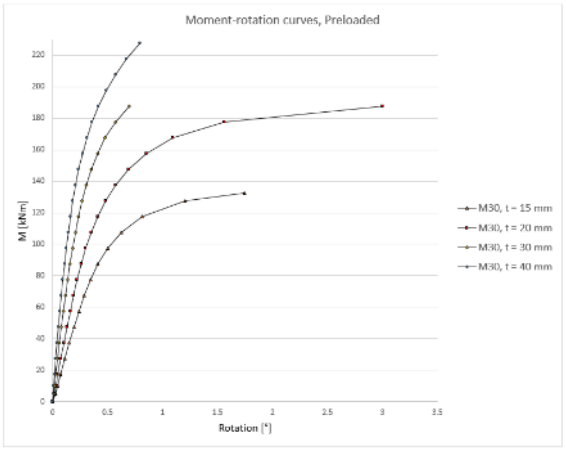
Moment-rotation curves, Preloaded
M [kNm]
Rotation [°]
M30, t = 15 mm
M30, t = 20 mm
M30, t = 30 mm
M30, t = 40 mm

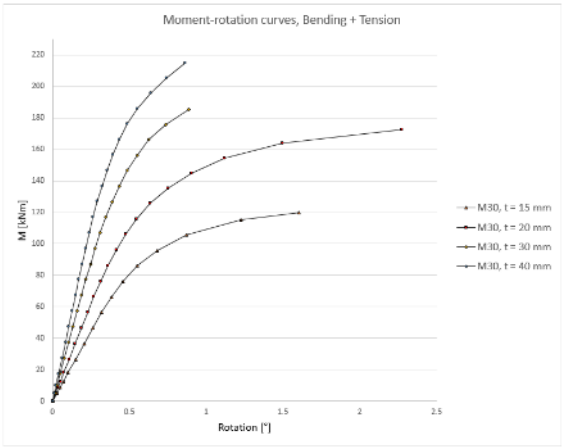
Moment-rotation curves, Bending + Tension
M [kNm]
Rotation [°]
M30, t = 15 mm
M30, t = 20 mm
M30, t = 30 mm
M30, t = 40 mm

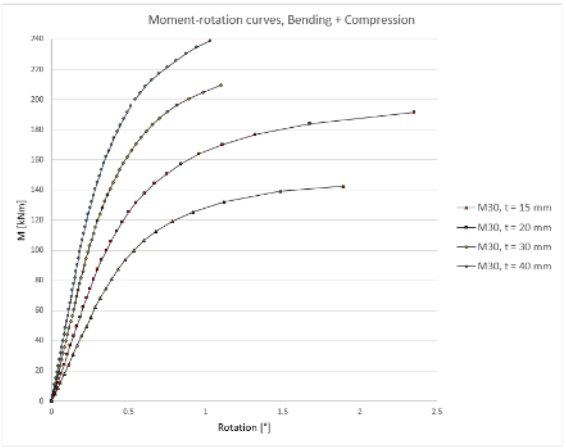
Moment-rotation curves, Bending + Compression
M [kNm]
Rotation [°]
M30, t = 15 mm
M30, t = 20 mm
M30, t = 30 mm
M30, t = 40 mm

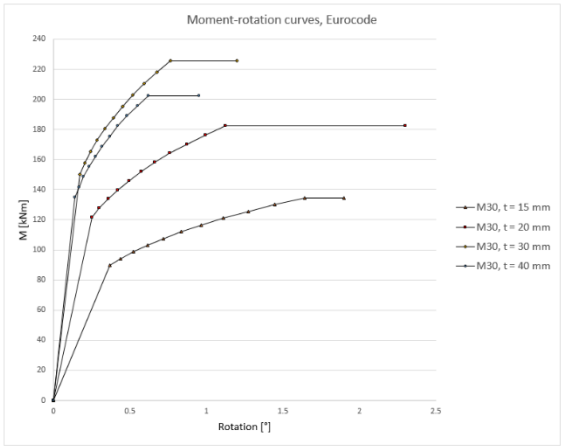
Moment-rotation curves, Eurocode
M [kNm]
Rotation [°]
M30, t = 15 mm
M30, t = 20 mm
M30, t = 30 mm
M30, t = 40 mm